The copyright of this thesis vests in the author. No quotation from it or information derived from it is to be published without full acknowledgement of the source. The thesis is to be used for private study or non-commercial research purposes only.

Published by the University of Cape Town (UCT) in terms of the non-exclusive license granted to UCT by the author.

University of Cape Town

Performance of Turbo Multi-User Detectors in Space-Time Coded DS-CDMA Systems

Derrick Bonginkosi Mashwama

University of Cape Town

Performance of Turbo Multi-User Detectors in Space-Time Coded DS-CDMA Systems

By:

Derrick Bonginkosi Mashwama

Supervised by:

Dr E.O. Bejide

Communications Research Group
Department of Electrical Engineering
University of Cape Town

A thesis presented to the University of Cape Town
In partial fulfilment of the thesis requirement for the degree of
Master of Science in Engineering

November 2007

University of Cape Town

Declaration

i) I hereby grant the University of Cape Town free licence to reproduce for the purpose of research either the whole or any portion of the contents in any manner whatsoever of the dissertation. I am presenting this dissertation in FULL fulfilment of the requirements for my degree.

ii) I know the meaning of plagiarism and declare that all of the work in the document, save for that which is properly acknowledged, is my own.

Signature:	Signed by candidate	**Date:** 22-11-07

Abstract

The continuous and growing demand for personal communication services has led both research and industry into the search for larger capacity systems. This research has led to the standardisation of Direct-Sequence Code Division Multiple Access (DS-CDMA) systems for the third generation of mobile communication systems. However, the system capacity of DS-CDMA systems is limited by Multiple-Access Interference (MAI). Multi-User Detection (MUD) has emerged as an effective technique for combating MAI in CDMA systems.

In this thesis we address the problem of improving the uplink capacity and the performance of a DS-CDMA system by combining MUD and turbo decoding. These two are combined following the turbo principle. Depending on the concatenation scheme used, we divide these receivers into the Partitioned Approach (PA) and the Iterative Approach (IA) receivers. To enable the iterative exchange of information, these receivers employ a Parallel Interference Cancellation (PIC) detector as the first receiver stage.

The performance of PA and IA receivers over an Additive White Gaussian Noise (AWGN) channel is first evaluated. These receivers are then extended to explore any possible benefits derived from utilizing a Minimum Mean Square Error (MMSE) detector as a front-end to both the PA and IA receivers. Simulation results show that, for this channel, the MMSE front-end IA receiver has substantially higher capacity and performance gains than all the other investigated receivers.

The proposed turbo multi-user receivers are then considered for Multiple-Input Multiple-Output (MIMO) CDMA systems in order to deal with channel fading. The performance of both the PA and IA receivers is evaluated in Rayleigh flat fading channels for the uplink scenario. Numerical results show that the MMSE front-end turbo space-time iterative approach receiver (IA) effectively combats the mixture of MAI and multipath fading.

University of Cape Town

To investigate the possible achievable data rates in the MIMO turbo MUD receivers, we introduce the puncturing of the mother code through the use of Rate Compatible Punctured Turbo Codes (RCPTC). Simulation results suggest that combining MUD, turbo decoding, MIMO techniques and RCPTC can significantly improve the system performance, capacity gains and greatly increase the achievable data rates for a synchronous DS-CDMA system for the uplink in Rayleigh fading channels.

University of Cape Town

Acknowledgements

Numerous people helped in bringing this work to fruition. Firstly, my sincere thanks go to my supervisor, Dr. E. O. Bejide for his advice, guidance, support, friendship and most of all for believing in me.

A special thanks goes to my friends and colleagues in the Communications Research Group who have been there to see me through hard academic and social times.

I would like to extend my sincere gratitude to my parents Dan and Busisiwe Mashwama for their unconditional support and giving me the opportunity to be who I want to be. Finally, I wish to express my heart-felt thanks to my beautiful sisters, Bhekiwe, Thuli and Bethu for their moral and financial support and for cheering me till the end, thank you.

University of Cape Town

Dedication

This thesis is dedicated to my mother, Busisiwe Yvonne Mashwama, who has given her all to make me the better man I am. Thank you mom, through your struggles, sacrifices and suffering I am who you have shaped me to be and whom and what I have always wanted to be. I love you so ever much.

University of Cape Town

University of Cape Town

University of Cape Town

List of Figures

University of Cape Town

University of Cape Town

University of Cape Town

Acronyms and abbreviations

2G	Second Generation
3G	Third Generation
APP	A Posteriori Probability
BER	Bit Error Rate
BLAST	Bell labs LAyered Space Time architecture
BPSK	Binary Phase Shift Keying
CDMA	Code-Division Multiple-Access
DCS	Digital Communication System
DD	Decision Device
DS	Direct Sequence
DS/SS	Direct-Sequence Spread-Spectrum
FDMA	Frequency-Division Multiple Access
FEC	Forward Error Correction
FF	Flat Fading
FM	Frequency Modulation
GPRS	General Packet Radio Service
GSM	Global System for Mobile Communications
HDD	Hard Decision Device
HIC	Hybrid Interference Cancellation
IA	Iterative Approach
IC	Interference Cancellation
ISI	Inter-Symbol Interference
K	Number of subscribers currently actively engaged in transmission
Ks	Number of subscribers
LLR	Log Likelihood Ratio
LOS	Line-of-Sight
MA	Multiple Access
MAI	Multiple Access Interference

University of Cape Town

MAP	Maximum A Posteriori
MF	Matched Filter
MIMO	Multiple-Input Multiple-Output
ML	Maximum-Likelihood
MLSE	Maximum Likelihood Sequence Estimator
MMSE	Minimum Mean Square Error
MRC	Maximum Ratio Combining
MS	Mobile Station
MUD	Multi-User Detection
NSC	Non-Systematic Convolutional
PA	Partitioned Approach
PG	Processing Gain
PIC	Parallel Interference Cancellation
PN	Pseudo-Noise
QoS	Quality of Service
RCPC	Rate Compatible Punctured Convolutional
RCPTC	Rate Compatible Punctured Turbo Codes
RSC	Recursive Systematic Convolutional
SDD	Soft Decision Device
SIC	Successive Interference Cancellation
SISO	Single-Input Single-Output
SM	Spatial Multiplexing
SNR	Signal-to-Noise Ratio
STBC	Space-Time Block Codes
STC	Space-Time Codes
ST-Demux	Space-Time Demultiplexer
ST-Mux	Space-Time Multiplexer
STTC	Space-Time Trellis Codes
TC	Turbo Codes
TDMA	Time-Division Multiple Access
ZF-DF	Zero-Forcing Decision-Feedback Detector

University of Cape Town

Chapter 1
Introduction

Contents

University of Cape Town

1.1 Wireless Mobile Communications

The ultimate goal of mobile communications is to enable everyone to communicate instantly with anyone else, at anytime they please, at any location and through all weather/channel conditions. Third Generation (3G) and beyond systems give the ability to provide seamless access to a variety of services, including the Internet, voice and video. As the demand to host multimedia content in wireless communication systems grows, so does the need to support more users per given communication channel grow. Once a user is accommodated in a given channel he/she expects a certain Quality of Service (QoS) and high-data-rate transmission in order to be able to efficiently utilize high-end services provided by his/her service provider.

To meet the capacity demand, Multiple Access (MA) technologies are used for cellular technologies. To ensure the effective utilization of the limited radio spectrum available, a choice of MA technology that efficiently shares the available but scarce bandwidth among a large number of users must be made. The evolution of telecommunication systems from Second Generation (2G) through 2.5G to 3G and beyond has seen a lot of research concentrated in finding the best MA scheme. A schematic of a multiple access communication system is shown in Figure 1.1.

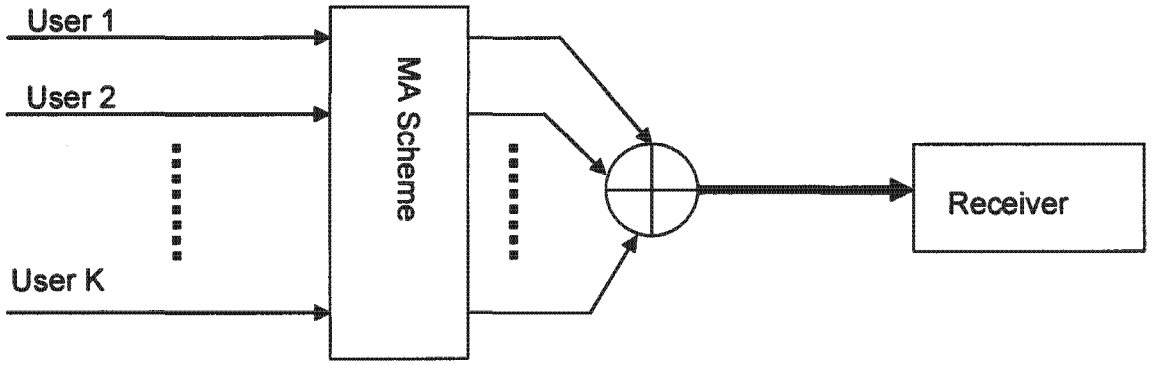

Figure 1.1: *Multiple Access Communication System*

MA systems are such that, corresponding messages from different transmitting sources that transmit simultaneously through the same communication channel, are separated in such a manner that they do not interfere with each other. This separation can be achieved by making the messages orthogonal to one another in the dimensions of frequency, time or space.

The first wireless communication systems saw the deployment of Frequency-Division Multiple Access (FDMA), where Frequency Modulation (FM) was used to divide the total available bandwidth into frequency channels/bands. Each frequency channel was allocated to a particular user thus ensuring minimum interference from other system users. Since each sub-channel is assigned to only one user at a time, as shown in Figure 1.2, an obvious disadvantage of FDMA is that the frequency spectrum is not used efficiently as no two users can share the frequency band at any given time and moreover, guard bands have to be maintained between adjacent signals spectra to minimize cross-talk between sub-channels.

University of Cape Town

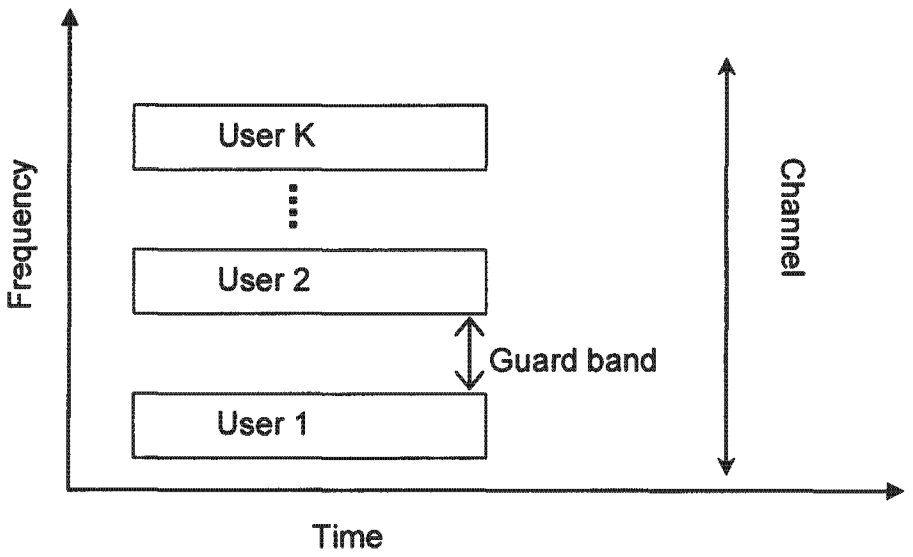

Figure 1.2: *Frequency Division Multiple Access (FDMA)*

Another type of MA technology is Time-Division Multiple Access (TDMA). In TDMA partitioning is in time (as opposed to frequency), where the signal is divided into different time slots, with each time slot assigned to a single user for data transmission. Thus each user utilizes the entire frequency spectrum available. Although TDMA offers increased efficiency of transmission, it however, requires a significant amount of signal processing in order to achieve synchronisation of all users' transmitted signals. As seen in

Figure 1.3, TDMA requires guard times between time intervals to reduce clock instabilities and transmission time delay, thus imposing a constraint on the maximum bit rate per channel.

University of Cape Town

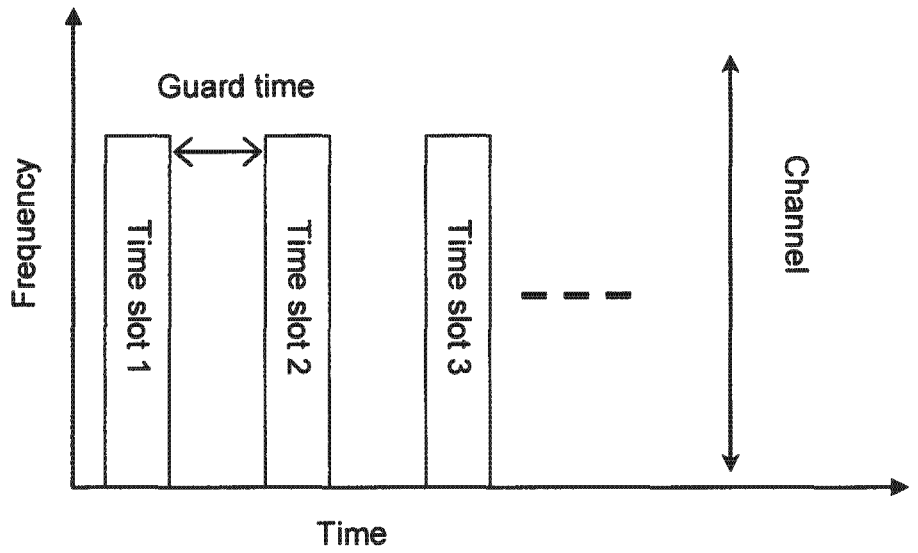

Figure 1.3: *Time Division Multiple Access (TDMA)*

In both FDMA and TDMA the frequency or time allocation for each user is fixed to that user (whether active or not) and cannot be utilized by any other user. As the demand for more services (i.e. data and video) and number of system users increases, both schemes have set an upper limit on the system capacity and available transmission rates.

Due to these inefficiencies, researchers have continued the search for more efficient, dynamic and reliable MA schemes that allow free use of idle frequency channels or time slots. Code-Division Multiple-Access (CDMA) implemented with Direct-Sequence Spread-Spectrum (DS/SS) signalling is among the most promising MA techniques currently used in 3G systems. The narrow band signal is spread using a very large-bandwidth signal called the spreading signal. The large redundancy inherent in the spreading of the signal allows for the overcoming of the severe levels of interference that maybe present in the communication channel. In a DS-CDMA system all users are operating in the same waveband and they can transmit at the same time using the same channel resources, where orthogonality is achieved by assigning unique spreadind codes to each user's signal. Figure 1.4 shows a general scheme of a CDMA system.

University of Cape Town

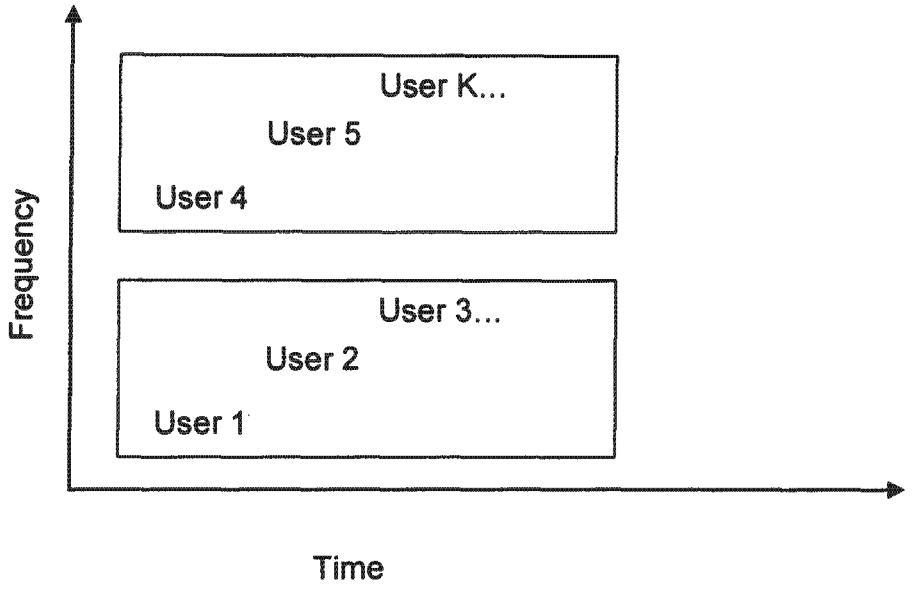

Figure 1.4: *Code Division Multiple Access (CDMA)*

In CDMA systems, the signal received at the detector/receiver is a sum of all users' signals, which overlap both in time and frequency. The conventional detector uses a bank of matched filters, each matched to a particular user's code waveform and sampled at that user's propagation delay.

Figure 1.5 shows a receiver-end baseband model of a direct sequence CDMA system. This detector acts as a single user detector and ignores the existence of all other users.

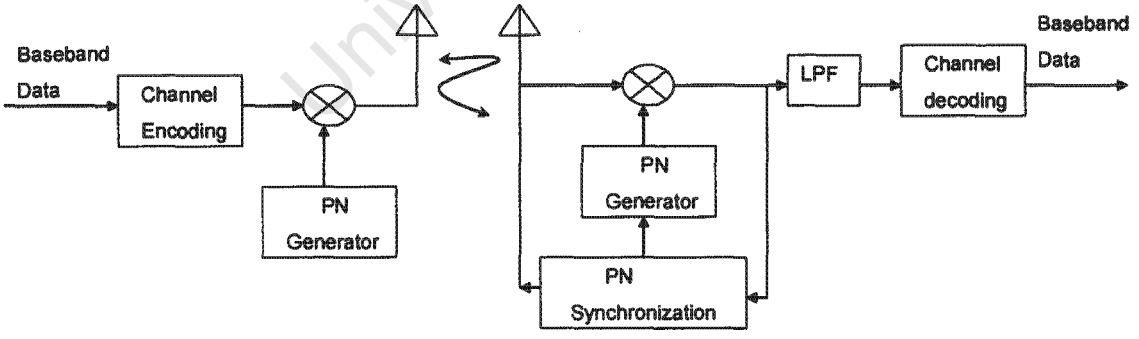

Figure 1.5: *DS-CDMA System*

University of Cape Town

Due mainly to the fact that the spreading waveforms used at transmission are not completely orthogonal; there exists correlation between transmitted users' signals. This Multiple Access Interference (MAI) increases with every user that is introduced into the system, thus setting a capacity and performance limit on the DS-CDMA system. In the uplink scenario, the overall MAI at the receiver is the sum of all MAI from all interfering users. We can thus say that CDMA systems are generally interference limited. MAI suppression in receiver design becomes an important aspect as its reduction leads to reduced transmit power required to meet a certain Signal-to-Noise Ratio (SNR), thus enabling more signals to be transmitted with the limited available transmitter power. When power levels of certain users are significantly high, weak users with single-user detectors may lose communication because of the overwhelming MAI. This phenomenon is known as the near-far effect and it can be mitigated by means of power control, where ideal power control ensures all users have identical signal power levels or SNR when they arrive at the base station thus guarantying superior performance as compared to TDMA and FDMA systems. To reduce complexity, MAI from a single cell is only considered in this work.

University of Cape Town

1.2 Motivation and Objectives of this work

This presence of MAI in DS-CDMA systems has led many researchers to investigate ways of exploiting the MAI to improve the system performance. Multi-User Detection (MUD) deals with the demodulation of mutually interfering digital streams of information, such techniques are viewed essential in the quest to achieve near optimal performance in communication systems.

Motivated by the growing demand for enhanced capacity and data services in current 3G and future generation systems, in this thesis we present investigations on various multi-user receiver structures and we focus mainly on such structures that employ the iterative turbo multi-user detection principle to improve the spectral efficiency and performance of cellular systems. Multiple-Input Multiple-Output (MIMO) antenna techniques and puncturing devices are also investigated as possible means of improving the system

performance in fading channels. Investigations are also taken on the possible achievable data rates in such cellular systems.

The objective of this work is to evaluate the performance of turbo space-time DS-CDMA multi-user detectors with a special emphasis on system capacity and data rates that these receivers can possibly achieve.

1.3 Thesis Contributions

The contributions of this thesis can be summarized as follows:

- The performance evaluation of iterative space-time turbo coded DS-CDMA multi-user detectors
- A comparative study of two classes of turbo space-time coded MIMO-CDMA receivers in Rayleigh fading channels. These two classes of receivers are classified, according to the concatenation scheme used, as either Partitioned Approach (PA) or Iterative Approach (IA).
- An MMSE linear detector is used as the front-end of both PA and IA receivers and performance studies of both MMSE/PA and MMSE/IA receivers are undertaken over both AWGN and Rayleigh fading channels.
- The performance evaluation of PA and IA receivers for systems employing Rate Compatible Punctured Turbo Codes (RCPTC) for transmission through Rayleigh fading channels

University of Cape Town

1.4 Thesis Outline

This thesis is organized into six chapters, the first being the introduction. The rest of the thesis is organized as follows:

In chapter 2, an introduction of the fundamental techniques used in this thesis is given. A general DS-CDMA system model with Forward Error Correction (FEC) is introduced and the basic elements that constitute this model, such as the transmitter, communication

channel and receiver are also discussed in detail. A brief review of convolutional codes is presented in this chapter since they are vital in the understanding of turbo codes. A detailed description of the algorithm used in turbo decoding is presented. Finally a brief discussion on decision devices is presented.

Chapter 3 addresses the problem of MAI in CDMA systems. First, the Matched Filter (MF) receiver is reviewed followed by a general overview of multi-user detectors. The principle of iterative MUD is introduced and such receivers are classified as either PA or IA receivers. An investigation into the use of Minimum Mean Square Error (MMSE) detectors as a front end to both the PA and IA receivers is presented with performance curves for transmission in an AWGN channel.

In chapter 4, the more realistic Rayleigh fading channel is considered. Here, MIMO antenna techniques are introduced as a means of suppressing channel fading. The receivers introduced in chapter 3 now take a different form, thus a new system model, i.e. turbo space-time MIMO CDMA system model, is introduced. The receivers are now divided into the MMSE front-end turbo space-time partitioned approach receiver and the MMSE front-end turbo space-time iterative approach receiver. Performance results are presented for these two receiver types under varying receiver parameters, such as the system load, number of decoding iterations and SNR levels.

Chapter 5 introduces the RCPTC concept into the PA and IA receivers of chapter 4. Performance results for punctured multiple user systems in Rayleigh fading channels are presented.

Finally, chapter 6 concludes this thesis. It summarises the work done in this thesis and highlights the contributions made. Suggestions for further work are also given.

University of Cape Town

Chapter 2

Turbo Coded DS-CDMA Systems

Contents

University of Cape Town

The main concern of this thesis is the performance investigation and application of the turbo multi-user detection principle in the design of multi-user receivers. The aim of this chapter is to present and review key concepts from existing literature that form the essence of the remaining chapters.

The system model for a FEC-CDMA system is first introduced in section 2.1 of this chapter. In section 2.2 a brief introduction to the theory behind Turbo encoding is presented. Section 2.3 looks at the degradation effect experienced by the transmitted signal as it propagates through the communication channel from the transmitter to the receiver. The Maximum a Posteriori (MAP) Turbo decoder, which is one of the key components in turbo-iterative multi-user detector is discussed in section 2.4. Section 2.5 presents simulation results for single user turbo coded CDMA systems. This chapter concludes with a brief summary in section 2.6.

2.1 Forward Error Coded DS-CDMA Systems

The distortions and disturbances inherent in mobile communication channels can significantly degrade the system performance. We are concerned with channel coding

schemes that have error control attributes. Error control coding enables the digital communication system to reduce the amount of erroneous data at the receiver. The ratio of erroneous bits to the total number of received bits is called the Bit Error Rate (BER) and is used as the measure of the system performance for a given SNR. By employing FEC coding helps improve the system performance as it lowers the required SNR for a desired BER. The measure of advantage gained by a FEC coded system on an uncoded system is called the FEC coding gain. A significant coding gain figure can be translated into an increase in the system capacity as this means less power is required to reach the desired BER.

A FEC encoder adds redundant bits, called parity bits, to the information bits. These parity bits are used by the channel decoder at the receiver to correct transmission channel errors. Generally FEC codes are classified into either block codes or convolutional codes. Some of the commonly used block codes include Hamming codes, Golay codes, Reed Solomon Codes and BCH codes. Convolutional codes have been however more accepted in wireless communications because of their properties in continuous transmission. For a detailed discussion on these two classes of FEC coding techniques the reader is referred to [1, 2].

FEC coded systems are considered in this chapter not only as a medium of resistance to the degrading effect introduced by the communication channel but also because they play a vital role in our study of iterative multi-user detection schemes which are discussed in consequent chapters. Convolutional codes are of interest in this work as they form part of the powerful subclass of FEC codes called Turbo Codes (TC) discussed in the remaining sections of this chapter.

A DS-CDMA system for Ks synchronous number of subscribers (where subscribers are the users authorized to use the CDMA system) is considered. To facilitate ease in analysis, we assume synchronous transmission throughout this thesis. We further denote the number of subscribers currently actively engaged in transmission by K. All subscribers in the system are assigned spreading codes or signatures. Each user's

University of Cape Town

spreading code will have a length of N chips, where the length N is termed the Processing Gain (PG). Figure 2.1 shows the FEC coded CDMA system modelling the uplink transmission scenario that is considered throughout this chapter.

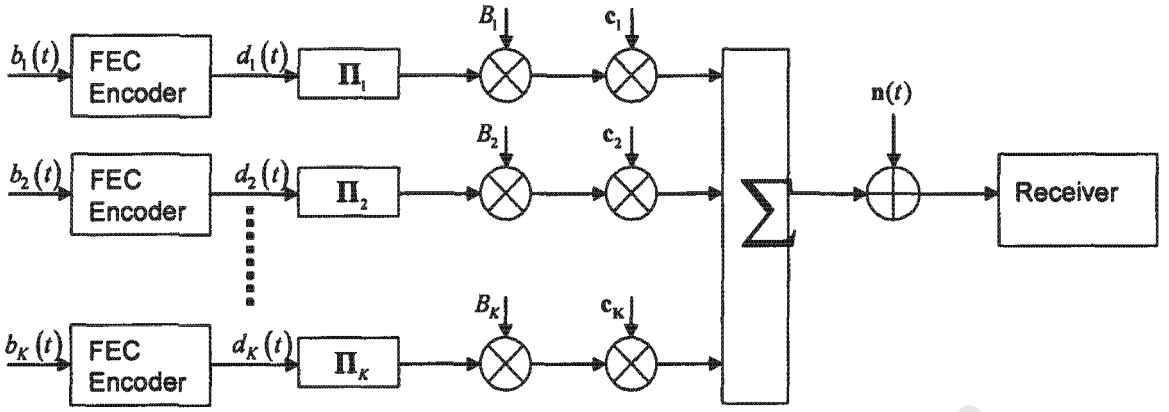

Figure 2.1: *FEC Coded Direct Sequence CDMA System in AWGN Channel*

Each user's input data stream $b_k(l) \in \{0,1\}$ of frame size L_{in} information bits, where $l \in \{1,2,\ldots,L_{in}\}$, is first encoded using a rate $r = L_{in}/L_{out}$ FEC channel encoder to produce L_{out} coded bits. The L_{out} coded bits at the output of the encoder are then passed through a channel interleaver. The interleaved coded bits of the *k*th user are BPSK symbol mapped, yielding the coded bits $d_k(t) \in \{-1,1\}$ where $t \in \{1,2,\ldots,L_{in}/r\}$ and then each coded bit is spread using a unique code sequence, $\mathbf{c}_k(t)$ which is assumed to be known only to the base station. Once modulated, the signals are then transmitted over the channel.

The *k*th user's baseband signal can be modelled as:

$$s_k(t) = B_k d_k(t)\mathbf{c}_k(t)\cos(\omega_c t\theta_k + (t)) \tag{2.1}$$

or

$$s_k(t) = \sqrt{E_k}\, d_k(t)\mathbf{c}_k(t)\cos(\omega_c t + \theta_k(t)) \tag{2.2}$$

$$E_k = B_k^2 = 2P_k \tag{2.3}$$

Where B_k is the received amplitude of the *k*th user's signal, and E_k is referred to as the

University of Cape Town

energy of the *k*th user's signal and $d_k(t) \in \{+1, -1\}$ is the coded bit transmitted by user k at time t, consisting of rectangular pulses of duration T_b (bit interval) that correspond to the transmitted symbol. Each user's data is multiplied by the spreading code $\mathbf{c}_k(t)$, and then the composite $d_k(t)$ modulates the carrier, we assume Binary Phase Shift Keying (BPSK) modulation. Here $k \in \{1, \cdots, K\}$ is the user number and E_k is the energy of the transmitted coded bit, and is related to the uncoded information bit through $E_k = rE_b$ and E_b is the energy per information bit, ω_c is the carrier frequency and θ_k is the carrier phase of the *k*th user. $\mathbf{c}_k(t) \in \{1, -1\}^N$ is the spreading code employed by user k at time t, consisting of N chips given by:

$$\mathbf{c}_k(t) = \sum_{j=0}^{N-1} c_k[j]\psi(t - jT_c) \tag{2.4}$$

Where $c_k[j] \in \{-1, 1\}$ is the *j*th element/chip of the spreading code for user k and $\psi(t)$ is the chip waveform with chip duration of T_c. We assume that $\mathbf{c}_k(t)$ has unit energy. We assume that all signature waveforms fall within the bit interval, T_b, and are zero outside this range.

By substituting (2.4) into (2.2) we can express the continuous time waveform transmitted by user k in symbol interval i as:

$$s_k(t) = \sqrt{E_k} \sum_{j=0}^{N-1} d_{k,j}[c_{k,j}]_j \psi(t - jT_c - iT_b) \tag{2.5}$$

Where $[c]_j$ is the *j*th element of c.

2.2 Encoding

2.2.1 Convolutional Codes

Convolutional codes are generated by shifting blocks of L_{in} input binary bits at a time into a shift register. The convolutional encoder produces L_{out} output symbols which are a

University of Cape Town

linear combination of the current set of L_{in} input bits and all bits stored in the shift register. This results in an encoder with a rate, $\frac{L_{in}}{L_{out}}$. The total number of input data blocks in the shift resister, v, is called the constraint length of the code and the term $v-1$ represents the memory of the code. Figure 2.2 below shows a Non-Systematic Convolutional (NSC) encoder.

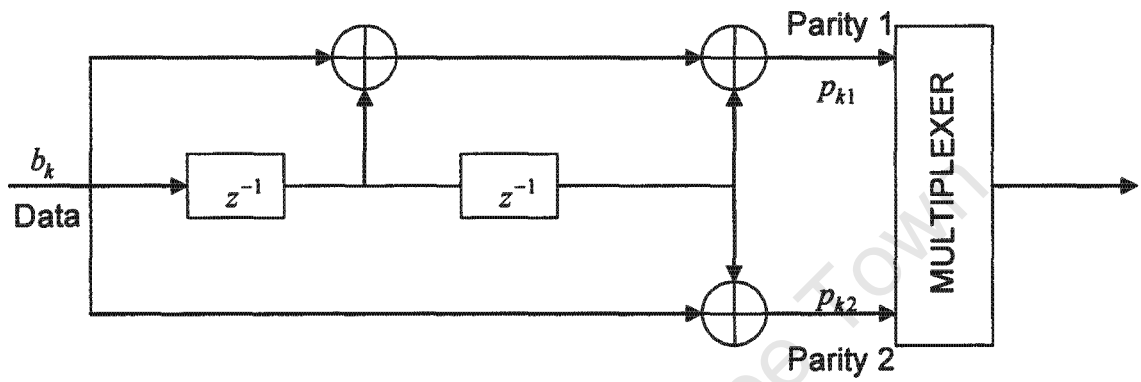

Figure 2.2: *Non-Systematic Convolutional (NSC) Encoder*

A convolutional encoder which has its current input block appearing unchanged in the current code block is classified as systematic (shown in Figure 2.3). Furthermore a convolutional encoder that is implemented by including feedback is known as a recursive convolutional encoder.

University of Cape Town

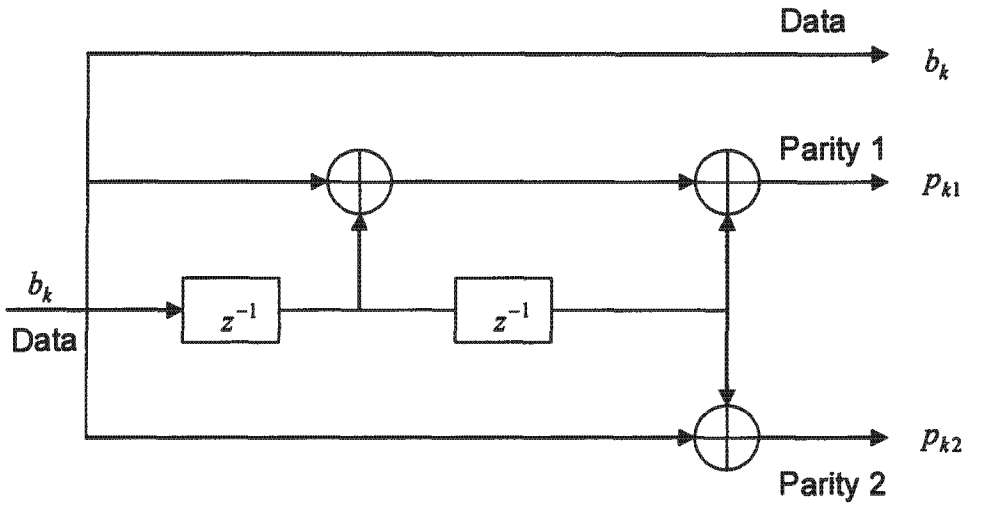

Figure 2.3: *Systematic Convolutional Encoder*

A recursive convolutional code can also be either systematic or non-systematic. Figure 2.4 below shows an example of a Recursive Systematic Convolutional (RSC) encoder with generator polynomials given by $(7,5)_{octal}$.

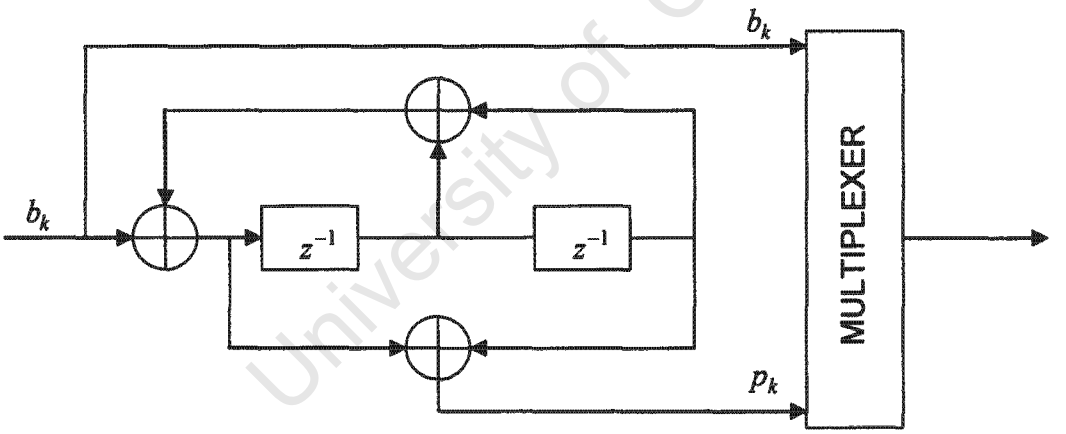

Figure 2.4: *Recursive-Systematic Convolutional (RSC) Encoder*

2.2.2 Turbo Encoder

A TC is the parallel concatenation of two RSC codes separated by an interleaver. The structure of a rate $r = 1/3$ turbo encoder formed by the parallel concatenation of two identical rate $r = 1/2$ RSC encoders, separated by an interleaver (represented by Π), is

University of Cape Town

shown in Figure 2.5.

The encoder produces binary codewords $d_k(t) \in \{d_k^s, d_k^{p1}, d_k^{p2}\}$ for each kth user's input bit $b_k(t)$ at time index t, where $d_k(t) = \pm 1$. Here d_k^s represents the systematic bit and the parity output (at time t) from RSC1 and RSC2 is represent by d_k^{p1} and d_k^{p2} respectively.

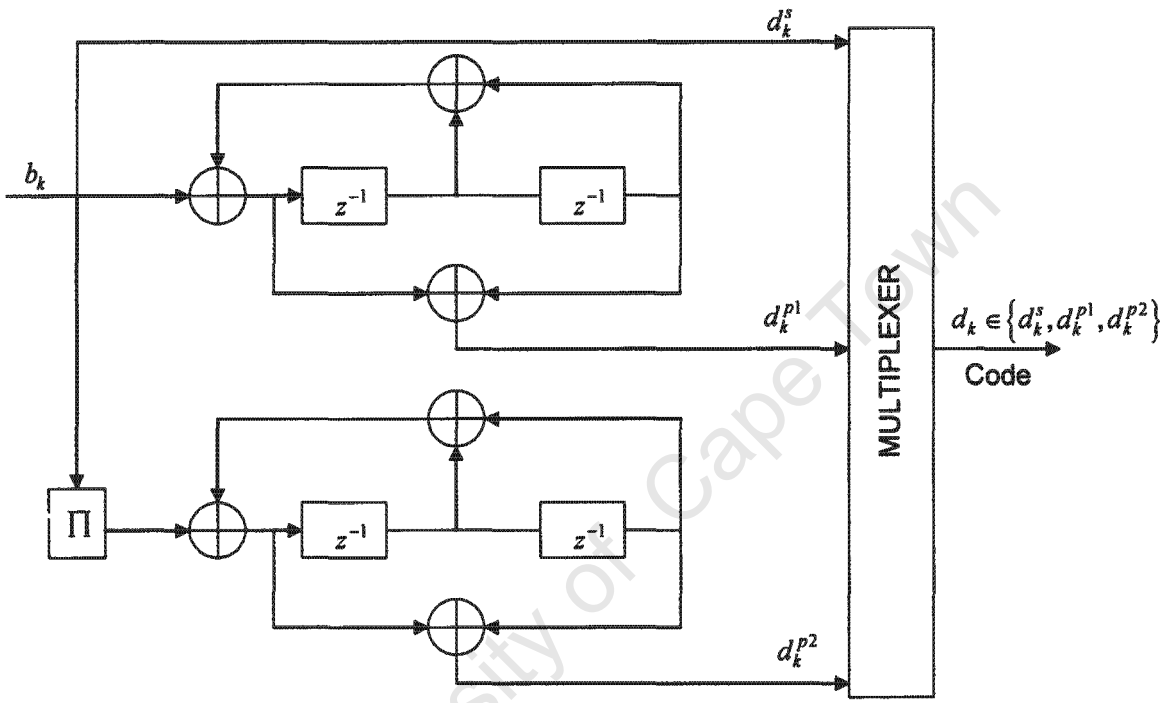

Figure 2.5: *Rate r=1/3 Turbo Encoder Structure*

University of Cape Town

Interleaver

The interleaver is an important aspect of the turbo encoding/decoding process. Its main function is to permute each incoming block of L information bits and rearrange them in a random order before encoding on RSC2. Since in practice the same random interleaving sequence used at encoding cannot be re-generated at decoding, we thus employ a pseudo-random interleaver (pseudo-random because there is no apparent order, although the arrangement is known at the decoder). In this work we utilize pseudo-random block interleaving, where the data is read in by rows and columns but read out in a pseudo-

random order [1, 2].

The two RSC encoders encode the same information bits, b_k (although RSC2 receives an interleaved version of the information bits). The structure in Figure 2.5 is an example of a TC with rate $r = 1/3$. This overall TC rate is due to the transmission of the systematic output of RSC1 and parity bits of both RSC1 and RSC2. Generally, for a rate $r = 1/M$ turbo encoder, only the systematic code symbols of the first encoder are transmitted and the non-systematic (parity) code symbols of all constituent encoders are transmitted. However, the code rate of the turbo encoder can be increased through puncturing.

2.3 Transmission Channel

The propagation of radio signals through a channel is subjected to free space loss or path loss and fluctuations in signal level called fading. Fading can be categorizes as either large-scale or small-scale fading. Large-scale fading is caused by shadowing effects due to energy absorbing objects along the propagation path (i.e. path loss due to motion over large areas). We concentrate on small-scale fading where changes in signal amplitude and phase are only due to the spatial positioning between a receiver and transmitter. This is relevant since wireless mobile communication systems suffer from multi-path fading, which is due to the signal from the transmitter arriving at the receiver through multiple reflective paths thus causing the signal's amplitude, phase, and angle of arrival to fluctuate [3]. The radio channel is a time varying, multipath fading channel, and its main characteristics are time spread and time variation [5]. The multi-path propagation results in spreading of the signal in three different dimensions — time spread, Doppler spread, and angular spread.

The fading channel will undergo different types of fading according to the relation between the signal parameters and the channel parameters. Based on multipath time spreading, the fading channel can be classified as either a frequency-nonselective fading channel or a frequency-selective fading channel, according to Doppler spread, the fading channels are classified as either fast fading channels or slow fading channels. It can thus

University of Cape Town

be said, that frequency non-selective fading and frequency selective fading channels describe the characteristics of the frequency variation while fast fading and slow fading channels describe characteristics of the time variation. Spread in the time domain appears as Flat Fading (FF) when the multipath delay spread is less than the symbol time. At the receiver frequency-selective fading causes Inter-Symbol Interference (ISI) distortion while flat fading causes a loss in SNR.

In a flat fading channel, the bandwidth of the transmitted signal is less than the bandwidth of the fading channel. The envelope of the received signal of a flat fading channel is assumed to follow the Rayleigh or Ricean distribution. A frequency-selective fading channel, on the other hand, consists of a number of multi-path components and the envelope of the received signal for each component follows the Rayleigh or Ricean distribution.

The fore mentioned communication channels can be modelled using the statistical models or probability density function (pdf) models as discussed below.

Ricean

The Rice pdf is used to characterize the statistical fluctuations of signals received from a multipath fading channel with presence of a Line-of-Sight (LOS) signal component. The pdf of the received signal envelope is represented as:

$$p(d) = \frac{d}{\sigma_R^2} \exp\left[-\left(\frac{d^2 + a^2}{2\sigma_R^2}\right)\right] I_0\left(\frac{da}{\sigma_R^2}\right) \tag{2.6}$$

where, σ_R^2 is the mean received scattered power of the diffuse component due to multipath propagation, $a^2/2$ is the mean received power of the LOS signal component and $I_0(.)$ is the modified zero order Bessel function of the first kind.

University of Cape Town

Rayleigh

The Rayleigh pdf is used to model the statistical fluctuations of signals received from a multipath fading channel with no LOS signal component. The pdf of the received signal envelope is represented as:

$$p(d) = \frac{d}{\sigma_R^2} \exp\left[-\left(\frac{d^2}{2\sigma_R^2}\right)\right] \tag{2.7}$$

where, σ_R^2 is the mean received scattered power of the diffuse component due to multipath propagation.

Other distributions include the lognormal and Nakagami distributions [2], however lognormal distribution is often used for large-scale shadowing fading and not for small-scale fading. Fading channels can be classified through the analysis of their three main mathematical characteristics. These are: the received amplitude distribution, LOS components and the Doppler power spectral density. Depending on the signal propagation environment, the envelope of the received signal can be described as either a Rayleigh or a Ricean distribution. If the in phase and quadrature components are zero-mean, the received signal amplitude distribution corresponds to the Rayleigh distribution and the phase is uniformly distributed in the interval $[0, 2\pi]$. If the in phase and quadrature components are not zero-mean, the received signal amplitude distribution corresponds to the Ricean distribution.

In the Rayleigh fading channel, there is no LOS component between the transmitter and the receiver. Thus, the in phase component and the quadrature component do not include a LOS component, and they are Gaussian random variables with zero-means [3-4]. However, in the Ricean fading channel, there exist a direct LOS component between the transmitter and the receiver. Therefore, the in phase component and the quadrature component are composed of a LOS component, but they are still Gaussian random variables with non-zero means.

University of Cape Town

It can thus be summarized that a Rayleigh fading channel is a channel whose received signal's envelope follows the Rayleigh distribution. In this thesis all transmitted signals are over the Rayleigh flat fading channel (unless stated otherwise).

For a more detailed discussion of radio propagation and statistical modelling of multidimensional fading channels the reader is referred to [2-5].

2.3.1 Rayleigh Flat Fading Channel

In a flat fading channel, the bandwidth of the signal is less than the coherence bandwidth of the channel or simply, the delay spread is less than the symbol period. We suppose to deal with flat fading channels such that the channel response does not vary with time. The multi-user CDMA system in a flat fading channel is structured as depicted in Figure 2.6 below.

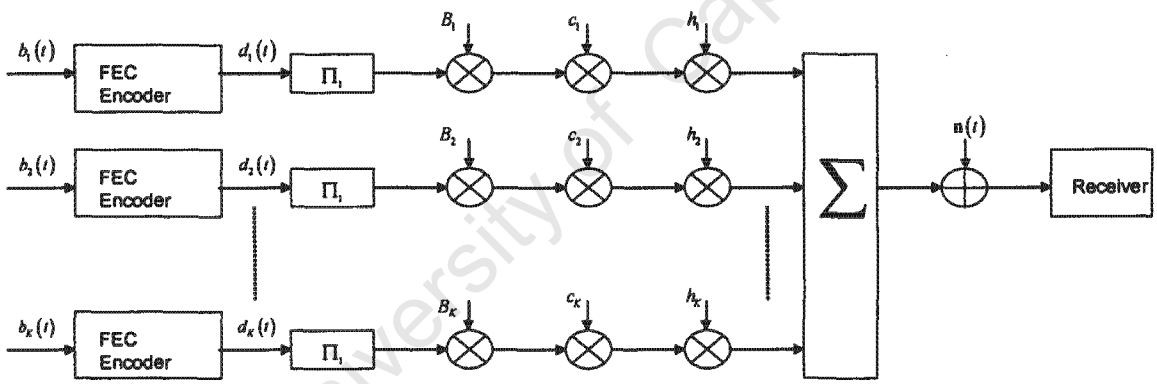

Figure 2.6: *FEC Coded Direct Sequence CDMA System in a Flat Fading Channel*

The continuous time signal at a receiver from a flat fading channel can be expressed as

$$r(t)=\sum_{n=0}^{+\infty}\sum_{k=1}^{K} d_k(t)c_k(t-nT)*h(t)+n(t) \tag{2.8}$$

University of Cape Town

Where $h(t)$ represents the channel coefficient subject to fading. We consider a Rayleigh fading channel, where $h(t)$ is a complex Gaussian random process, given as

$$h(t) = |h(t)| e^{j\theta} \tag{2.9}$$

Where $|h(t)|$ is Rayleigh distributed and θ is the phase value.

Here * represents the convolution operation, and $n(t)$ is a zero mean additive Gaussian noise with a two-sided power spectral density of $N_0/2$.

2.4 Receiver

The receiver structure for a FEC coded CDMA system is shown in Figure 2.7. This structure consists of a simple approach to demodulating CDMA signals called the single-user MF also known as the conventional detector. This receiver is optimal in the case of a single-user CDMA channel but suffers from MAI in a multi-user CDMA channel. The MF receiver structure is discussed in detail in section 3.2.

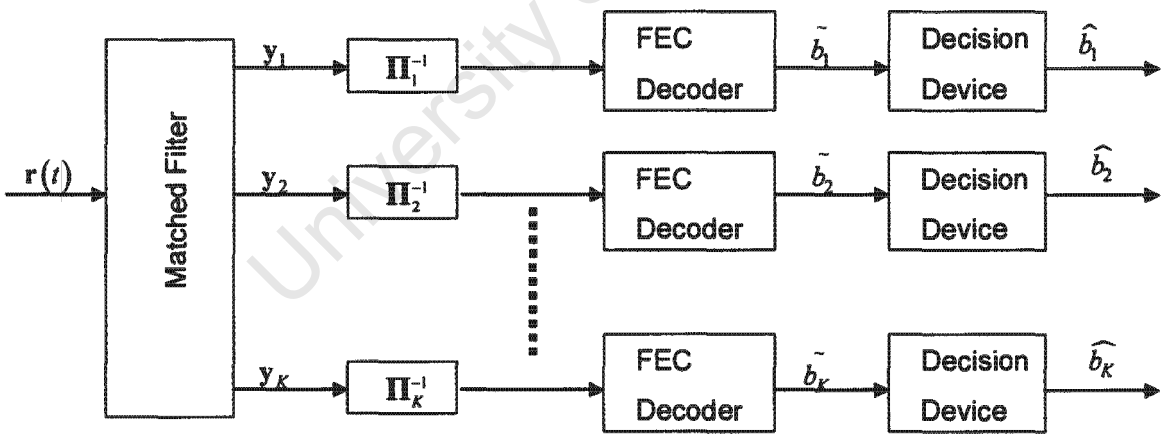

Figure 2.7: *Structure of FEC Coded CDMA System Receiver*

The de-interleaved output of the conventional detector is then decoded by a FEC decoder

University of Cape Town

to give a soft estimate of the kth user's encoded bit, b_k .

Convolutional codes are decoded using the Maximum-Likelihood (ML) solution and the Viterbi algorithm. This decoding algorithm cannot however be applied for turbo decoding as the presence of the interleaver increases the complexity of the Viterbi algorithm to $O(2^L)$, where L is the combined size of the data frame and the interleaver. Due to the prohibitive complexity of the ML decoding in turbo codes, we use suboptimal decoding solutions. The MAP algorithm is an example of a suboptimal decoding solution. By taking the logarithmic of the MAP algorithm we obtain the log-MAP algorithm which merely, for convenience reasons, converts all likelihoods (that are present in MAP) to a logarithmic form thus removing the exponentiations and converting the multiplications to additions. A simplified version of both the MAP and log-MAP algorithms that further reduces calculation complexity is the max-log-MAP algorithm. In this thesis we consider the MAP algorithm.

2.4.1 MAP Decoding Algorithm

In this section, we assume a rate $1/n$ constituent RSC code, which produces binary codewords $\mathbf{d}_l = \{d_l^i\}$ at time index l, $(0 \le i < n)$, where $d_l^i = \pm 1$. As an example, we consider two rate 1/2 constituent RSC codes, thus at time l the binary codeword produced is $\mathbf{d}_l = \{d_l^s, d_l^1\}$ where d_l^s represents the systematic bit and d_l^1 is the parity bit due to the present RSC encoder. We thus differentiate the parity output (at time l) from RSC1 and RSC2 by expressing it as d_l^{P1} and d_l^{P2} respectively.

We further assume that the encoder is initially in the all-zero state and terminates either at an arbitrary state after L_{in} bits (if no tail bits are transmitted) or at the all-zero state after $L_{in} + v$ bits (with tail bits transmitted).

For the encoded and transmitted word $\mathbf{d}_l$ the corresponding received noisy word is $\mathbf{y}_l$ and $\mathbf{y}$ represents the vector for all received codewords.

University of Cape Town

In the symbol-by-symbol MAP decoding algorithm of Bahl *et al.* [6] we need to calculate the Log Likelihood Ratio (LLR) of the a posteriori probabilities (APPs). The MAP algorithm gives the probability for each decoded bit u_l, that at transmission this bit was +1 or -1, given the received symbol y_l. This is done by formation of APPs for each data bit, which is followed by choosing the data-bit value that corresponds to the MAP probability for that data bit [7]. The LLR of the APPs $L(u_l \mid \mathbf{y})$ are given as

$$L(u_l \mid \mathbf{y}) = \left(\frac{P_r(u_l = +1 \mid \mathbf{y})}{P_r(u_l = -1 \mid \mathbf{y})} \right) \tag{2.10}$$

Where $P_r(u_l \mid \mathbf{y})$ is the likelihood ratio and $\mathbf{y}$ is the vector containing the received decision variables.

The input bit d_l^s will be known if the previous state $s_{l-1} = s'$ and the present state $s_k = s$ are known in the trellis. Thus (2.10) becomes

$$L(u_l \mid \mathbf{y}) = \left(\frac{\sum_{S^+} P_r(s_{k-1} = s', s_k = s, \mathbf{y})}{\sum_{S^-} P_r(s_{k-1} = s', s_k = s, \mathbf{y})} \right) \tag{2.11}$$

Transition from the previous state $s_{k-1} = s'$ to the present state $s_k = s$ can occur if the input bit $u_l = +1$, given as

$$(s', s) \Rightarrow u_l = +1 \tag{2.12}$$

while this can also occur when the input bit $u_l = -1$ given as

$$(s', s) \Rightarrow u_l = -1 \tag{2.13}$$

Using (2.12) and (2.13) above, we can express $P_r(s_{k-1} = s', s_k = s, \mathbf{y})$ in (2.11) as:

University of Cape Town

$$P_r(s_{l-1}=s', s_l=s, \mathbf{y}) = P_r(s', s, \mathbf{y}) = P_r(s', s, \mathbf{y}_{l-1}, \mathbf{y}_l, \mathbf{y}_{l+1}) \tag{2.14}$$

If we use Baye's rule in (2.14) and assume that the channel is memoryless, then the future received sequence $\mathbf{y}_{l+1}$ will only depend on the present state s and not on the previous state s' or the present and previous received channel sequences $\mathbf{y}_l$ and $\mathbf{y}_{l-1}$, thus equation (2.14) becomes:

$$\begin{aligned} P_r(s', s, \mathbf{y}) &= P_r(s', s, \mathbf{y}_{l-1}, \mathbf{y}_l, \mathbf{y}_{l+1}) \\ &= P_r(\mathbf{y}_{l+1} \mid s) P_r(s', s, \mathbf{y}_{l-1}, \mathbf{y}_l) \\ &= P_r(\mathbf{y}_{l+1} \mid s) P_r(\mathbf{y}_l, s \mid s') P_r(s', \mathbf{y}_{l-1}) \\ &= \beta_l(s) \gamma_l(s', s) \alpha_{l-1}(s') \end{aligned} \tag{2.15}$$

The above equation can be split into three terms:

$$\alpha_{l-1}(s') = P_r(s_{l-1}=s', \mathbf{y}_{l-1}) \tag{2.16}$$

Where (2.16) is the probability that the trellis is in state s' at time *l-1* and the received channel sequence up to this point is $\mathbf{y}_{l-1}$.

$$\beta_l(s) = P_r(\mathbf{y}_{l+1} \mid s_k = s) \tag{2.17}$$

Where (2.17) is the probability that the trellis is in state s at time l and the future received channel sequence will be $\mathbf{y}_{l+1}$.

$$\begin{aligned} \gamma_l(s', s) &= P_r(s_l = s, \mathbf{y}_l \mid s_{l-1} = s') \\ &= P_r\left(s_l = s \mid s_{l-1} = s'\right) P_r\left(\mathbf{y}_l \mid s_l = s, s_{l-1} = s'\right) \\ &= P_r\left(s \mid s'\right) P_r\left(\mathbf{y}_l \mid s', s\right) \end{aligned} \tag{2.18}$$

Where (2.18) is the probability that given the trellis was in state s' at time *l-1*, it moves to state s and the received channel sequence for this transition is $\mathbf{y}_l$.

The above definitions, transform Equation (2.11) into:

$$L(u_l \mid \mathbf{y}) = \left(\frac{\sum_{S^+} \alpha_{l-1}(s') \gamma_l(s', s) \beta_l(s)}{\sum_{S^-} \alpha_{l-1}(s') \gamma_l(s', s) \beta_l(s)} \right) \tag{2.19}$$

University of Cape Town

Definitions

The Forward Recursive Calculation of the $\alpha_l(s)$ values

$\alpha_l(s)$ is called the forward state metric, calculated as:

$$\alpha_l(s) = \sum_{all\,S'} \alpha_{l-1}(s')\gamma_l(s',s) \tag{2.20}$$

The values of $\alpha_l(s)$ are calculated recursively as soon as $\gamma_l(s',s)$ values are known. If we assume a trellis initial state $s_0 = 0$, the initial conditions are:

$$\begin{aligned} \alpha_0(s_0 = 0) &= 1 \\ \alpha_0(s_0 \neq 0) &= 0 \end{aligned} \tag{2.21}$$

The Backward Recursive Calculation of the $\beta_l(s)$ values

$\beta_l(s)$ is called the reverse state metric

$$\beta_{l-1}(s') = \sum_{all\,S} \beta_l(s)\gamma_l(s',s) \tag{2.22}$$

Once the values of $\gamma_l(s',s)$ are known, a backward recursion can be used to calculate the values of $\beta_{l-1}(s')$ from the values of $\beta_l(s)$ with the initial values:

$$\begin{aligned} \beta_L(s_0 = 0) &= 1 \\ \beta_L(s_0 \neq 0) &= 0 \end{aligned} \tag{2.23}$$

The Branch Metric Calculation

γ_l is called the branch metric. It is calculated from the received channel sequence and any *a-priori* information that is available. Since the event u_l corresponds to the event $s' \rightarrow s$, we can represent equation (2.18) as

$$\gamma_l(s',s) = P_r(u_l)P_r(\mathbf{y}_l \mid u_l) \tag{2.24}$$

It is observed from [7] that $P_r(u_l)$ and $P_r(\mathbf{y}_l \mid u_l)$ can be represented by

$$P_r(u_l) = A_l \exp\left(u_l L^e(u_l)/2\right) \tag{2.25}$$

and

University of Cape Town

$$P_r(\mathbf{y}_l \mid y_l) = B_l \exp\left(\frac{y_l^s u_l + y_l^p d_l^p}{\sigma^2}\right) \tag{2.26}$$

Where the extrinsic LLR of u_l is

$$L^e(u_l) = \frac{P_r(u_l = +1)}{P_r(u_l = -1)} \tag{2.27}$$

and A_l and B_l are normalization constants that will cancel when $\gamma_l(s', s)$ is substituted into equation (2.19) since it appears in both in the numerator (where $u_l = +1$) and the denominator (where $u_l = -1$). Substituting equations (2.25) and (2.26) into (2.24) we obtain

$$\gamma_l(s', s) = \exp\left[\frac{1}{2} u_l \left(L^e[u_l] + L_c y_l^s\right)\right] \bullet \gamma_l^e(s', s) \tag{2.28}$$

Where the channel reliability measure is given by $L_c = \frac{4E_c}{N_0}$ and $E_c = rE_b$ is the energy per channel bit and

$$\gamma_l^e(s', s) = \exp\left(\frac{1}{2} L_c y_l^p d_l^p\right) \tag{2.29}$$

Where y_l^p, d_l^p represent the received and transmitted parity bit, respectively.

The above metrics are written using the modified BCJR-MAP algorithm [6] with the modified probabilities defined as:

$$\tilde{\alpha}_l(s) = \frac{\sum_{S'} \tilde{\alpha}_{l-1}(s')\gamma_l(s', s)}{\sum_{S}\sum_{S'} \tilde{\alpha}_{l-1}(s')\gamma_l(s', s)} \tag{2.30}$$

$$\tilde{\beta}_{k-1}(s') = \frac{\sum_{S} \tilde{\beta}_k(s)\gamma_l(s', s)}{\sum_{S}\sum_{S'} \tilde{\alpha}_{l-1}(s')\gamma_l(s', s)} \tag{2.31}$$

By substituting the results of equations (2.30) and(2.31), into equation (2.19) giving the a-posteriori[1] LLR $L(u_l \mid \mathbf{y})$ calculated with the BCJR-MAP algorithm as:

University of Cape Town

$$L(u_l \mid \mathbf{y}) = \left(\frac{\sum_{S^+} \tilde{\alpha}_{l-1}(s')\gamma_l(s',s)\tilde{\beta}_l(s)}{\sum_{S^-} \tilde{\alpha}_{l-1}(s')\gamma_l(s',s)\tilde{\beta}_l(s)} \right) \tag{2.32}$$

2.4.1.2 Soft-Input Soft-Output MAP Decoder

The MAP algorithm provides not only the estimated bit sequence, but also the probability for each bit that it has been decoded correctly.

The a-posteriori[1] LLR $L(u_l \mid \mathbf{y})$ calculated with the MAP algorithm can be thought of as comprising of three terms, $L_c y_l^s$, $L(u_l)$ and $L^e(u_l)$

$$L(u_l \mid \mathbf{y}) = L_c y_l^s + L(u_l) + L^e(u_l) \tag{2.33}$$

Where

$$L^e(u_l) = \log \left(\frac{\sum_{S^+} \tilde{\alpha}_{l-1}(s')\gamma^e{}_l(s',s)\tilde{\beta}_l(s)}{\sum_{S^-} \tilde{\alpha}_{l-1}(s')\gamma^e{}_l(s',s)\tilde{\beta}_l(s)} \right) \tag{2.34}$$

The first term, $L_c y_l^s$ is the soft channel output for the systematic bit that was directly transmitted across the channel and received as y_l. The second term, $L(u_l)$ represents any a-priori[2] information about u_l provided by a previous decoder. In the case of an iterative turbo decoder, each component decoder provides the other decoder(s) with an estimate of the a-priori LLR $L(u_l)$.

[1] The a-posteriori information about a bit is the information that the decoder gives taking into account all available sources of information about u_l. It is the *a-posteriori* LLR, $L(u_l \mid \mathbf{y})$ that the MAP algorithm gives as its output.

[2] The *a-priori* information about a bit is information available, before decoding starts, from a source other than the received sequence.

University of Cape Town

The channel values y_l are received, and they and the a-priori LLRs $L(u_l)$ are used to calculate $\gamma_l(s',s)$ using equations (2.28) and (2.29). As the channel values y_l are received and the branch matrices $\gamma_l(s',s)$ are calculated, the forward state metrics $\alpha_l(s)$ are calculated using Equation (2.30). Once all channel values of y_l have been received and $\gamma_l(s',s)$ calculated for all bits, then the reverse state metric $\beta_{l-1}(s')$ is calculated using equation (2.31). With all values of $\gamma_l(s',s)$, $\alpha_l(s)$ and $\beta_{l-1}(s')$ calculated, then equation (2.32) is used to calculate the values of $L(u_l|\mathbf{y})$.

2.4.1.3 Iterative Algorithm

Notation

$L_{11}(u_l|\mathbf{y})$, the subscript 11 indicates that this is the a-priori LLR in the first iteration from the first component decoder

$L_{12}(u_l|\mathbf{y})$, is the extrinsic information from the first iteration from the second component decoder

$L_{21}(u_l|\mathbf{y})$, is the extrinsic information from the second iteration passed from the first component decoder to the second component decoder

$L_{22}(u_l|\mathbf{y})$, is the extrinsic information from the second iteration passed from the second component decoder.

Figure 2.8 shows the structure of the iterative (turbo) decoder which uses two MAP decoders, where $D1$ and $D2$ represent component decoder 1 and component decoder 2 respectively.

University of Cape Town

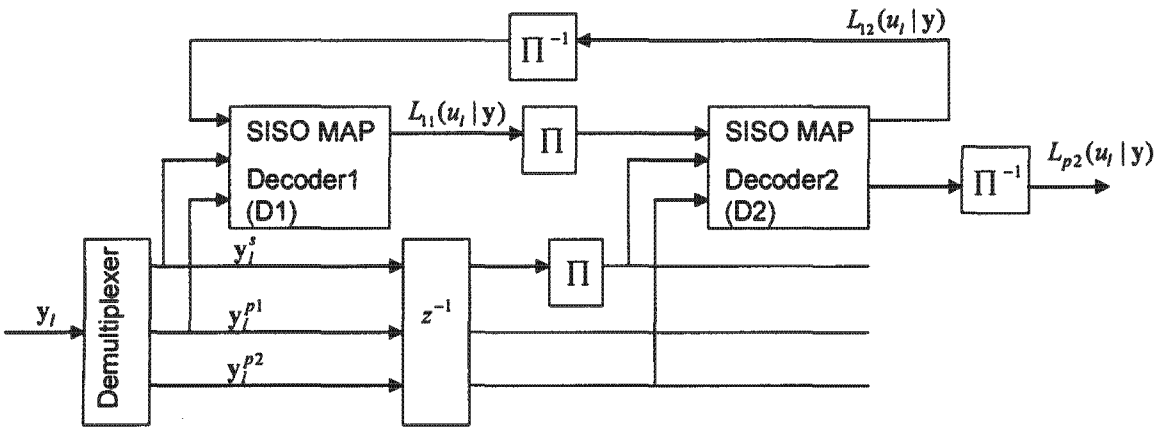

Figure 2.8: *Structure of a Turbo Decoder*

2.4.1.3.1 First Iteration

D1 receives the channel sequence $\mathbf{y}_1$ containing the received versions of the transmitted bits $L_c y_1^{ls}$, and the parity bits $L_c y_1^{p1}$ from RSC1(in case this bit has been punctured, the turbo decoder must insert dummy bits – zeros, in the soft channel output $L_c y_1^{p1}$).

D1 then processes the soft channel inputs and produces its estimate $L_{11}(u_l \mid \mathbf{y})$ of the conditional LLRs of the data bits. In the first iteration D1 will have no a-priori information about the bits, hence $P_r(u_l)$ in $\gamma_l(s', s)$ will be 0.5.

D2 receives the channel sequence $\mathbf{y}_2$, and uses the conditional LLR $L_{11}(u_l \mid \mathbf{y})$ provided by D1 to generate a-priori LLRs $L(u_l)$. Here the a-priori LLRs $L(u_l)$ are derived by interleaving the extrinsic LLRs $L^e(u_l)$ of D1 to produce D2's a-posteriori LLRs $L_{12}(u_l \mid \mathbf{y})$.

This is the last step done on the first iteration.

2.4.1.3.2 Second Iteration

D1 processes its received channel sequence $\mathbf{y}_1$, but now it also has a-priori LLRs $L(u_l)$ provided by the extrinsic portion $L^e(u_l)$ of the a-posteriori LLRs

University of Cape Town

$L_{12}(u_l \mid \mathbf{y})$ calculated by D2.

D1 can now produce an improved a-posteriori LLR $L_{21}(u_l \mid \mathbf{y})$. D2 processes its received channel sequence $\mathbf{y}_2$, and uses the improved a-posteriori LLRs $L_{21}(u_l \mid \mathbf{y})$ from the first decoder to derive improved a-priori LLRs $L(u_l)$. D2 now produces an improved a-posteriori LLR $L_{22}(u_l \mid \mathbf{y})$.

The iterative process is repeated until the desired number of iterations have been reached (we assume p iterations). At the end of the pth decoding iteration, the output from the turbo decoder is given by the de-interleaved a-posteriori LLRs of D2, $L_{p2}(u_l \mid \mathbf{y})$.

2.4.1.4 Data Estimation

Decision Devices (DDs) are used to convert the LLRs of the decoded data in such a way that they approximate the encoded data. These decision techniques can be classified either as hard decision or soft decision devices.

A hard decision is usually taken in conventional methods, this means that, for BPSK, any LLR above 0 will be converted to 1 and any LLR below 0 will be converted to -1.

$$\hat{u}_l = \begin{cases} 1 \ \textit{if} \ L_{p2}(u_l \mid \mathbf{y}) > 0 \\ -1 \ \textit{otherwise} \end{cases} \tag{2.35}$$

The sign of these a-posteriori LLRs gives the hard decision output, that is, whether the decoder believes that the transmitted bit u_l was +1 or -1 and the magnitude of these LLRs gives the confidence the decoder has in its decision.

University of Cape Town

This decision device is shown in Figure 2.9.

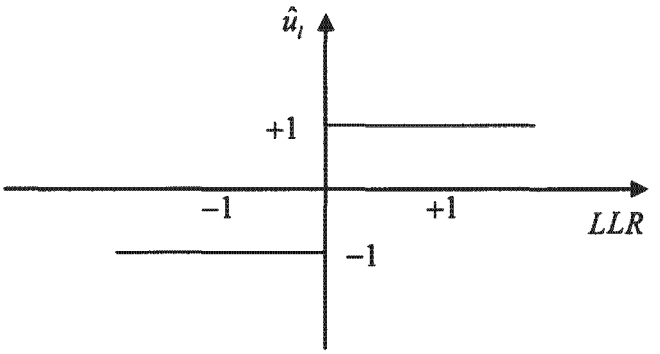

Figure 2.9: *Hard Limiter*

It is clear from Figure 2.9 that the Hard Decision Device (HDD) discards the reliability of the information given by the LLR of the data. Making an incorrect decision, leads to an erroneous value and error propagation might result.

Instead of hard decisions, soft decision techniques can be used to estimate the data. Among the soft decisions possible are the linear, null-zone, the unit clipper, and the hyperbolic tangent decision. These are all shown in Figure 2.10. These Soft Decision Devices (SDDs) give reliable data values between 1 and -1 and an unreliable bit leads to a value close to 0. This gives an advantage over the HDD as this unreliable bit is more helpful in reducing the error propagation due to an erroneous decision.

University of Cape Town

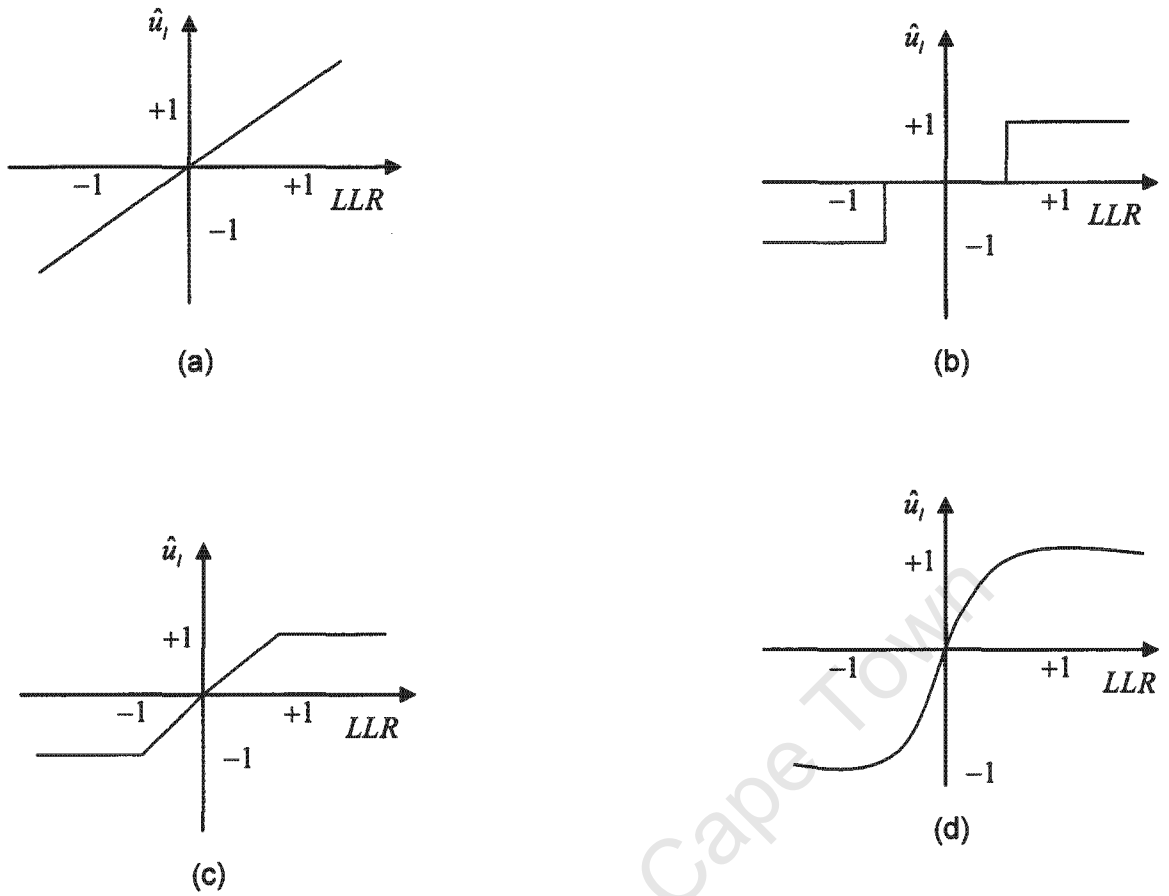

Figure 2.10: *Tentative decision devices. (a) Linear. (b) Null zone. (c) Unit clipper. (d) Hyperbolic tangent*

Soft decision techniques such as the linear decision [8] produce no error propagation but still cannot significantly reduce the MAI effect in CDMA system. In order to achieve the combined advantage of both hard and soft decision functions, hybrid functions have been proposed. These include the unit clipper [9], null-zone and hyperbolic tangent decision algorithms shown in Figure 2.10.

In [10] it is observed that the null zone device provides slightly better performance than the hard decision device but is still inferior to the hyperbolic tangent device. Due to its superior performance, the hyperbolic tangent function as derived in [11] is used for soft decisions throughout this thesis.

University of Cape Town

We derive the hyperbolic tangent device threshold as follows [11]. The generalized form of the LLR of the kth user's lth symbol $u_k^l = \alpha\left[u_k^l\right]$ is given by:

$$\alpha_k^l = L\left(\alpha\left[u_k^l\right]\right) = \ln\left(\frac{P_r\left(u_k^l = +1\right)}{P_r\left(u_k^l = -1\right)}\right) \tag{2.36}$$

with

$$P_r\left(u_k^l = +1\right) + P_r\left(u_k^l = -1\right) = 1 \tag{2.37}$$

becomes:

$$P_r\left(u_k^l = +1\right) = \frac{\exp\left(\alpha\left[u_k^l\right]\right)}{1+\exp\left(\alpha\left[u_k^l\right]\right)} \tag{2.38}$$

and

$$P_r\left(u_k^l = -1\right) = \frac{\exp\left(-\alpha\left[u_k^l\right]\right)}{1+\exp\left(-\alpha\left[u_k^l\right]\right)} \tag{2.39}$$

By defining $\bar{u} \in \{+1, -1\}$ we write both equations (2.38) and (2.39) in one expression as:

$$\begin{aligned} P_r\left(u_k^l = \bar{u}\right) &= \frac{\exp\left(\bar{u}\alpha\left[u_k^l\right]\right)}{1+\exp\left(\bar{u}\alpha\left[u_k^l\right]\right)} \\ &= \frac{\exp\left(\frac{1}{2}\bar{u}\alpha\left[u_k^l\right]\right)}{\exp\left(-\frac{1}{2}\bar{u}\alpha\left[u_k^l\right]\right)+\exp\left(\frac{1}{2}\bar{u}\alpha\left[u_k^l\right]\right)} \\ &= \frac{\cosh\left(\frac{1}{2}\bar{u}\alpha\left[u_k^l\right]\right)\left(1+\bar{u}\tanh\left(\frac{1}{2}\bar{u}\alpha\left[u_k^l\right]\right)\right)}{2\cosh\left(\frac{1}{2}\bar{u}\alpha\left[u_k^l\right]\right)} \\ &= \frac{1}{2}\left(1+\bar{u}\tanh\left(\frac{1}{2}\bar{u}\alpha\left[u_k^l\right]\right)\right) \end{aligned} \tag{2.40}$$

Then the soft estimates of the symbol $d_k[l]$ can be given as [12]:

University of Cape Town

$$\tilde{d}_k^l = \sum_{\bar{u}\in\{+1,-1\}} \bar{u} P_r\left(u_k^l\right)$$
$$= \sum_{\bar{u}\in\{+1,-1\}} \frac{\bar{u}}{2}\left(1+\tanh\left(\frac{1}{2}\alpha\left[u_k^l\right]\right)\right) \tag{2.41}$$
$$= \tanh\left(\frac{1}{2}\alpha\left[u_k^l\right]\right)$$

This hyperbolic tangent threshold is shown in Figure 2.10.

2.4.1.5 Modified Turbo Decoder

As seen in equation (2.35) above, the outputs of the turbo decoding process are the LLR values of the users' information data. This means that the knowledge gleaned from the parity bits is discarded. For iterative decoding, as will be discussed in section 3.5.2, we however pay close attention to both the systematic and parity bits since these are vital in the accurate reconstruction of the interference.

We thus calculate the LLRs of both information and parity bits as:

$$\alpha_l^s = L\left(u_l^s\right) = L_c y_l^s + L_{p1}^e\left(u_l^s\right) + L_{p2}^e\left(u_l^s\right) \tag{2.42}$$

and

$$\alpha_l^{p1} = \left(u_l^{p1}\right) = L_c y_l^{p1} + L_{p1}^e\left(u_l^{p1}\right) + L_{p2}^e\left(u_l^{p1}\right) \tag{2.43}$$

$$\alpha_l^{p2} = \left(u_l^{p2}\right) = L_c y_l^{p2} + L_{p1}^e\left(u_l^{p2}\right) + L_{p2}^e\left(u_l^{p2}\right) \tag{2.44}$$

respectively, where in equations (2.42), (2.43) and (2.44) the first term is called the channel value of the bit, the second term is the a priori information about the bit provided by D1, and the third term represents extrinsic information for the bit.

University of Cape Town

2.5 Numerical Results on the Performance of Turbo Codes

In this section, the performance of a turbo coded single user system transmitting through both AWGN and Rayleigh fading channels is evaluated through Monte Carlo simulation techniques. The component encoder used in all simulations in this section is the RSC encoder with generator polynomial $(7,5)_{octal}$ and code rate $r = 1/3$. The user input frame is $L_{in} = 1024$ and the BER per SNR is computed after each decoding step.

The performance results are given in Figure 2.11 for an AWGN channel and in Figure 2.12 for a Rayleigh flat fading channel. Also presented are the results for an uncoded single-user CDMA system for both AWGN and Rayleigh fading channels.

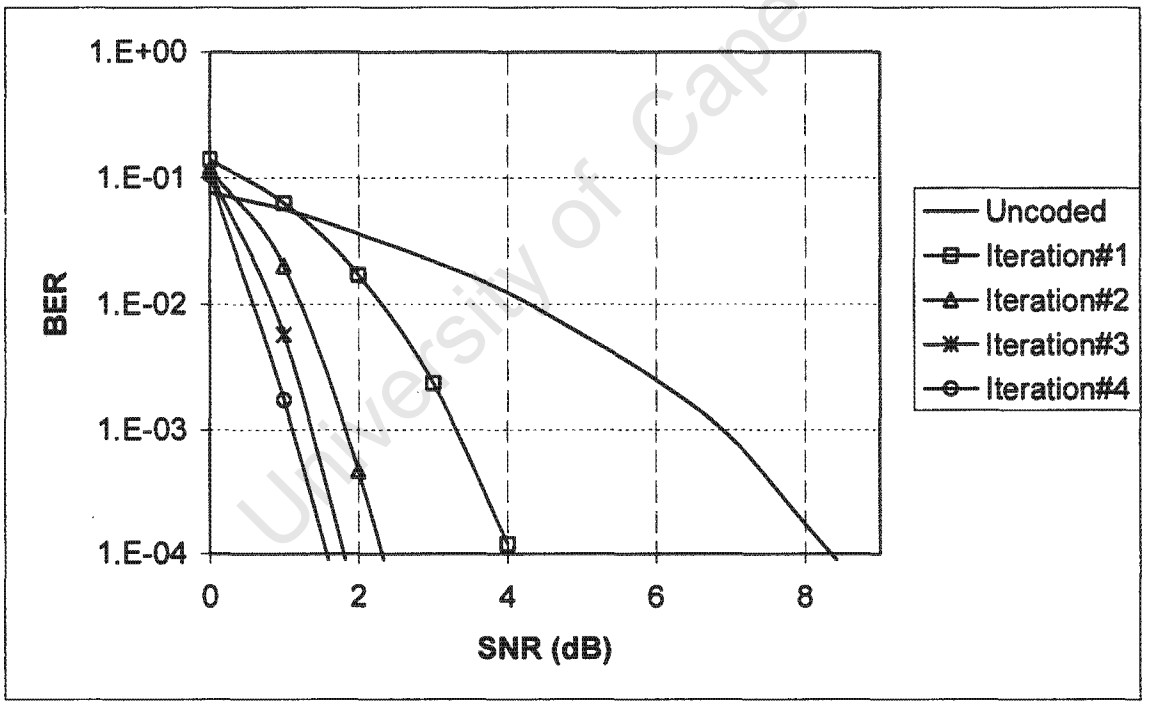

Figure 2.11: *Single user BER Turbo-coded performance as a function of SNR and multiple iterations for an AWGN channel*

University of Cape Town

In Figure 2.11 we observe a performance improvement as the number of decoder iterations increases. This improvement with increased number of iterations has, however, been observed to follow the law of diminishing returns. An approximate fourfold coding gain is achieved between the uncoded and first decoder iteration performance for a BER threshold of 10^{-3} while four decoder iterations have an approximate 3dB gain over a single decoder iteration for the same performance threshold.

Figure 2.12 demonstrates a 3dB loss on the Rayleigh fading fourth decoder iteration to the equivalent AWGN channel performance. This loss in performance can be attributed to the distortions and disturbances inherent in wireless communication channels.

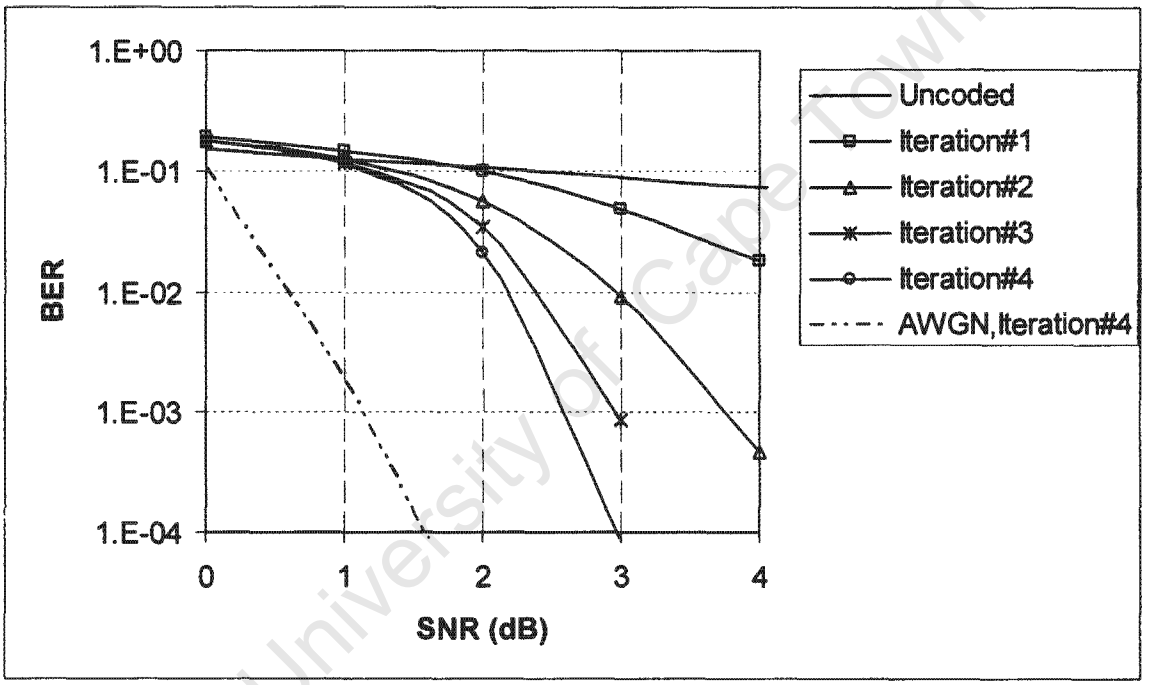

University of Cape Town

Figure 2.12: *Single user BER Turbo-coded performance as a function of SNR and multiple iterations for a flat fading channel*

Turbo codes are seen to be a realistic means of power efficient FEC codes in wireless communications due to their outstanding performance at low SNR values.

2.6 Summary

In this chapter we introduced Turbo codes, a fundamental class of FEC codes used in this thesis. The MAP decoding technique is introduced and its algorithm is explained. Moreover a modified decoding algorithm that is used in later chapters in this work was also introduced. The introduction of Turbo codes on a Digital Communication System (DCS) is shown, through simulations, to provide a considerable coding gain over an uncoded DCS. This coding gain can be further improved by increasing the number of decoding iterations.

Data estimation techniques such as hard and soft decision devices used in the decoding process and in subsequent chapters are introduced. Furthermore the Rayleigh fading wireless communication channel was also introduced. Simulations are used to demonstrate the signal degradation in wireless communications due to the propagation channel. It is seen that in systems where there are no diversity schemes employed, Rayleigh fading channels can pose serious problems during a deep fade as this can result in a received signal that is below the background noise level, making communication unreliable.

University of Cape Town

Chapter 3
Turbo Multi-user Detection in AWGN CDMA Systems

Contents

Objective: To introduce the turbo multi-user detection principle.

We start by introducing, in section 3.1, the Single-Input Single-Output (SISO) AWGN CDMA system used throughout this chapter. The conventional match filtering technique is reviewed in Section 3.2. In section 3.3 through 3.4 we review multi-user detection methods that are used in combating the MAI that limits the capacity of a CDMA communication system.

In section 3.5 we introduce the turbo decoding structure. Since this structure involves the concatenation and iterative exchange of information between the MUD (in sections 3.3 and 3.4) and turbo decoder (in chapter 2), we call this structure the Turbo multi-user detector. Section 3.6 summarizes this chapter.

University of Cape Town

3.1 Introduction

In this chapter we consider the system introduced in Section 2.1, where all K users transmit using symbol synchronous CDMA over an additive white Gaussian noise (AWGN) channel, then the waveform $s_k(t)$,given by (2.5), is said to arrive at the common receiver in an attenuated form.

Due to the assumption that all K users transmit simultaneously over the AWGN channel, the received signal at the receiver, is a continuous time waveform, expressed as

$$r(t)=\sum_{k=1}^{K}s_k(t)+n(t) \tag{3.1}$$

Where the first term is the multiple access signal coming from K independent users and $n(t)$ is a zero mean additive Gaussian noise with a two-sided power spectral density of $\sigma^2 = N_0/2$.

Equation (3.1) can be better shown by expressing $r(t)$ explicitly for each symbol interval i as

$$r_i(t)=\sum_{k=1}^{K}s_{k,i}(t)+n_i(t) \tag{3.2}$$

and substituting (2.5) into (3.1) we obtain

$$r_i(t)=\sum_{k=1}^{K}\sqrt{E_{k,i}}\sum_{j=0}^{N-1}d_{k,j}\left[c_{k,j}\right]_j\psi(t-jT_c)+n_i(t) \tag{3.3}$$

From the chip view point, the signal $r_i(t)$ is a continuous signal. By performing chip waveform matched filtering (for all $0 \le j \le N-1$ chip intervals), followed by sampling at the chip rate T_c, the waveform can be made discrete.

The discrete-time received signal can be expressed in matrix notation as

$$\mathbf{r}=\mathbf{CPd}+\mathbf{n} \tag{3.4}$$

$$\mathbf{r}=\left[r[1],r[2],\cdots,r[N]\right]^T \tag{3.5}$$

Where the channel matrix $\mathbf{C}$ is a $N\times K$ matrix containing all K spreading codes utilized and is defined as

University of Cape Town

$$\mathbf{C} = \begin{pmatrix} c_{1,1} & c_{2,1} & \cdots & c_{K,1} \\ c_{1,2} & c_{2,2} & \cdots & c_{K,2} \\ \vdots & \vdots & \vdots & \vdots \\ c_{1,N} & c_{2,N} & \cdots & c_{K,N} \end{pmatrix} \tag{3.6}$$

$\mathbf{P}$ is a K by K diagonal matrix containing the received signal amplitude (B_k or $\sqrt{E_k}$ or $\sqrt{2P_k}$) and is defined as

$$\mathbf{P} = diag\left[P_1, P_2, \cdots, P_K\right]^T = \begin{bmatrix} \sqrt{E_1} & 0 & \cdots & 0 \\ 0 & \sqrt{E_2} & \cdots & \vdots \\ \vdots & 0 & \ddots & 0 \\ 0 & 0 & \cdots & \sqrt{E_K} \end{bmatrix} \tag{3.7}$$

$\mathbf{d}$ is a K-vector that holds the data for all users, given by

$$\mathbf{d} = \left[d_1, d_2, \cdots, d_K\right]^T \tag{3.8}$$

while $\mathbf{n}$ is an N-vector that holds the filtered samples of the noise and is expressed as

$$\mathbf{n} = \left[n[1], n[2], \cdots, n[N]\right]^T \tag{3.9}$$

University of Cape Town

3.2 Matched Filter

The common receiver needs to be able to distinguish each user's data. Due to the fact that each user is assigned a unique spreading code, this unique code can thus be used by the receiver to demodulate the user of interest's signal. However, orthogonality is almost impossible to achieve in DS-CDMA spreading codes, this correlation in spreading codes leads to the increase of the level of interference.

Throughout this thesis we assume that the receiver has perfect knowledge of all the spreading sequences. Furthermore all spreading sequences used are Pseudo-Noise (PN) sequences, and each element of $a_{k,j}$ is chosen independently and identically distributed (*i.i.d.*) according to some distribution.

The conventional detector for the received signal $\mathbf{r}$ consists of a bank of K correlators or matched filters. This is the simplest approach to demodulating the CDMA signals and the structure is illustrated in Figure 3.1 below.

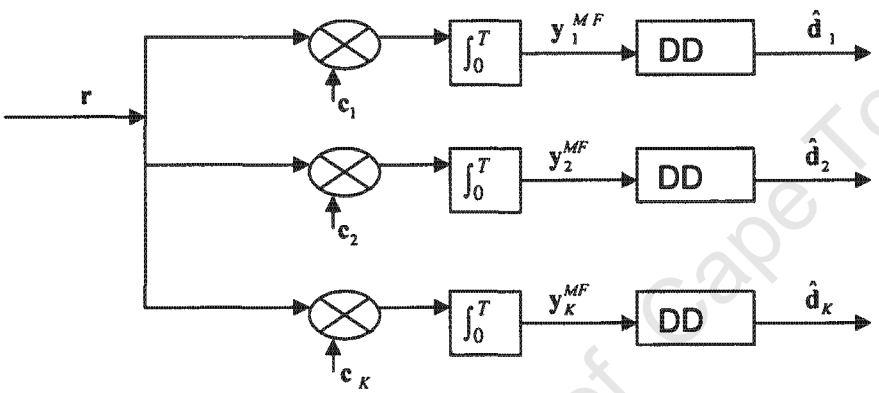

Figure 3.1: *Matched Filter Structure for CDMA Systems*

Each of the K matched filters regenerates the unique spreading code assigned (at transmission) to that user. This regenerated code is then correlated with the received signal $r(t)$ whose output is sampled at every bit interval, thus giving a soft estimate of the transmitted data, given as

$$y_k^{MF} = \frac{1}{T_b}\int^{T_b} c_k(t)\,r(t)\,dt \qquad (3.10)$$

Upon substituting (2.5) and (3.1) into (3.10), the transmitted data can be expressed as

University of Cape Town

$$y_k^{MF} = \sqrt{E_k} d_k + \sum_{j \neq k}^{K} \sqrt{E_j} \rho_{jk} d_j + n_k' \tag{3.11}$$

Where

$$n_k' = \frac{1}{T_b} \int^{T_b} c_k(t) n(t) dt \tag{3.12}$$

and

$$\rho_{jk} = \frac{1}{T_b} \int^{T_b} c_k(t) c_j(t) dt \tag{3.13}$$

is the cross-correlation between the *j*th and *k*th user.

Equation (3.11) can be expressed in discrete-time form as

$$\begin{aligned} \mathbf{y}^{MF} &= \mathbf{C}^T \mathbf{r} \\ &= \mathbf{C}^T \mathbf{C} \mathbf{P} \mathbf{d} + \mathbf{C}^T \mathbf{n} \\ &= \mathbf{R} \mathbf{P} \mathbf{d} + \mathbf{z} \end{aligned} \tag{3.14}$$

Where

$$\mathbf{y}^{MF} = \left[y_1^{MF}, y_2^{MF}, \cdots, y_K^{MF} \right]^T \tag{3.15}$$

$$\mathbf{z} = \left[z_1, z_2, \cdots, z_K \right]^T = \mathbf{C}^T \mathbf{n} \tag{3.16}$$

is Gaussian noise correlated by the MF operation, and

$$\mathbf{R} = \mathbf{C}^T \mathbf{C} = \left\{ \rho_{j,k} \right\} \tag{3.17}$$

is a $K \times K$ correlation matrix whose entries are values of the correlation between spreading signatures for all $k, j \in \{1, 2, \ldots, K\}$ users.

By breaking up $\mathbf{R}$ as shown in [13] into two matrices, $\mathbf{R} = \mathbf{I} + \mathbf{Q}$ where $\mathbf{Q}$ is the cross-correlation matrix and $\mathbf{I}$ is the identity matrix, $\mathbf{y}$ becomes

$$\begin{aligned} \mathbf{y}^{MF} &= (\mathbf{Q} + \mathbf{I}) \mathbf{P} \mathbf{d} + \mathbf{z} \\ &= \mathbf{P} \mathbf{d} + \mathbf{Q} \mathbf{P} \mathbf{d} + \mathbf{z} \end{aligned} \tag{3.18}$$

The first term $\mathbf{Pd}$ is the decoupled data weighted by the received amplitudes (i.e. correlation with the *k*th user itself gives rise to the recovered data term). The second term is the MAI introduced in the signal (i.e. correlation with other users gives rise to MAI).

University of Cape Town

The hard decision made by the decision device on the received data can be expressed as

$$\begin{aligned}\hat{d}_k(t) &= \operatorname{sgn}\left\{y_k^{MF}(t)\right\} \\ &= \operatorname{sgn}\left\{\sqrt{E_k}d_k(t)+\sum_{j\neq k}^{K}\sqrt{E_j}\rho_{j,k}d_j(t)+n_k'(t)\right\}\end{aligned} \tag{3.19}$$

As can be seen from (3.19), as the absolute value of the sum of noise and MAI increases so does the probability of making an erroneous decision at the output of the conventional detector. It is obvious that the existence of MAI has a significant impact on the capacity and performance of the conventional detector system and as the number of interfering users increase, so does the amount of MAI increase.

If the user of interest is further to the receiver it undergoes more amplitude attenuation than the signals that are closer to the receiver. This worsens the effective MAI due to the stronger power interfering users, thus overwhelming the desired signal. This is known as the near-far problem. Because of this effect, well-defined power control is essential for proper functioning of CDMA systems. In this work we assume that all users transmit with equal and constant power of $P_k = 1W$.

University of Cape Town

Figure 3.2 shows the uncoded BER performance as a function of the SNR for 1, 5 and 15 users with a processing gain of $N = 15$ chips, over an AWGN channel for a conventional match filtered receiver.

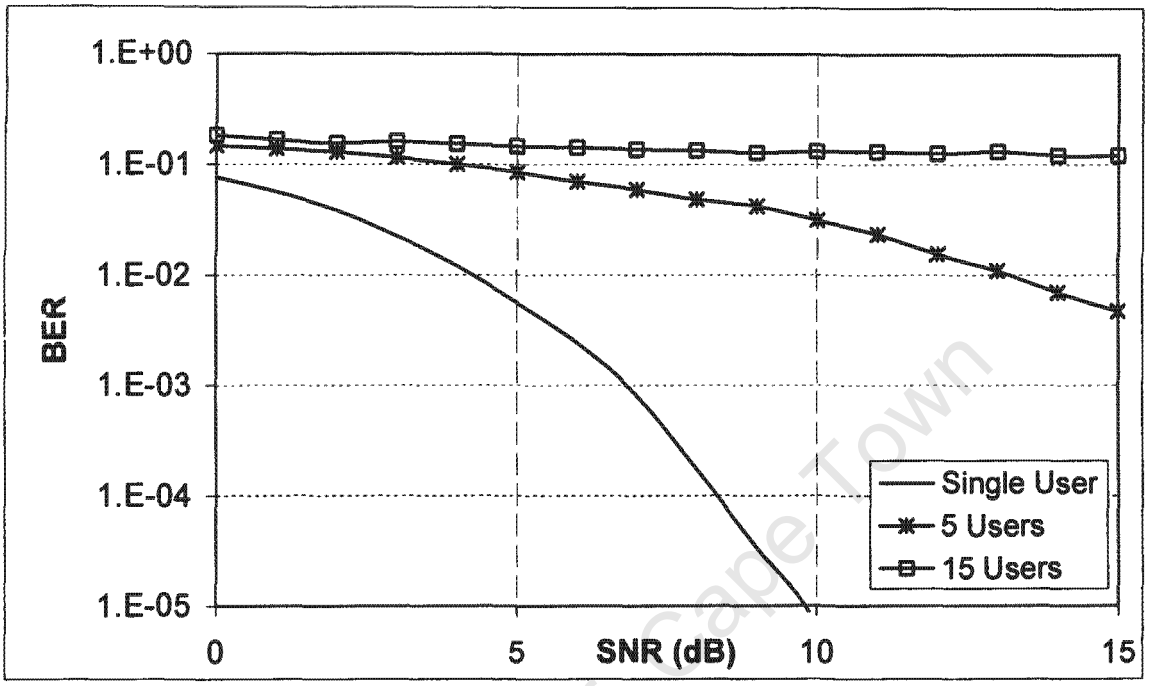

Figure 3.2: *MF receiver performance for an uncoded system over an AWGN channel*

It is observed from Figure 3.2 that as the system load increases the performance of the MF receiver degrades. The fully loaded system with $K = 15$ is seen to reach an error floor of about 10^{-1}, making reliable communications at this level unfeasible.

The system capacity of the conventional CDMA system is mainly limited by interference, thus to increase this system capacity we need to find ways to mitigate the effects of MAI.

University of Cape Town

3.3 Multi-user Detection

The two major limits to the conventional CDMA system were discussed in the preceding section, these are: Firstly, the near-far problem poses a serious problem and tight power control, with attendant complexity, is needed to combat it. We thus assume equal power transmission from all active system users. Secondly, the conventional detector performs as if other users do not exist and ignores the presence of MAI in the received signal. When MUD is employed in a CDMA system it can reduce/eliminate MAI caused by other active users leading to potential increases in capacity. For the sake of simplicity, we assume that there is no inter-cell interference in the work presented in this thesis.

The optimum multi-user detector proposed in [14] that consists of the Maximum Likelihood Sequence Estimator (MLSE) based on the Viterbi decoding algorithm, has shown huge improvement (i.e. a substantial increase in system capacity) over the conventional correlation receiver. Unfortunately as the number of users introduced into the system increase so does its computational complexity. This complexity grows exponentially with the number of active users and constraint length of the code making any practical implementation very prohibitive. This has led to the search for suboptimal MUDs that can achieve a large capacity gain, with lower complexity and less explicit information about the received signals. The Verdu algorithm is normally used as a benchmark against which all sub-optimal schemes are compared.

University of Cape Town

Various suboptimum detectors have been proposed, most of which can be classified into linear multi-user detectors and non-linear multi-user detectors. An overview of different receiver techniques can be found, for example, in [13],[15] and [14].

3.3.1 Linear Multi-user Detectors

Linear multi-user detectors are those multi-user detectors based on linear techniques. A linear transformation is applied to the soft outputs of the conventional detector in order to produce a new set of decision variables with MAI greatly decoupled (or completely decoupled in the decorrelation detectors). A linear MUD is simply a filter that is designed

to attenuate MAI according to a specific criterion. There are two important types of linear MUDs, and they are known as: the Decorrelating detector and the MMSE detector.

3.3.1.1 Decorrelator Detector

The decorrelating receiver attempts to completely eliminate the MAI for all the users. It linearly transforms each vector of matched filter outputs by multiplying it with the inverse of the correlation matrix. This is done by multiplying both sides of (3.14) with $\mathbf{R}^{-1}$ (the inverse of $\mathbf{R}$), to give a decoupled user signal given by:

$$\begin{aligned}\mathbf{y}^{Decor} &= \mathbf{R}^{-1}\mathbf{y}(t) = \mathbf{P}\mathbf{d}(t) + \mathbf{R}^{-1}\mathbf{z}(t) \\ &= \mathbf{P}\mathbf{d}(t) + \mathbf{z}^{Decor}(t)\end{aligned} \tag{3.20}$$

where $\mathbf{z}^{Decor}(t)$ is a noise vector with zero mean and covariance of $\sigma^2\mathbf{R}^{-1}$.

As can be seen from the first term of (3.20), the decorrelator completely decouples the MAI, thus leading to substantial performance gain over the conventional detector. Moreover the decorrelator detector is near-far resistant, and has a suboptimum performance and more importantly its complexity increases linearly with the number of users. This detector, however, has its drawback. As can be seen on the last term, the detector causes noise enhancement and this noise term, $\mathbf{R}^{-1}\mathbf{z}(t)$, is always greater or equal to the noise term at the output of the conventional detector.

The decorrelating receiver tries to completely remove MAI and this often results in unacceptable noise enhancements. As the number of active users becomes large and approaches system capacity, the performance starts to degrade, this is due to noise enhancement that results from trying to invert the MAI of a large number of users. For an overloaded system (i.e. $K > N$) the decorrelating algorithm becomes undefined since it becomes impossible to drive the interference to zero.

University of Cape Town

3.3.1.2 Minimum Mean Squared Error (MMSE) Detector

The MMSE detector, as compared to the decorrelator, has far smoother degradation in performance since it balances MAI mitigation with noise enhancement – as loading increases its capacity also decreases asymptotically to zero [14].

The dispread signal (3.18) from the MF is passed into the MMSE detector, as shown in Figure 3.3

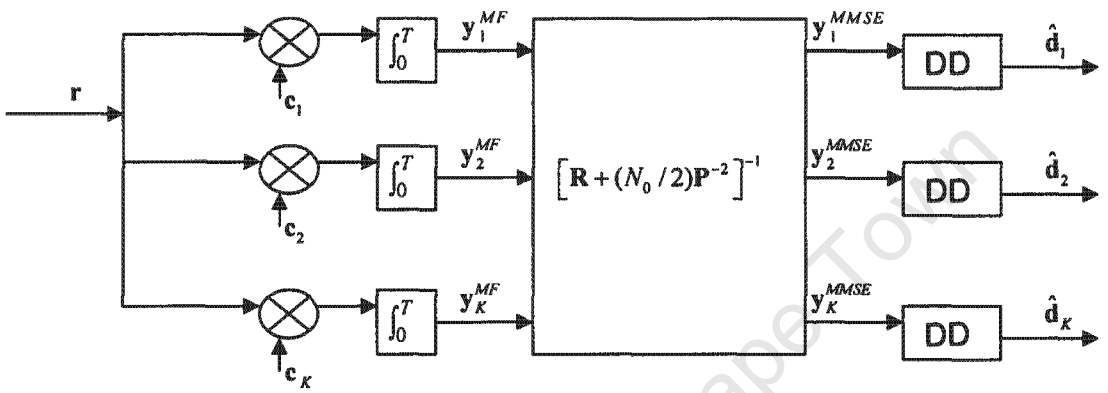

Figure 3.3: *Structure of the MMSE Detector for CDMA Systems*

The MMSE detector utilizes a linear mapping that minimizes the mean-squared error, $E\left[\left|\mathbf{d}-\mathbf{M}_{MMSE}\mathbf{y}^{MF}\right|\right]$, between the actual data $\mathbf{d}$ and the soft output of the conventional detector $\mathbf{y}^{MF}$.

The result of the $K\times K$ matrix $\mathbf{M}_{MMSE}$ that achieves the minimum square-error is given in [14] and [16] as:

$$\mathbf{M}_{MMSE}=\left[\mathbf{R}+\sigma^2\mathbf{P}^{-2}\right]^{-1} \tag{3.21}$$

The soft estimate vector of the MMSE detector is

$$\begin{aligned}\mathbf{y}^{MMSE}&=\mathbf{M}_{MMSE}\mathbf{y}^{MF}\\&=\left[\mathbf{R}+\sigma^2\mathbf{P}^{-2}\right]^{-1}\mathbf{y}^{MF}\end{aligned} \tag{3.22}$$

University of Cape Town

As can be seen in (3.22), the MMSE detector takes into account the background noise, thus giving better performance than the decorrelating detector. Worth noting is that as the background noise in equation (3.22) goes to zero, the MMSE detector converges in performance to the decorrelating detector. On the other hand, if the background noise increases considerably, then the MMSE detector approximates the conventional detector. Due to the fact that the performance of the MMSE detector depends on the powers of the interfering users' signals, it is thus less resistant to the near-far problem, but due to our earlier assumption of equal power users, our system is immune to this problem. The MMSE detector output signal has reduced or suppressed MAI.

3.3.2 Interference Cancellation Schemes

Interference Cancellation (IC) techniques are non-linear and use previously made decisions to reduce the MAI seen by each user. This is achieved by using data estimates to reconstruct the interference which is then subtracted from the received signal. This category of IC schemes can be classified into three sub-categories: Parallel Interference Cancellation (PIC), Successive Interference Cancellation (SIC) and Hybrid Interference Cancellation (HIC) techniques.

3.3.2.1 Successive Interference Cancellation

In SIC, the performance of the system is improved by demodulating and cancelling each user's signal from the strongest to the weakest according to their received signal power. This is done serially, where at each stage only one user's signal is removed from the overall received signal, so that all remaining users see less MAI in the next cancellation stage. This is repeated until all but one user have been demodulated. Removing the strongest user first is advantageous for the remaining users, meaning that the strongest user does not gain any MAI reduction advantages while the weaker users benefit the most in terms of MAI reduction. This single user-single stage serial cancellation introduces an unacceptable delay in the system, meaning that the more users in the system the larger the delay [13].

University of Cape Town

3.3.2.2 Parallel Interference Cancellation

PIC estimates and subtracts out all the MAI for each user in parallel. In this approach, each user's estimates are calculated separately at first, after which the decisions made (assuming hard-decision approach) are used to reconstruct the MAI that is then subtracted from the received signal. Figure 3.4 shows one stage of the multistage PIC detector. As can be seen on Figure 3.4, the initial bit estimates, $\hat{d}_k(t)$, are obtained by taking a decision on the output of the conventional detector, as given by (3.19).

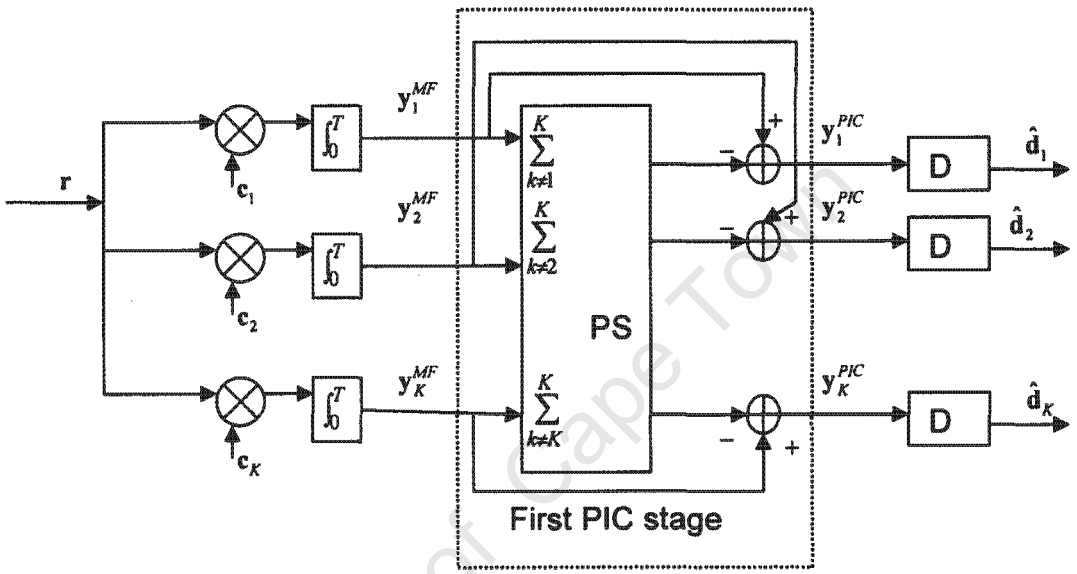

Figure 3.4: *Parallel Interference Cancellation for CDMA Systems*

The bit estimates are scaled by the amplitude estimates and re-spread by the signature codes and added in order to regenerate the MAI estimates for each user. This interference is then cancelled from the received signal, providing an input to the bank of conventional detectors whose output yields a new set of more improved signals, $\mathbf{y}^{PIC,1}$ as the output of the first PIC stage. On the next stage the data estimates of the previous stage are used as input, thus providing a better estimate that can be used to further improve the signal.

The output of the PIC first stage, $\mathbf{y}^{PIC,1}$ can thus be represented as:

$$\mathbf{y}^{PIC,1} = \left[y_1^{PIC,1}, y_2^{PIC,1}, \ldots, y_K^{PIC,1} \right] \tag{3.23}$$

University of Cape Town

where

$$y_k^{PIC,1}(t) = y_k^{MF}(t) - \sum_{j\neq k}^{K} \sqrt{E_j}\rho_{j,k}\hat{d}_j(t)$$
$$= \sqrt{E_k}d_k(t) - \sum_{j\neq k}^{K} \sqrt{E_j}\rho_{j,k}\left[d_j(t) - \hat{d}_j(t)\right] + n_k'(t) \tag{3.24}$$

At the output of the first stage PIC decision device (assuming HDD), we have:

$$\hat{d}_k^{PIC,1}(t) = \text{sgn}\left\{y_k^{PIC,1}(t)\right\}$$
$$= \text{sgn}\left\{\sqrt{E_k}d_k(t) - \sum_{j\neq k}^{K} \sqrt{E_j}\rho_{j,k}\left[d_j(t) - \hat{d}_j(t)\right] + n_k'(t)\right\} \tag{3.25}$$

This iterative process can be repeated for multiple stages (say p stages). Where each stage takes as inputs the data estimates of the previous stage $y_k^{PIC,(p-1)}$ and produces a new set of estimates at its output, $y_k^{PIC,p}$ related by:

$$y_k^{PIC,p}(t) = y_k^{MF}(t) - \sum_{j\neq k}^{K} \sqrt{E_j}\rho_{j,k}\hat{d}_j^{PIC,(p-1)}(t) \tag{3.26}$$

and at the output of the last stage (pth) decision device we have:

$$\hat{d}_k^{PIC,p}(t) = \text{sgn}\left\{y_k^{PIC,p}(t)\right\}$$
$$= \text{sgn}\left\{\sqrt{E_k}d_k(t) - \sum_{j\neq k}^{K} \sqrt{E_j}\rho_{j,k}\left[d_j(t) - \hat{d}_j^{PIC,(p-1)}(t)\right] + n_k'(t)\right\} \tag{3.27}$$

Following the matrix-vector formulation in equation (3.18), the soft output of the pth PIC stage for all transmitted bits and all K users is

$$\hat{\mathbf{d}}^{PIC,p} = \mathbf{y}^{MF} - \mathbf{QP}\hat{\mathbf{d}}^{PIC,(p-1)}$$
$$= \mathbf{Pd} + \mathbf{QP}\left(\mathbf{d} - \hat{\mathbf{d}}^{PIC,(p-1)}\right) + \mathbf{z} \tag{3.28}$$

Where $\mathbf{QP}\hat{\mathbf{d}}^{PIC,(p-1)}$ represents the estimated MAI during the $(p-1)$ PIC stage [13].

University of Cape Town

In Figure 3.5 the BER performance as a function of the number of users for a MF receiver and a PIC detector is shown. These graphs are plotted for a system with no FEC coding and are taken at an SNR value of 9dB with a processing gain of $N = 15$.

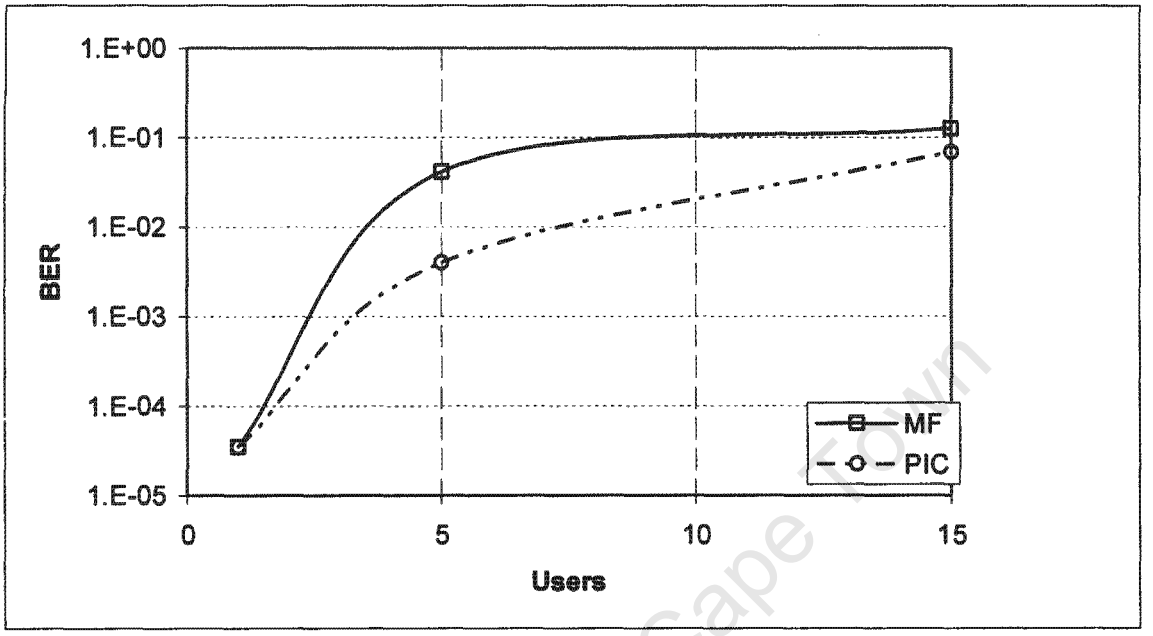

Figure 3.5: *AWGN channel Capacity Performance of the MF receiver and PIC Detector, evaluated at SNR value of 9dB*

The capacity improvements attainable through the use of PIC detectors over the MF receiver are seen to be as much as double for a given BER performance threshold. However, these gains diminish as the system gets heavily loaded and converge towards the MF performance for an overloaded system.

It has been shown [10] that as the estimates from the previous stages improve, the performance of the multistage PIC can also be improved. Although the iterative process can be performed as many times as required it has been seen that the PIC saturates after the third iteration [17]. Moreover if an erroneous decision is made during the iterative process, then the error is propagated leading to a doubling of the final error, oscillation and failure of convergence [10].

University of Cape Town

The oscillatory behaviour described above happens as a result of error propagation. If during the hard decision stage an error is made, then the reconstructed MAI signal will also be in error, resulting in the addition of MAI in equation (3.28) instead of subtraction. This means that the current PIC iteration can become worse than a previous lower order iteration, resulting in oscillations in system performance. This means that the PIC MUD is most effective if correct decisions are made at the decision device, otherwise serious oscillatory behaviour will manifest itself in the detection process.

In [11] several possible measures are suggested to avoid incurring wrong MAI estimates, these are:

i) Firstly we can try and improve the first iteration by employing a linear MUD as a front-end to the PIC detector's first stage. This approach is known as combined detection and is discussed in Section 3.4.

ii) Secondly by using soft decisions rather than hard decisions in all the PIC stages (except the last), helps give reliable estimates that can be fed to the PIC detector. This is the soft decision PIC detection approach. Decision devices or algorithms were discussed in Section 2.4.1.4.

iii) Lastly we can try to improve the data estimates, before they are used to reconstruct the MAI, by using a FEC decoder in each iteration.

University of Cape Town

3.4 Combined Detection

As stated earlier in the previous section, an incorrect or erroneous decision leads to error propagation, which can be avoided by making confident initial decisions. Stabilizing the first stage of PIC detection through the use of a linear MUD as a front-end to the PIC detector's first stage aids in reducing erroneous initial decisions that may lead to this oscillatory behaviour and failure of convergence.

The combined detection schemes combine a linear detection scheme with an interference cancellation technique. These can be classified into: the Zero-Forcing Decision-Feedback

(ZF-DF) detector, decorrelator/PIC, MMSE/PIC, and many others as discussed in [13] and [14].

Since the interference cancellation scheme depends on the linear detector for its initial data estimates, then we need reliable data estimates that will not easily succumb to error propagation.

3.4.1 MMSE-based Parallel Interference Cancellation Detection

Since the MMSE detector balances MAI mitigation with noise enhancement it makes it more attractive, as opposed to the decorrelator, to be used as a linear MUD front-end to the PIC detector's first stage. The MMSE front-end PIC receiver is shown in Figure 3.6

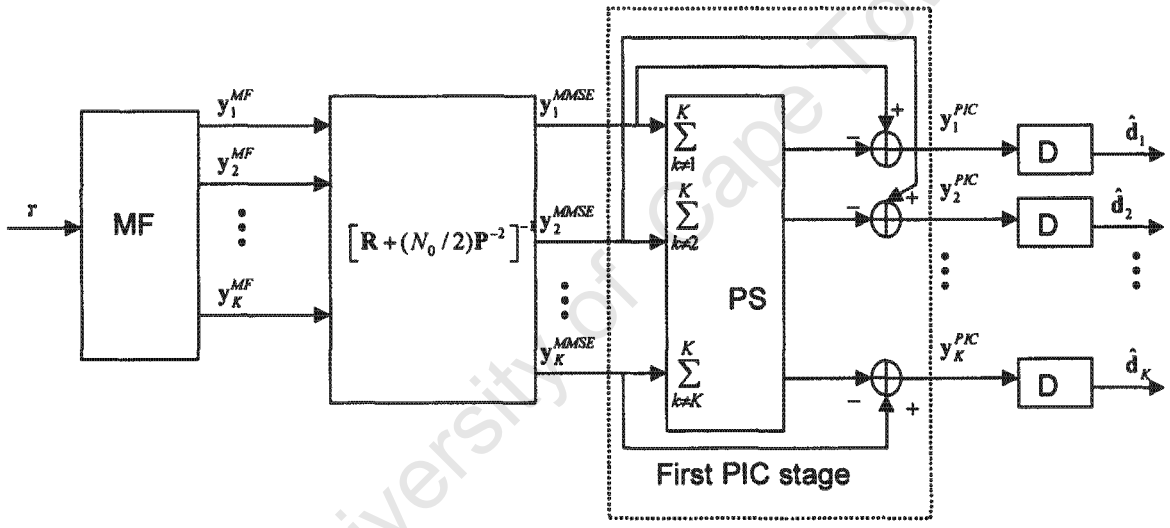

Figure 3.6: *MMSE Front-end PIC Receiver for CDMA Systems*

Recalling Equations (3.14) and (3.22), the PIC detector depicted in Figure 3.6 can be represented in discrete-time form, by rewriting Equation (3.26) as:

$$\mathbf{y}^{PIC} = \mathbf{y}^{MMSE} - \left(\mathbf{R} - diag[\mathbf{R}]\right)\mathbf{A}\tilde{\mathbf{d}} \tag{3.29}$$

Where $\mathbf{y}^{MF}$, $\mathbf{R}$ and $\mathbf{A}$ are given by Equations (3.14), (3.17) and (3.7) and

University of Cape Town

$$diag[\mathbf{R}] = \begin{bmatrix} \rho_{1,1} & 0 & \cdots & 0 \\ 0 & \rho_{2,2} & \cdots & 0 \\ \vdots & \vdots & \vdots & \vdots \\ 0 & 0 & \cdots & \rho_{K,K} \end{bmatrix} \tag{3.30}$$

$$\hat{\mathbf{d}} = \left[\hat{d}_1, \hat{d}_2, \cdots, \hat{d}_K \right]^T \tag{3.31}$$

3.5 Turbo Multi-user Detection

Here the single-input single-output synchronous CDMA uplink AWGN channel system of Figure 2.1 is considered. As demonstrated in previous sections of this work, neither MUD alone nor channel coding techniques can completely eliminate the effects of MAI. Joint detection and decoding in multi-user systems has been an active research area for the past decade. Researchers like [18] have investigated the combined optimum detector [14] and convolutional decoding system performance. Due to the exponential complexity of the receiver in [14], the authors of [18] propose suboptimal MUD with convolution coding in [19]. By integrating a combination of various suboptimal MUDs with iterative channel decoding, the authors of [20] introduce a convolutionaly coded iterative interference canceller. The powerful error correction ability of turbo codes [21] has been combined with interference cancellation in [22] to produce the turbo interference cancellation detection approach. The work of [22] has further been studied in [23], [24] with further work being done by [25] and [26].

The turbo multi-user detection principle follows that of turbo decoding discussed in section 2.4. This involves the joint channel decoding and multi-user detection through the iterative exchange/use of soft information. In [27] multi-user receivers are divided into two classes, namely, the partitioned approach (PA) and the integrated/iterative approach (IA).

University of Cape Town

3.5.1 Partitioned Approach Receiver

In PA the multi-user detector precedes the decoder and does not utilize the decoder output. Decoding is only performed after the last PIC stage, thus the tentative decisions produced by the PIC of each stage treats each user data as if it were not coded. Figure 3.7 shows the partitioned approach turbo PIC MUD. As can be seen in this suboptimal approach, symbol detection and decoding are done separately and there is no exchange of soft information between the bank of turbo decoders and the PIC detector.

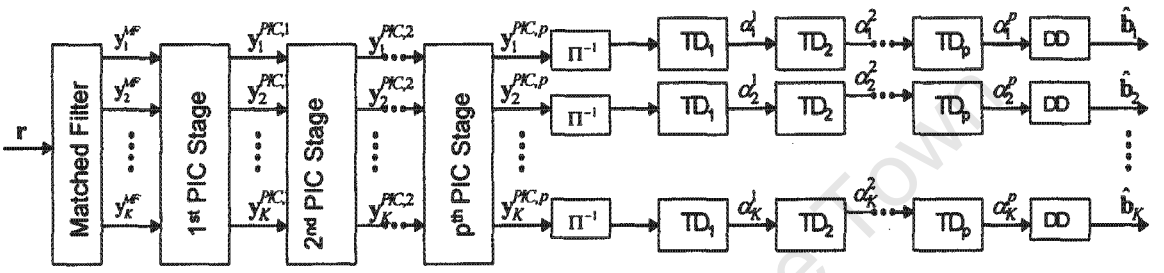

Figure 3.7: *Partitioned Approach Multi-user Receiver for CDMA Systems*

The conventional MF receiver acts as the first stage of the detector, it dispreads the signals, giving, at each MF output $\mathbf{y}^{MF}$ as given by Equation (3.18). The MF output is then fed to the PIC, where p iterative interference cancellation steps are carried out. The output of the pth PIC iteration, $\mathbf{y}^{PIC,P}$ is defined and can be calculated similar to (3.24).

The output soft signal of the last iteration $y_k^{PIC,P}$ is then deinterleaved before it is decoded by the relevant turbo decoder to produce the soft decoded output α_k. The turbo decoder used in this receiver is that discussed in Section 2.4.1 and only yields the LLR value of the information bits. For ease of comparison we assume that the bank of turbo decoders performs p iterations, where p is the same as the number of PIC stages. After the last iteration (pth iteration) a hard decision is then taken on α_k to give an estimate $\hat{b}_k$ of the transmitted symbol.

University of Cape Town

3.5.2 Iterative Approach Receiver

For each iterative detect/decode stage, this structure performs detection and decoding separately and exchanges soft information through an iterative process. The structure of the iterative turbo PIC multi-user detector is shown in Figure 3.8.

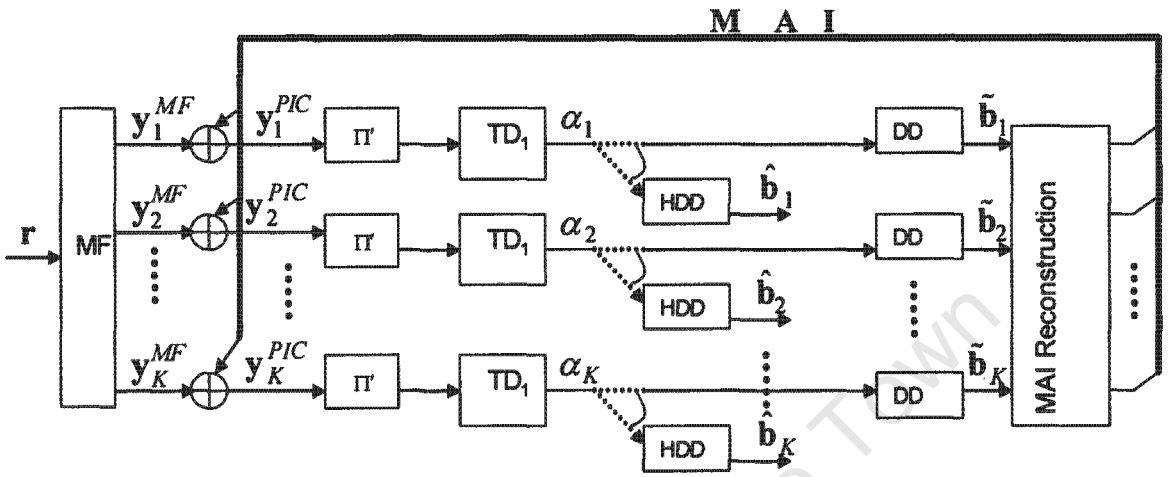

Figure 3.8: *Iterative Approach to Multi-user Detection for CDMA Systems*

The signals are first dispread using a MF and then a single PIC detector stage followed by de-interleaving is performed. This gives a cleaner PIC output signal that is taken as the input to the turbo decoder. The modified decoder of Section 2.4.1.5 is used and it yields the LLR values of both information bits and the parity bits, all which are vital in the reconstruction of the MAI. This iterative process is repeated p times after which a hard decision is taken to estimate the user's input data.

The soft MAP decoding algorithm outputs the a posteriori LLRs of the coded bits based on the soft codeword provided by the PIC detector. In this case we describe the extrinsic information as the information about the coded bits gleaned from the a priori information about user's coded bits based on the trellis structure of the code [28]. This iterative process is repeated for p joint PIC and turbo iterations (as described above) and on the last iteration a hard decision is taken on the soft decoder to give the input data estimate. In the following section we introduce the MMSE front-end PIC detectors for the turbo coded SISO CDMA system.

University of Cape Town

3.5.3 MMSE Front-End Turbo Multi-user Detectors

As stated in earlier sections, an incorrect or erroneous decision can lead to error propagation; this error propagation can be avoided by making confident initial decisions. Stabilizing the first stage of PIC detection through the use of a linear MUD as a front-end to the PIC detector's first stage can aid in reducing erroneous initial decisions that may lead to oscillatory behaviour and failure of convergence.

Since the MMSE detector balances MAI mitigation with noise enhancement it makes it more attractive, as opposed to the decorrelator, to be used as a linear MUD front-end to the PIC detector's first stage. The signal at the receiver is first dispread by the matched filter as discussed in Section 3.2. The match filtered signal is then passed on to the MMSE detector (introduced in Section 3.3.1.2) which suppresses the MAI, resulting in a cleaner signal.

To further suppress the MAI, the signal at the output of the MMSE receiver is fed into the PIC detector. The immediate output (in the case of IA) or the final output (in the PA scenario) of the PIC detector is then fed as input to the bank of turbo decoders. The turbo decoders will yield LLR values of the users' data on which a soft or hard decision may be appropriately taken as discussed in Section 2.4.1.4. The MMSE front-end turbo PIC receiver can be divided into either PA or IA schemes which operate similarly to the schemes described in Sections 3.5.1 and 3.5.2 above.

3.5.3.1 MMSE Front-End Partitioned Approach Receiver

The MMSE front-end PA receiver can be described by combining the MMSE based PIC detector described in Section 3.4.1 with the PA receiver of Section 3.5.1. The overall structure of the MMSE front-end PA receiver is as depicted in Figure 3.9.

University of Cape Town

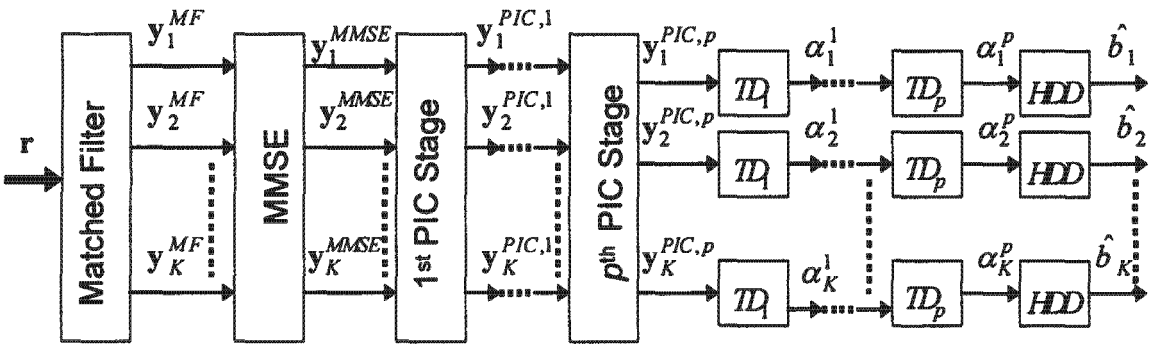

Figure 3.9: *MMSE Front-end PA Receiver*

There is no exchange of soft information between the PIC and decoder modules. This means that the PIC detector will perform all p cancellation stages, after which the soft output of the pth PIC stage is fed into a channel de-interleaver whose output becomes input to the first decoding iteration. For comparative reasons, the decoder is assumed to perform an equal number of iterations to that of the PIC detector.

The output of the pth stage can be expressed in discrete-time form as:

$$\mathbf{y}^{PIC,p} = \mathbf{y}^{MMSE} - \left(\mathbf{R} - diag\left[\mathbf{R}\right]\right)\tilde{\mathbf{y}}^{PIC,(p-1)} \tag{3.32}$$

where

$$\tilde{\mathbf{y}}^{PIC,p} = \left[\tilde{y}_1^{PIC,p}, \tilde{y}_2^{PIC,p}, \cdots, \tilde{y}_K^{PIC,p}\right] \tag{3.33}$$

is the users' codeword at the pth PIC output stage.

University of Cape Town

3.5.3.2 MMSE Front-End Iterative Approach Receiver

An MMSE receiver is used as the front-end to the IA receiver of Section 3.5.2. Figure 3.10 shows the structure of the MMSE front-end IA receiver.

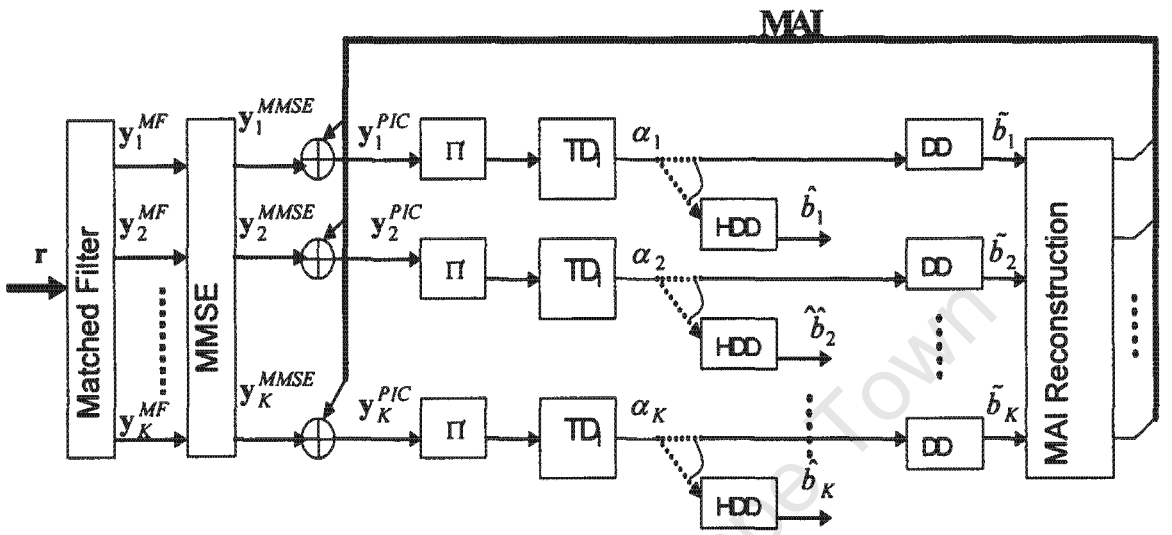

Figure 3.10: *MMSE Front-end IA Receiver*

The signal at the output of the MMSE receiver is fed into the PIC detector. The immediate output of the PIC detector is then fed as input to the bank of turbo decoders. This receiver uses the modified decoder of Section 2.4.1.5 that yields the LLR values of both information bits and the parity bits which are all used in the interference reconstruction process. The reconstructed MAI is then subtracted from the MMSE output $\mathbf{y}^{MMSE}$ thus producing a cleaner signal for consequent PIC stage outputs $\mathbf{y}^{PIC,i}$, where $i \in \{1,2,\cdots,p\}$. Each PIC output stage signal is fed into the modified turbo decoders which yield the LLR of the received codeword.

To estimate the users' transmitted data, a hyperbolic tangent soft decision device (introduced in Section 2.4.1.4) is taken on the LLR of the information and parity bits. In the signal interference reconstruction stage, the soft estimates of all users are multiplied by the users' received amplitudes, then spread and finally dispread.

University of Cape Town

The MAI reconstruction is done so that the estimates are as close as possible to the original users' data, as this will result in near accurate estimation of the MAI, thus translating to limited interference desired signals after each PIC stage. The cleaner PIC output signal (consisting of LLR values of information and data bits) leads to cleaner extrinsic information thus improved decoder output results. This cycle repeats for each iteration and expectedly yielding better and better results.

The output of the pth stage can be expressed in discrete-time form as:

$$\mathbf{y}^{PIC,p} = \mathbf{y}^{MMSE} - \left(\mathbf{R} - diag\left[\mathbf{R}\right]\right)\mathbf{P}\tilde{\mathbf{b}}^{PIC,(p-1)} \tag{3.34}$$

where $\mathbf{y}^{MMSE}$, $\mathbf{R}$ and $\mathbf{P}$ are given by Equations (3.14), (3.17) and (3.7) respectively and

$$\tilde{\mathbf{b}}^{PIC,p} = \left[\tilde{b}_1^{PIC,p}, \tilde{b}_2^{PIC,p}, \cdots, \tilde{b}_K^{PIC,p}\right] \tag{3.35}$$

is the users' data estimates given by the soft decision on LLR of the users' pth stage output.

3.5.4 Numerical Results

Because of complexity of analysis of multistage interference cancellation systems, most of this work relies heavily on Monte-Carlo simulation techniques to help supplement analysis. The synchronous uplink DS-CDMA system introduced in section 2.1 is considered. Transmission is over an AWGN channel and equal-power users are assumed. The receivers all assume perfect knowledge of the channel state information. The number of active system users is $K = 15$ and each user transmits an information frame size of $L_{in} = 1024$ data bits. The FEC code used is a rate $r = 1/3$ turbo code with a component encoder with generator polynomial $(7,5)_{octal}$. All spreading codes are of length $N = 15$ and are generated in a pseudo-random manner for each user. All presented performance curves in this section are evaluated at the fourth receiver iteration.

University of Cape Town

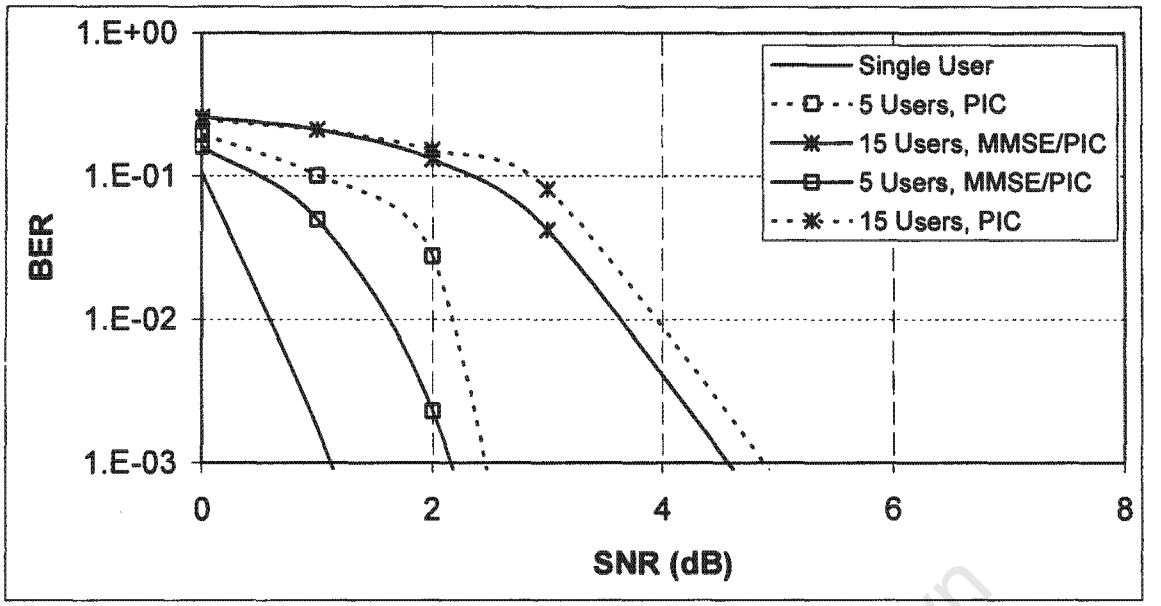

Figure 3.11: *PA-PIC and PA-MMSE/PIC Detector Performance comparison; Iterations=4*

Figure 3.11 shows the BER performance as a function of the SNR for the partitioned approach receiver with and without an MMSE front-end for a 5 and 15 user system, lower bounded by the single user performance curve.

In the above figure we consider 4 interference cancellation stages and 4 turbo decoding iterations. For a given BER performance threshold of 10^{-2}, the 5 user MMSE/PIC performance graph demonstrates a performance gain of approximately 0.6dB over the 5 user non-front-end curve. For the same BER performance threshold of 10^{-2}, the 15 user MMSE/PIC performance curve has a performance gain of approximately 0.3dB over the 15 user non-front-end curve. We observe that the MMSE front-end PA receiver offers a much better performance gain than its non-Front-end counterpart. This observation is valid for both $K=5$ and $K=15$ graph sets, however the performance gains are minimized as the system becomes overloaded.

The latter observation is clearly illustrated in Figure 3.12 where the BER performance as a function of the number of users is graphed for both the PA receiver with and without

University of Cape Town

the MMSE front-end at a SNR value of 2dB. The conventional MF capacity acts as an upper bound for the PA receiver system capacity.

For a given BER of 10^{-3} it is observed that the PA-PIC receiver achieves a capacity of only about 3 users while the MMSE front-end PA receiver achieves more than double the PA-PIC receiver capacity for the same performance threshold. These capacity gains are however seen to diminish as the system load increases and both receivers with and without the MMSE front-end are seen to converge towards the MF capacity limit for a fully loaded system.

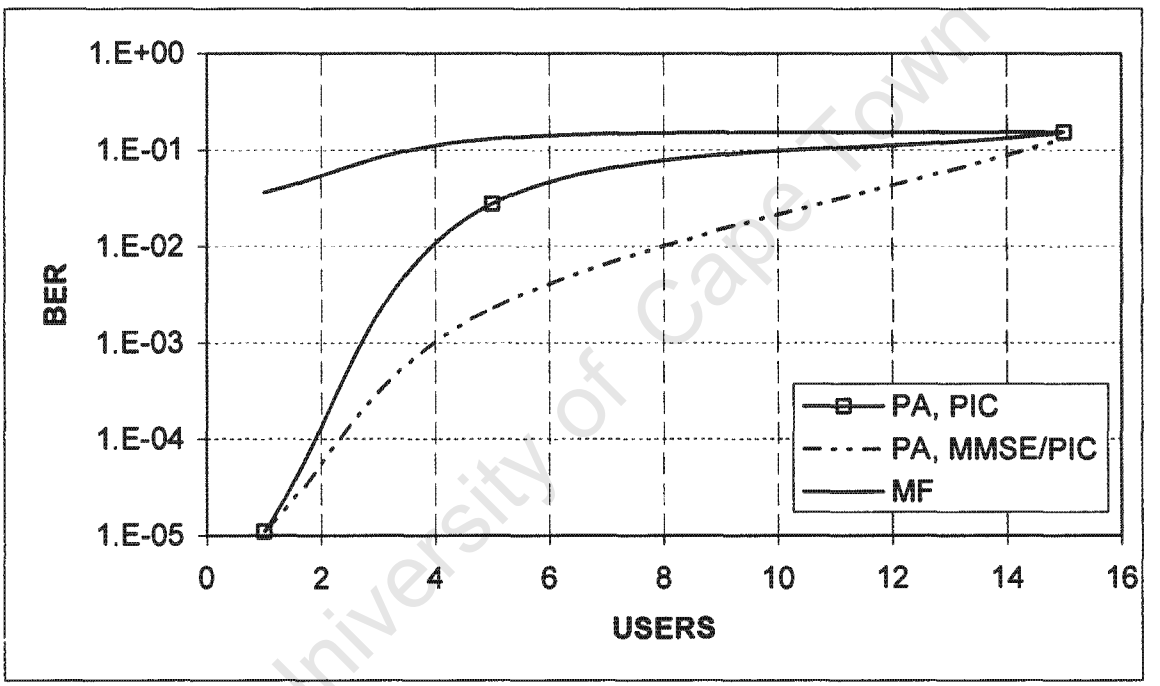

Figure 3.12: *PA-PIC and PA-MMSE/PIC system capacity; SNR=2dB, Iterations=4*

Figure 3.13 shows the BER performance as a function of the SNR for the iterative approach receiver with and without an MMSE front-end for a 5 and 15 user system, lower bounded by the single user performance curve. As in the previous PA graphs, we consider 4 iterative decoding steps for the IA receiver, as discussed in section 3.5.2.

University of Cape Town

As with the PA scheme, we observe that the MMSE front-end IA receiver offers an improved performance gain than the IA-PIC receiver. Again, this observation is valid for both $K = 5$ and $K = 15$ graph sets.

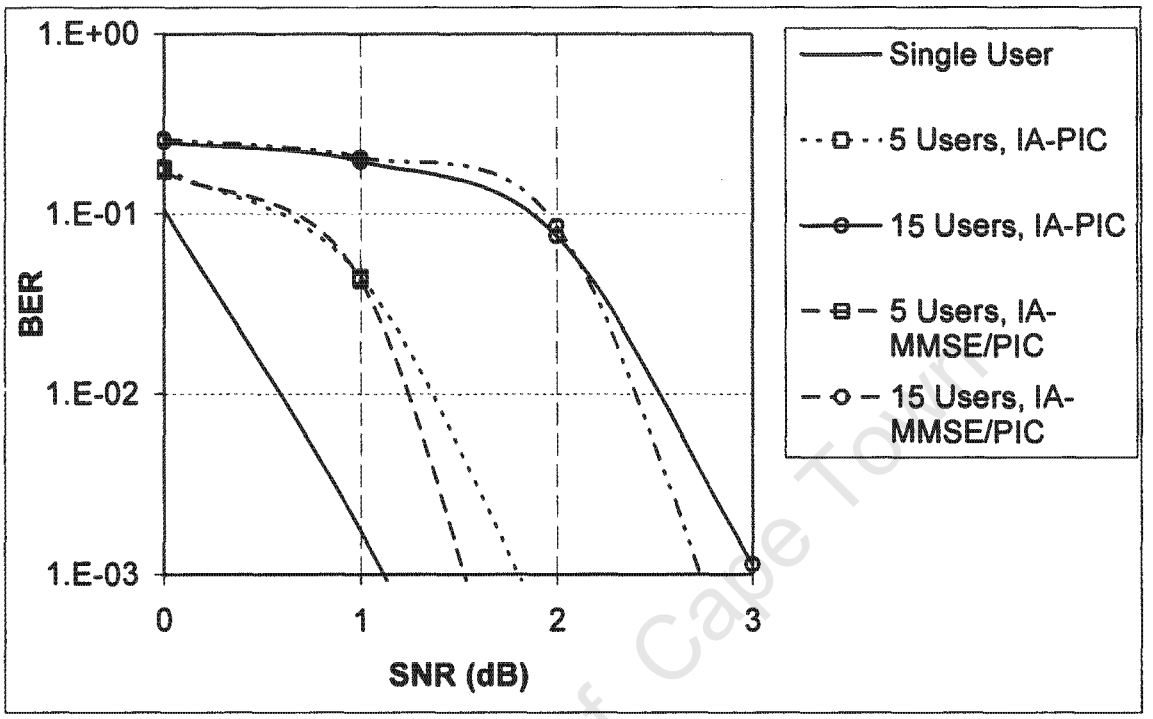

Figure 3.13: *IA-PIC and IA-MMSE/PIC Detector Performance comparison; Iterations=4*

Figure 3.14 shows the BER performance as a function of the number of users for both the IA receiver with and without the MMSE front-end at a SNR value of 2dB. For a given BER of 10^{-4} it is observed that the IA-PIC receiver achieves a capacity of $K = 3$ users while the MMSE front-end IA receiver achieves a capacity of $K = 13$ users, indicating a more than fourfold capacity improvement over the IA-PIC receiver capacity for the same performance threshold. These capacity gains are seen to be degrading gracefully as the system becomes overloaded.

University of Cape Town

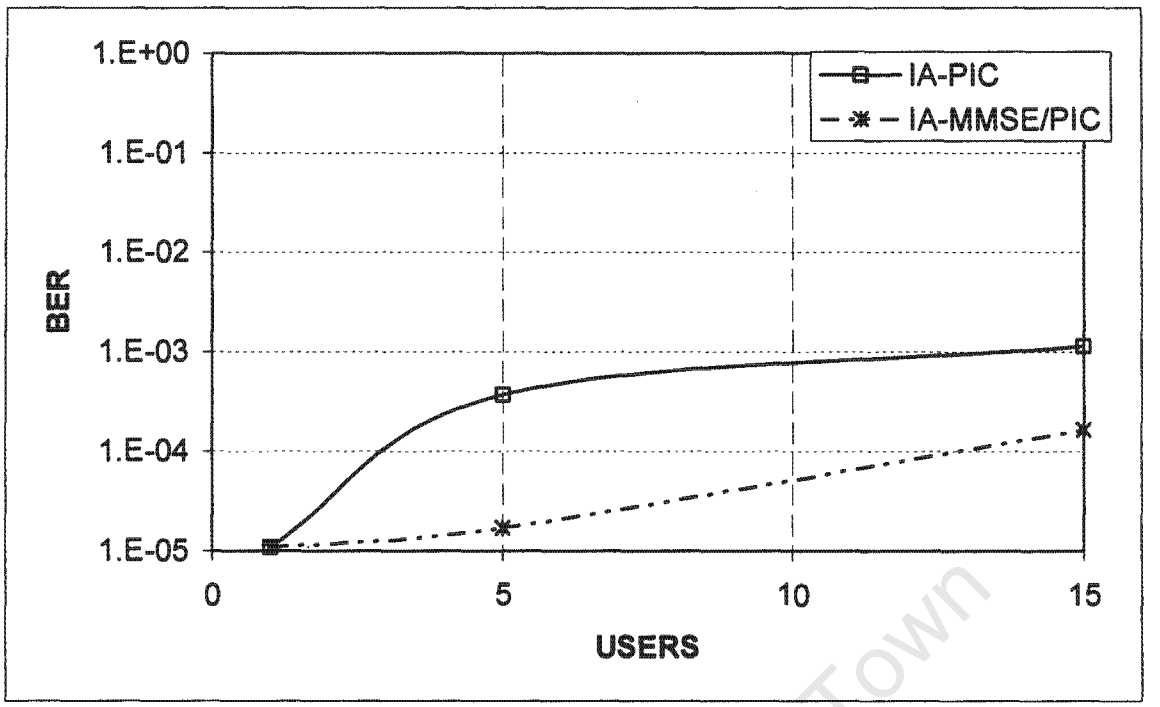

Figure 3.14: *IA-PIC and IA-MMSE/PIC system capacity; SNR=2dB,Iterations=4*

A performance comparison, in terms of system capacity, is given in Figure 3.15 where the BER performance as a function of the number of active users for both PA and IA receivers with and without an MMSE front-end is shown for a SNR of 2dB. In each case 4 cancellation stages and or iterations are performed. For any given performance measure, the IA MMSE front-end receiver is observed to give the best capacity improvements.

University of Cape Town

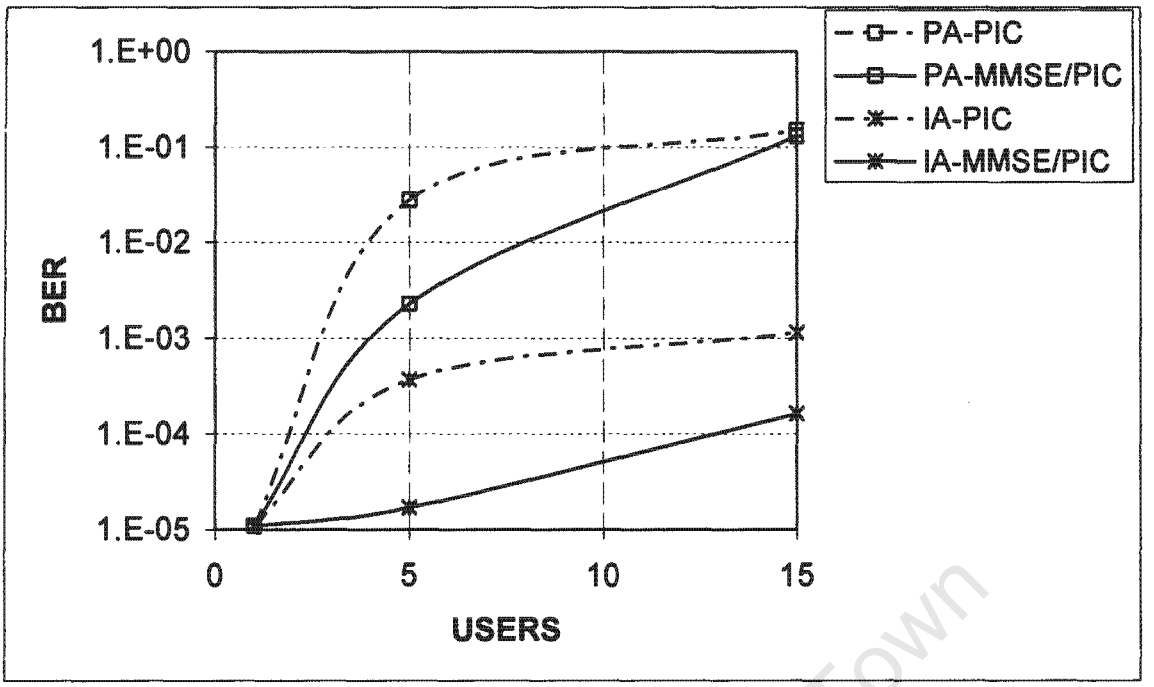

Figure 3.15: *PA and IA System Capacity comparison as a function of BER vs. Users; SNR=2dB, Iterations=4*

University of Cape Town

3.6 Summary

The main contribution in this chapter is the application and choice of a turbo multi-user concatenation scheme as a receiver in a turbo coded synchronous DS-CDMA system in an AWGN channel. The turbo multi-user detection principle is introduced and such receivers are divided into partitioned approach (PA) and iterative approach (IA) receivers. Simulation results demonstrate that the IA receiver that employs an MMSE detector as its front end provides outstanding capacity gains in comparison: to the IA receiver with no MMSE front end and also to the PA receiver with and without an MMSE front end detector.

Chapter 4
Turbo Space-Time Multi-user Detection in MIMO Flat Fading CDMA Systems

Contents

University of Cape Town

4.1 Introduction

Though the work in previous chapters investigates the combined MUD and error control coding performance it still does not investigate these in conjunction with diversity techniques. The work done in this chapter draws heavily from concepts already introduced in previous chapters of this thesis. To highlight the motivation behind the work in this chapter, we first review/introduce work previously done by other authors and authors of the same thesis.

The presence of MAI in CDMA systems has led many researchers to investigate ways of exploiting the MAI to improve the system performance. The optimum MUD proposed in [14] that consists of the MLSE based on the Viterbi decoding algorithm has shown huge improvements (i.e. a substantial increase in system capacity) over the conventional correlation receiver. Unfortunately as the number of users increases so does its computational complexity. This complexity grows exponentially with the number of active users and constraint length of the code making any practical implementation very

prohibitive. Various suboptimum detectors have been proposed, which include, but not limited to, decorrelator, MMSE, SIC and PIC receivers [13, 15].

The demand on higher system capacity and higher data rates has led researchers to the investigation of MIMO wireless systems [29]. The implementation of MIMO is particularly appealing because of its relative simplicity of implementation and the feasibility of multiple antennas at the base station where the MIMO costs can be evenly shared by the system users [30]. Moreover MIMO systems have been shown to offer much higher capacity gains over single antenna systems [29, 31]. Work done by [29] and [32] predicts a remarkable capacity increase for MIMO systems in the presence of multipath fading. Space-Time Codes (STCs) have recently gained much attention as an effective MIMO algorithm [33] and [30]. There are two main types of STCs; these being Space-Time Block Codes (STBCs) [18] and Space-Time Trellis Codes (STTCs) [30]. When many users are in the system, strong MAI will occur. In this case, diversity processing alone cannot improve the system performance.

As discussed in section 3.5, neither MUD alone nor channel coding techniques can fully eliminate the effects of MAI. Joint detection and decoding in multi-user systems has been an active research area for the last decade. Researchers like [18] have investigated the combined optimum detector [14] and convolutional decoding system performance. Due to the exponential complexity of the receiver in [14], the authors of [18] propose suboptimal MUD with convolution coding in [19]. By integrating a combination of various suboptimal MUDs with iterative channel decoding, the authors of [20] introduce a convolutionaly coded iterative interference canceller.

The powerful error correction ability of the turbo codes [34] has been combined with interference cancellation in [22] to produce the turbo interference cancellation detection approach. The work of [22] has further been studied in [23], [24] with further work being done by[25] and [26]. Though the above work investigates the combined MUD and error control coding performance it still does not investigate these in conjunction with diversity techniques. Recently, much work has been done on combining diversity techniques with

University of Cape Town

MUD algorithms [35], [36], [37]. Some authors like [38] have proposed iterative MUD techniques using error control coding and antenna arrays while [39] proposes a soft iterative multisensor array receiver for coded MUD CDMA wireless uplink. Most recently work in [40] investigates the joint DS-CDMA space-time MUD system with error control coding over a multi-path fading channel. The authors of [24] use convolutional coding for error control coding and a space-time MMSE detector at the receiver end. The authors of this thesis in [41] investigate the performance of IA and PA schemes for a turbo coded asynchronous DS-CDMA system that employs space-time multi-user detection in a Rayleigh fading channel. However, as seen in chapter 3 (for a synchronous system), a non-MMSE front-end turbo receiver does not provide as much capacity gains as its MMSE front-end counterpart.

Objective: The objective of this chapter is to investigate the performance (through simulation) of a synchronous turbo coded DS-CDMA system that employs an MMSE front-end turbo space-time multi-user detector at reception propagating through a Rayleigh fading channel. We use an MMSE/PIC MUD coupled with STBC to achieve space-time multi-user detection. Depending on the concatenation scheme used, we divide these into MMSE front-end partitioned approach and MMSE front-end iterative approach receivers, herein thereafter referred to as PA and IA receivers, respectively.

University of Cape Town

4.2 Diversity Techniques

Many wireless communication transmissions happen under various channel conditions, most of which undergo time-varying multipath fading that further complicates synchronization. This is a problem that is predominant in urban and indoor environments, which are of great interest for cellular mobile radio applications. Although direct sequence spread spectrum (DS/SS) systems have an inherent property of interference rejection, most radio channels exhibit such sever multipath effects that even the strict autocorrelation properties of the spreading waveforms are inadequate for rejecting multipath interference. Due to multipath fading, the receiver might not be able to discern

the transmitted signal; however this can be mitigated through statistically independent fading reception such that strong replicas of the transmitted signal are received. Diversity exploits the random nature of radio propagation by finding independent or largely uncorrelated signal paths for communication. Most mobile communication channels must combat the effects of fading caused by multipath propagation and diversity is a key technique aimed at addressing this problem. Diversity involves the sending of a less-attenuated signal replica that assists the receiver in determining the original transmitted signal [4].

Diversity types can be classified as: space, frequency, time and polarization diversity.

Space diversity: in space diversity, multiple antennas with independent fades are used to receive the signal.

Frequency diversity: the signal is transmitted in several frequency bands.

Time diversity: the signal is transmitted in different time slots. Techniques such as channel coding and interleaving are used to provide time diversity.

Polarization diversity: uses two antennas with different polarization for reception and/or transmission.

We suppose to deal with a Rayleigh flat fading channel such that the channel response does not vary with time. The continuous time signal at a receiver from a flat fading channel can be expressed as:

$$r(t)=\sum_{n=0}^{+\infty}\sum_{k=1}^{K} d_k(t)c_k(t-nT)*h(t)+n(t) \tag{4.1}$$

where $h(t)$ is a complex Gaussian random process, given as

$$h(t)=\beta(t)e^{j\theta} \tag{4.2}$$

Where $\beta(t)$ is Rayleigh distributed and θ is the phase value. Here * represents the convolution operation, and $n(t)$ is a zero mean additive Gaussian noise with a two-sided power spectral density of $N_0/2$.

University of Cape Town

In systems where there are no diversity schemes employed, Rayleigh fading channels can pose serious problems during a deep fade as this can result in a received signal that is below the background noise level, making communication unreliable [42].

4.3 MIMO System Model

Transmit diversity can help in improving the performance of the receiver in the presence of fading. It achieves this by sending multiple independent copies of the digitally modulated waveform at the receiver, where the chance that all copies are simultaneously in a fade is very minimal.

The demand for higher system capacity and higher data rates has led researchers to the investigation of multiple-input multiple-out MIMO wireless systems [29]. The implementation of MIMO is particularly appealing because of its relative simplicity of implementation and the feasibility of multiple antennas at the base station where the MIMO costs can be evenly shared by the system users [30]. MIMO uses an appropriate algorithm at transmission and reception to respectively de-multiplex and multiplex the original data stream.

The point-to-point MIMO system of Figure 4.1 is considered. This structure consists of a transmitter process characterized by n_T transmit antennas and a receiver process that has n_R receiver antennas. Both transmitter and receiver processes are characterized by a MIMO signal processing technique. Such signal processing techniques are discussed in the section that follows.

University of Cape Town

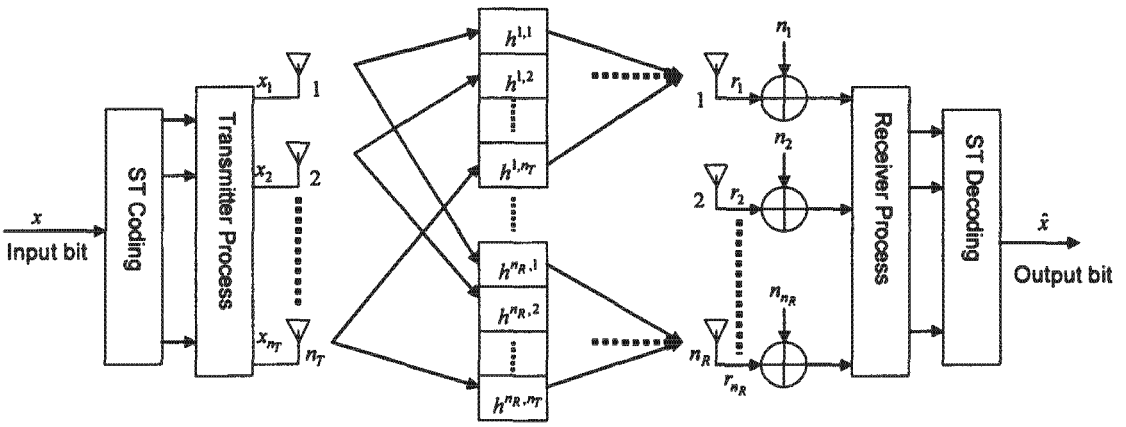

Figure 4.1: *Structure of a generalized point-to-point MIMO Communication System*

Transmitter Process

The user's information data is transformed into a column vector by the MIMO signal processing technique being employed. This vector can be represented as:

$$\mathbf{x} = \left[x_1, x_2, \cdots, x_{n_T} \right] \tag{4.3}$$

where x_m is the signal that is transmitted by the mth transmit antenna. All the n_R signals of $\mathbf{x}$ are transmitted simultaneously from each transmit antenna and have equal transmit average power of $P_t = \frac{P}{n_T}$, where P is the total transmitted signal power.

Propagation Channel

A channel is quasi-static if the channel coefficients are time-invariant for the duration of the entire block of symbols; this is also known as slow fading channel. However, if the channel coefficients change every symbol, the channel is known as a fast fading channel. In this work, a quasi-static channel is assumed.

There are $n_R \times n_T$ slowly varying sub-channels that make up the overall channel with each sub-channel considered to be Rayleigh fading. During transmission, n_R signals that undergo independent fading, are transmitted simultaneously from each transmit antenna.

University of Cape Town

The complex random variable that describes the channel between receiver antenna η and transmit antenna m is represented as $h^{\eta,m}$. This can be expressed similar to Equation (4.2) as:

$$h^{\eta,m}(t) = \beta^{\eta,m}(t)e^{j\theta(t)} \tag{4.4}$$

where the fade coefficients are assumed to be fixed during a time slot but are independent from one slot to another, $m \in \{1,2,\cdots,n_T\}$ and $\eta \in \{1,2,\cdots,n_R\}$.

Receiver Process

All signals transmitted by different transmit antennas are assumed to arrive simultaneously at each receiver antenna. Perfect knowledge of CSI at the receiver is assumed.

The total received signal at receiver antenna η is:

$$r_\eta = \sum_{m=1}^{n_T} h^{\eta,m} x_m + n_\eta \tag{4.5}$$

the total received signal at the receiver can be expressed in discrete-time form as:

$$\mathbf{r} = \mathbf{Hx} + \mathbf{n} \tag{4.6}$$

where

$$\mathbf{H} = \begin{bmatrix} h^{1,1} & h^{1,2} & \cdots & h^{1,n_T} \\ h^{2,1} & h^{2,2} & \cdots & h^{1,n_T} \\ \vdots & \vdots & \ddots & \vdots \\ h^{n_R,1} & h^{n_R,1} & \cdots & h^{n_R,n_T} \end{bmatrix} \tag{4.7}$$

is a $n_R \times n_T$ matrix representing the MIMO channels.

And

$$\mathbf{n} = \begin{bmatrix} n_1, n_2, \cdots, n_{n_R} \end{bmatrix} \tag{4.8}$$

is the noise vector at the receiver.

University of Cape Town

4.3.1 MIMO Signal Processing Techniques

Several signal processing techniques exist for MIMO communication systems.

These MIMO signal processing techniques can be divided into two main categories, namely Spatial Multiplexing (SM) and space-time codes. Figure 4.2 gives a summary of the MIMO signal processing techniques.

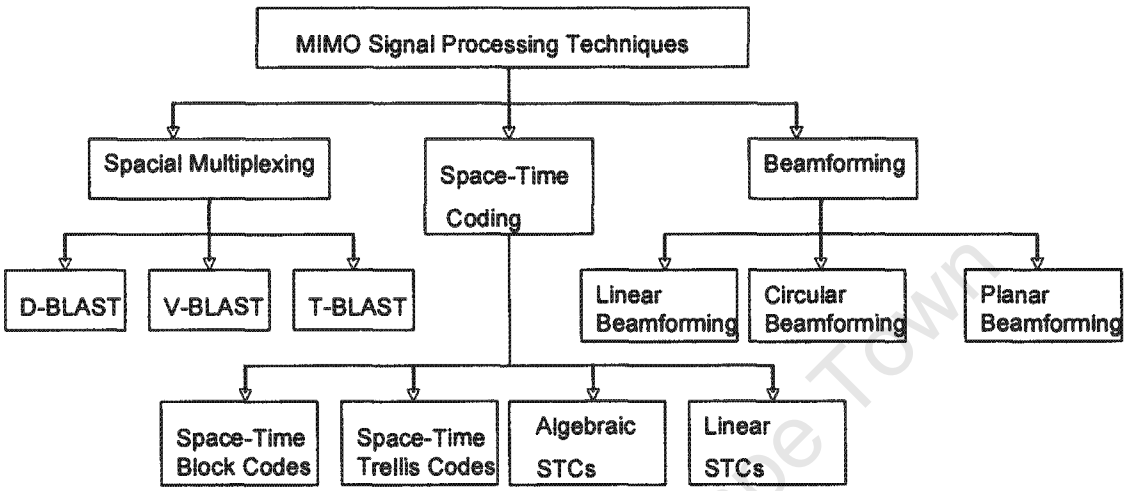

Figure 4.2: *Classification of MIMO techniques*

The main goal of SM is to achieve the maximum link capacity while that of STC is to achieve the maximum diversity order available. An example of spatial multiplexing is the Bell labs LAyered Space Time architecture (BLAST) whose basic principle is to transmit independent data from each transmit antenna. STCs simultaneously transmit multiple signals that undergo independent fading, increasing the chances of at least one reliable data stream copy being received. STCs include space-time trellis codes [43] which aim to provide coding and diversity gains and STBCs [30],[33], which aim at increasing diversity and thus improving the robustness of the communications link.

4.3.2 Space-Time Block Coding

STC is a more efficient technique for providing transmit diversity for a multiple antenna system. This has an advantage over the diversity schemes discussed in Section 4.2 as it enables the multiple antennas to be deployed at the base stations where the complexity is

University of Cape Town

not a major concern and all expenses can be equally shared among the system users, thus removing the diversity burden from the Mobile Station (MS).

As stated in the previous section, space-time coding can be implemented as either in a trellis form or block form. STB Encoders transform a data stream into a matrix whose columns represent the time dimension (i.e. time slots) and the rows represent the spatial dimension (i.e. transmit antennas). STBCs cannot provide coding gain, unless concatenated with an outer code, but they however do provide diversity gain, therefore increasing the reliability of the system.

STT Encoders operate on one input symbol at a time, producing a vector of symbols that has a length equal to the number of transmit antennas. STTCs provide coding gain and also provide full diversity gain. The STTC coding gain advantage over STBCs is however eclipsed by their extremely hard design and demand for highly complex encoders and decoders.

The STBC scheme is thus seen as the better choice for providing space-time diversity gain in real systems as it has a much less decoding complexity compared to the STTC scheme. This section gives a brief overview of STBCs. Figure 4.3 shows the scheme for a block transmission using one and two transmit antennas [44].

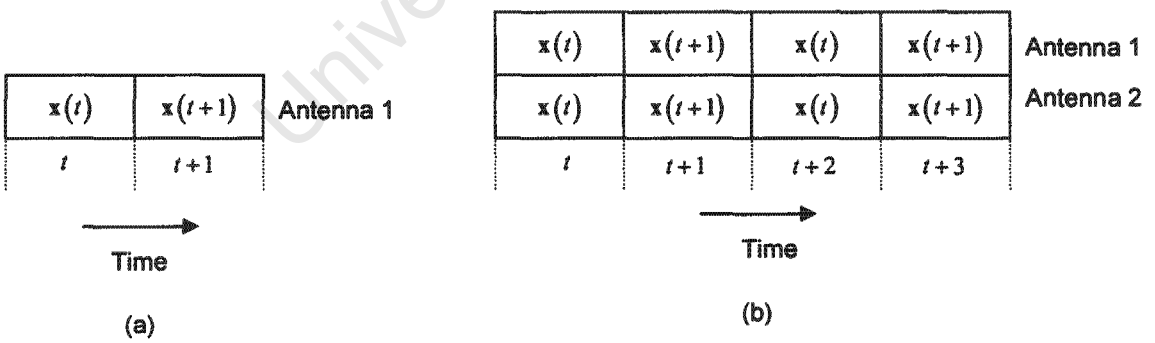

Figure 4.3: *Block Transmission through the STB encoder using (a) one transmit antenna and (b) two transmit antennas*

University of Cape Town

When the number of transmitting antennas is one, the STB encoder output sequence is given directly by its input. However for the case of two transmit antennas, the STC symbols transmitted at the tth time slot are $\mathbf{x}(t)$ and $\mathbf{x}(t+1)$ from antenna 1 and 2 respectively. During the next time slot, $-\mathbf{x}(t+1)$ and $\mathbf{x}(t)$ are transmitted from antenna 1 and 2 respectively.

A matrix is usually used to represent STBC with each row representing a time slot and each column representing one antenna's transmission over time. Alamouti [33] proposed a simple transmission scheme using two transmit antennas. The space-time block code proposed by [33] contains two variables (that maybe complex) x_1, x_2 and their negative (and complex conjugates, if complex) such that the columns are orthogonal. This 2 x 2 complex orthogonal design is given by

$$G_2 = \begin{pmatrix} x_1 & x_2 \\ -x_2^* & x_1^* \end{pmatrix} \tag{4.9}$$

Motivated by Alamouti, [30] extended this transmit diversity scheme to include the use of more than two transmit antennas. [30] used the theory of orthogonal code design in order to construct these STB codes, and defined half-rate STB codes G_3 and G_4 having three and four transmitters, respectively. These STB codes are shown below

$$G_3 = \begin{pmatrix} x_1 & x_2 & x_3 \\ -x_2 & x_1 & -x_4 \\ -x_3 & x_4 & x_1 \\ -x_4 & -x_3 & x_2 \\ x_1^* & x_2^* & x_3^* \\ -x_2^* & x_1^* & -x_4^* \\ -x_3^* & x_4^* & x_1^* \\ -x_4^* & -x_1^* & x_2^* \end{pmatrix} \tag{4.10}$$

University of Cape Town

$$G_4 = \begin{pmatrix} x_1 & x_2 & x_3 & x_4 \\ -x_2 & x_1 & -x_4 & x_3 \\ -x_3 & x_4 & x_1 & -x_2 \\ -x_4 & -x_3 & x_2 & x_1 \\ x_1^* & x_2^* & x_3^* & x_4^* \\ -x_2^* & x_1^* & -x_4^* & x_3^* \\ -x_3^* & x_4^* & x_1^* & -x_2^* \\ -x_4^* & -x_1^* & x_2^* & x_1^* \end{pmatrix} \tag{4.11}$$

In all generator matrices, the rows correspond to time-slots while the columns correspond to antennas. Thus during each symbol period the symbols from one time-slot are transmitted, one on each transmit antenna. This means that (with G_2 for instance), during the first time-slot symbols x_1 and x_2 are transmitted simultaneously from antennas one and two, respectively and during the second time-slot, signals $-x_2^*$ and x_1^* are transmitted simultaneously from antennas one and two, respectively. For an in-depth discussion of the space-time transmission and decoding process the reader is referred to [45].

Since in G_2 each symbol is transmitted by any one antenna only once it is thus referred to as a unit/full rate STB code, whereas G_3 and G_4 are half rate STB codes, since in both cases only four symbols are transmitted in eight time-slots.

Figure 4.4 shows the BER performance of uncoded coherent BPSK for the Alamouti [33] scheme in Rayleigh fading. We assume that the amplitudes of fading from each transmit antenna to each receive antenna are mutually uncorrelated Rayleigh distributed and that the average signal powers at each receive antenna from every transmit antenna are the same. Furthermore, it is assumed that the receiver has perfect knowledge of the CSI. It is observed that introducing diversity to a system limited by multipath fading can improve the system performance, data rate, or capacity of wireless communication systems [33].

University of Cape Town

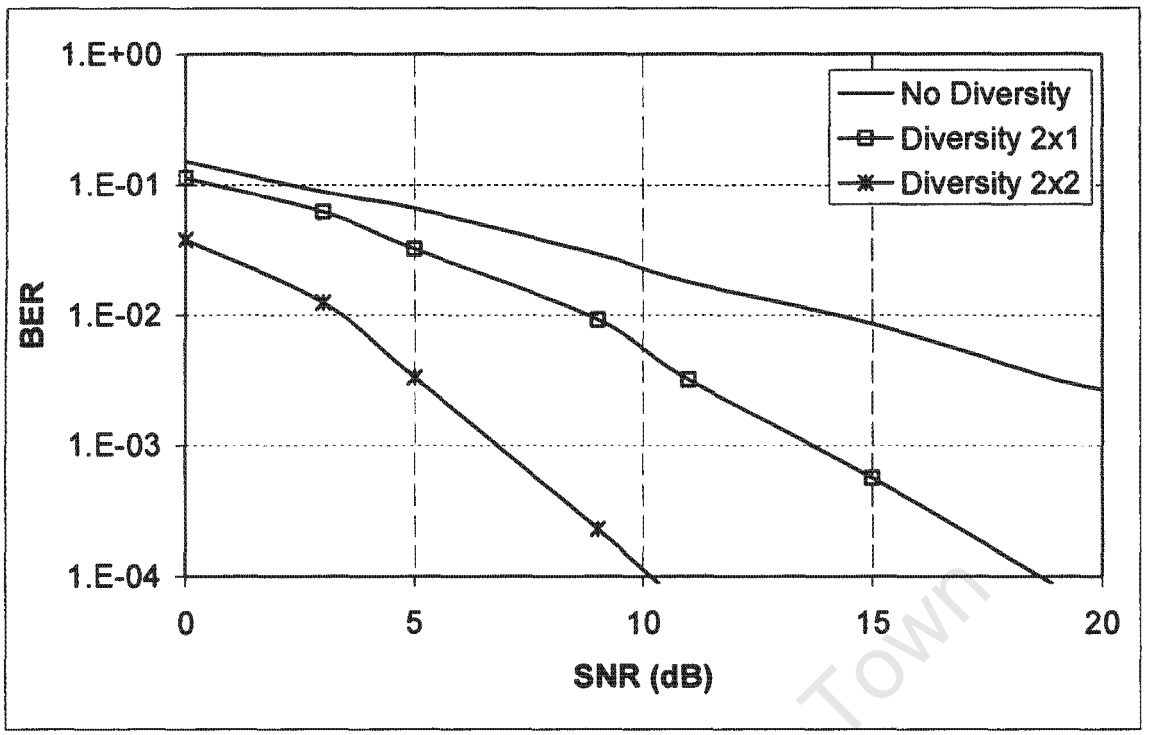

Figure 4.4: *Uncoded Single User BER vs. SNR Performance for a Rayleigh Flat Fading Channel with Diversity*

University of Cape Town

4.4 Space-Time MIMO-CDMA System Model

The MIMO communication system, discussed in Section 4.3 has been shown as the most practical approach to providing significant capacity improvements in a fading channel system.

In this section we expand this point-to-point MIMO system to a multiple user CDMA system dubbed as MIMO-CDMA. Figure 4.5 depicts the system model for the MIMO-CDMA system. This model considers the uplink scenario of a single cell system with K synchronous active users.

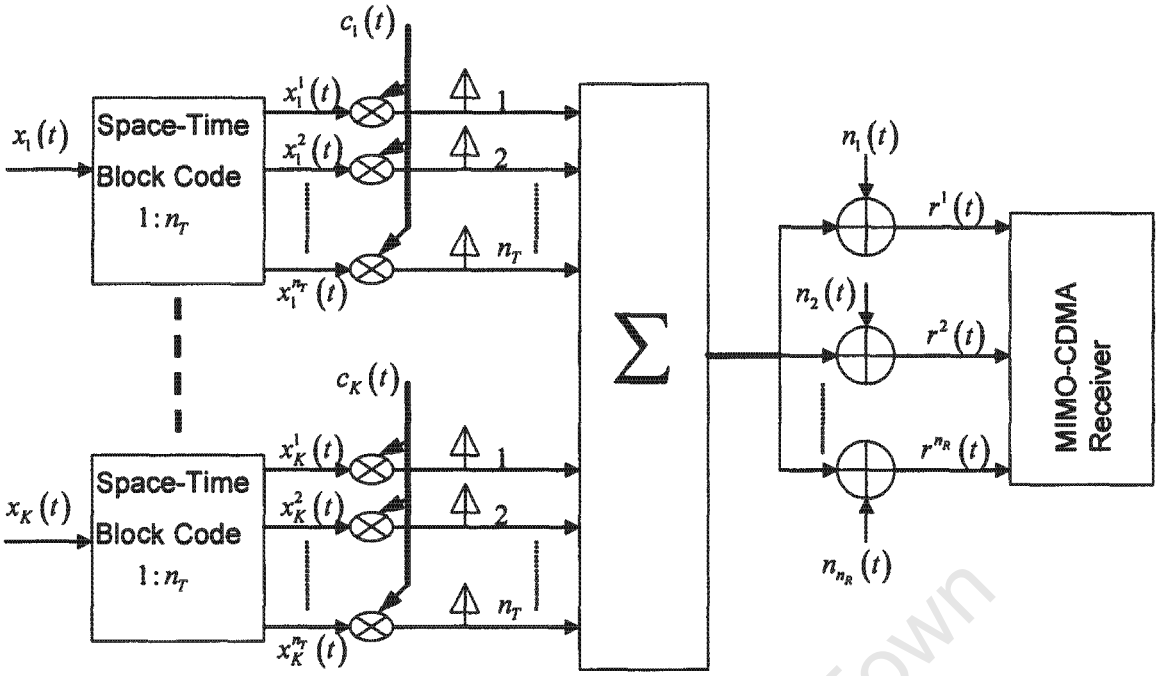

Figure 4.5: *Structure Diagram of a Space-Time MIMO-CDMA System*

Each MS is equipped with n_T transmit antennas and the base station has n_R receiver antennas. This can be easily extended to any arbitrary number of antennas [30],[45]. Following the approach in [33], during the first STBC symbol period, two signals x_1^k and x_2^k are simultaneously transmitted from the two antennas ($n_{T=1}$ and $n_{T=2}$, respectively). On the second symbol period, $-x_2^{k*}$ is transmitted from antenna $n_{T=1}$ and x_1^{k*} is transmitted from antenna $n_{T=2}$. We assume that the channel is constant across all consecutive symbols.

Considering a multi-user DS-CDMA system with STBC, the received signals for user k, $r^k(t)$ and $r^k(t+T_b)$ during time t and $t+T_b$, respectively, for the uplink scenario can be expressed as

$$r_1^k(t) = \sum^{K} (h_k^1 x_1^k + h_k^2 x_2^k) + n_1 \tag{4.12}$$

University of Cape Town

$$r_2^k(t) = \sum^{K}(-h_k^1 x_2^k + h_k^2 x_1^k) + n_1 \tag{4.13}$$

Where from (2.5) x_1^k and x_2^k are written as:

$$x_1^k = s_k^1 = \sqrt{E_k} d_k^1(t) c_k(t) \cos(\omega_c t + \theta_k(t)) \tag{4.14}$$

$$x_2^k = s_k^2 = \sqrt{E_k} d_k^2(t) c_k(t) \cos(\omega_c t + \theta_k(t)) \tag{4.15}$$

and d_k^1 and d_k^2 are the bits transmitted by user k during the first and second STBC symbol period, respectively.

Considering user k to be our user of interest, we can expressed the dispread signal at the MF output as

$$\begin{aligned} \mathbf{y}^{\mathbf{MF}} &= \left[\mathbf{y}_1^{\mathbf{MF}}, \cdots, \mathbf{y}_{\mathbf{K}}^{\mathbf{MF}}\right] \\ \mathbf{y}_k^{\mathbf{MF}} &= \left[y_k^{MF,1}, \cdots, y_k^{MF,n_T}\right] \end{aligned} \tag{4.16}$$

$$\begin{aligned} y_k^{MF,1} &= \frac{1}{T_b}\int^{T_b} c_k(t) r_1^k \\ &= \sqrt{E_k} d_k^1 h_k^1 + \sqrt{E_k} d_k^2 h_k^2 + \sum_{j\neq k}^{K}\left[\sqrt{E_j}\rho_{jk1}\begin{pmatrix} d_k^1 h_j^1 \cos\left(\theta_{k1} - \theta_{j1}\right) + \\ + d_k^2 h_j^2 \cos\left(\theta_{k2} - \theta_{j2}\right) \end{pmatrix}\right] + n_1' \end{aligned} \tag{4.17}$$

$$\begin{aligned} y_k^{MF,2} &= \frac{1}{T_b}\int^{T_b} c_k(t) r_2^k \\ &= -\sqrt{E_k} d_k^2 h_k^1 + \sqrt{E_k} d_k^1 h_k^2 + \sum_{j\neq k}^{K}\left[\sqrt{E_j}\rho_{jk2}\begin{pmatrix} -d_k^2 h_j^1 \cos\left(\theta_{k1} - \theta_{j1}\right) + \\ d_k^1 h_j^2 \cos\left(\theta_{k2} - \theta_{j2}\right) \end{pmatrix}\right] + n_2' \end{aligned} \tag{4.18}$$

where

$$n_1' = \frac{1}{T_b}\int^{T_b} n_1 c_k(t) \cos(\omega_c t) dt \tag{4.19}$$

$$n_2' = \frac{1}{T_b}\int^{T_b} n_2 c_k(t) \cos(\omega_c t) dt \tag{4.20}$$

and

University of Cape Town

$$\rho_{jki} \leq \frac{1}{T_b}\int^{T_b} c_k(t-\tau_{ki})c_j(t)dt \tag{4.21}$$

is the cross-correlation between the *j*th and *k*th user during the *i*th STBC symbol period. At the combiner the signals $y_k^{MF,1}$ and $y_k^{MF,2}$ are combined to extract x_1^k

$$\begin{aligned}\tilde{x}_1^k &= h_k^1 y_k^{MF,1} + h_k^2 y_k^{MF,2} \\ &= \left[\left(\beta_k^1\right)^2 + \left(\beta_k^2\right)^2\right]\sqrt{E_k}d_k^1 + \sum_{j\neq k}^{K} h_k^1\left[\sqrt{E_j}\begin{pmatrix}\rho_{jk}^1 h_j^1 \cos\left(\theta_k^1-\theta_j^1\right)d_k^1 + \\ \rho_{jk}^2 h_j^2 \cos\left(\theta_k^2-\theta_j^2\right)d_k^2\end{pmatrix}\right] \\ &+ \sum_{j\neq k}^{K} h_k^2\left[\sqrt{E_j}\begin{pmatrix}-\rho_{jk}^2 h_j^1 \cos\left(\theta_k^1-\theta_j^1\right)d_k^2 + \\ \rho_{jk}^1 h_j^2 \cos\left(\theta_k^2-\theta_j^2\right)d_k^1\end{pmatrix}\right] + h_k^1 n_1' + h_k^2 n_2'\end{aligned} \tag{4.22}$$

and to extract x_2^k

$$\begin{aligned}\tilde{x}_2^k &= -h_k^1 y_k^{MF,2} + h_k^2 y_k^{MF,1} \\ &= \left[\left(\beta_k^1\right)^2 + \left(\beta_k^2\right)^2\right]\sqrt{E_k}d_k^2 + \sum_{j\neq k}^{K} -h_k^1\left[\sqrt{E_j}\begin{pmatrix}-\rho_{jk}^2 h_j^1 \cos\left(\theta_k^1-\theta_j^1\right)d_k^2 + \\ \rho_{jk}^1 h_j^2 \cos\left(\theta_k^2-\theta_j^2\right)d_k^1\end{pmatrix}\right] \\ &+ \sum_{j\neq k}^{K} h_k^2\left[\sqrt{E_j}\begin{pmatrix}\rho_{jk}^1 h_j^1 \cos\left(\theta_k^1-\theta_j^1\right)d_k^1 + \\ \rho_{jk}^2 h_j^2 \cos\left(\theta_k^2-\theta_j^2\right)d_k^2\end{pmatrix}\right] - h_k^1 n_2' + h_k^2 n_1'\end{aligned} \tag{4.23}$$

For notational convenience, the combined estimates of (4.22) and (4.23) can be expressed as

$$\tilde{x}_1^1 = X_1^1 + MAI_1^1 + N_1'^1 \tag{4.24}$$

and

$$\tilde{x}_2^1 = X_2^1 + MAI_2^1 + N_2'^1 \tag{4.25}$$

Where X_1^1 and X_2^1 denote the first user's desired signal during the first and second STBC symbol periods, respectively, given by

$$X_1^1 = \left[\left(\beta_k^1\right)^2 + \left(\beta_k^2\right)^2\right]\sqrt{E_k}d_k^1 \tag{4.26}$$

$$X_2^1 = \left[\left(\beta_k^1\right)^2 + \left(\beta_k^2\right)^2\right]\sqrt{E_k}d_k^2 \tag{4.27}$$

University of Cape Town

MAI_1^1 and MAI_2^1 denote the multiple access interference on user 1's signal during the first and second STBC symbol periods, respectively, given as

$$MAI_1^1 = \sum_{j\neq k}^{K} h_k^1 \left[\sqrt{E_j} \begin{pmatrix} \rho_{jk}^1 h_j^1 \cos\left(\theta_k^1 - \theta_j^1\right) d_k^1 + \\ \rho_{jk}^2 h_j^2 \cos\left(\theta_k^2 - \theta_j^2\right) d_k^2 \end{pmatrix} \right] + \sum_{j\neq k}^{K} h_k^2 \left[\sqrt{E_j} \begin{pmatrix} -\rho_{jk}^2 h_j^1 \cos\left(\theta_k^1 - \theta_j^1\right) d_k^2 + \\ \rho_{jk}^1 h_j^2 \cos\left(\theta_k^2 - \theta_j^2\right) d_k^1 \end{pmatrix} \right] \tag{4.28}$$

$$MAI_2^1 = \sum_{j\neq k}^{K} -h_k^1 \left[\sqrt{E_j} \begin{pmatrix} -\rho_{jk}^2 h_j^1 \cos\left(\theta_k^1 - \theta_j^1\right) d_k^2 + \\ \rho_{jk}^1 h_j^2 \cos\left(\theta_k^2 - \theta_j^2\right) d_k^1 \end{pmatrix} \right] + \sum_{j\neq k}^{K} h_k^2 \left[\sqrt{E_j} \begin{pmatrix} \rho_{jk}^1 h_j^1 \cos\left(\theta_k^1 - \theta_j^1\right) d_k^1 + \\ \rho_{jk}^2 h_j^2 \cos\left(\theta_k^2 - \theta_j^2\right) d_k^2 \end{pmatrix} \right] \tag{4.29}$$

and $N_1'^1$ and $N_2'^1$ denotes the AWGN introduced at the receiver and is expressed as

$$N_1'^1 = \int^{T_b} h_1^1 n_1 \sqrt{2/T_b} c_1(t) \cos(\omega_c t) dt + \int^{T_b} h_1^2 n_2 \sqrt{2/T_b} c_1(t) \cos(\omega_c t) dt \tag{4.30}$$

$$N_2'^1 = \int^{T_b} -h_1^1 n_2 \sqrt{2/T_b} c_1(t) \cos(\omega_c t) dt + \int^{T_b} h_1^2 n_1 \sqrt{2/T_b} c_1(t) \cos(\omega_c t) dt \tag{4.31}$$

4.5 Turbo Space-Time Coded MIMO-CDMA System

A MIMO-CDMA system that employs turbo codes and space time block codes is investigated. The main focus is at the receiver end where two multi-user receiver structures are investigated and compared. The MMSE Front-end turbo receivers of section 3.5 are modified to produce the turbo space-time MIMO-CDMA receivers. The turbo space-time MIMO-CDMA system depicted in Figure 4.6 is considered. The system has K active users, with each kth user's data b_k, of duration T_b, being first encoded by a rate $r = 1/3$ turbo encoder resulting in coded bits d_k.

University of Cape Town

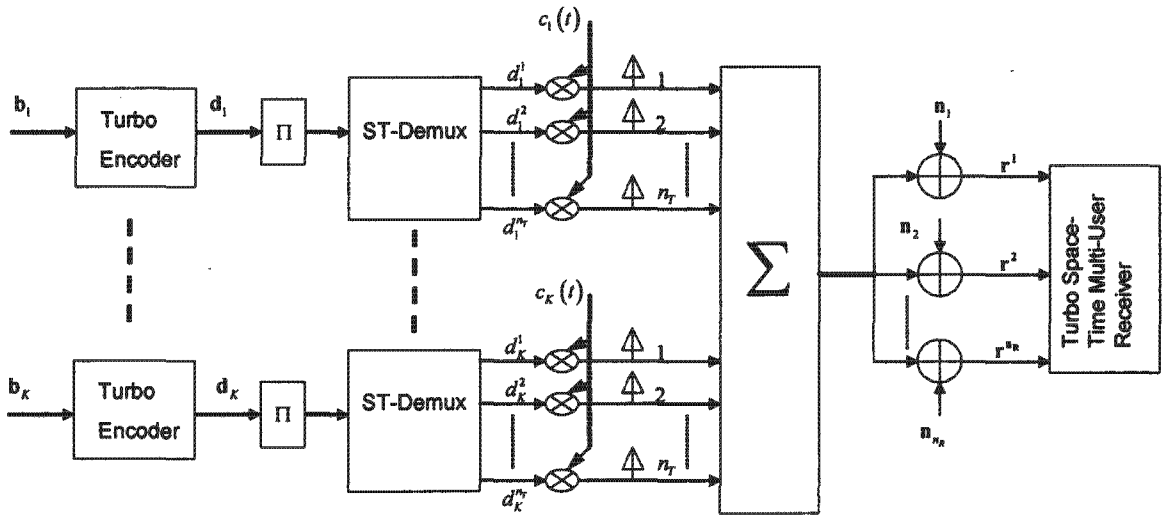

Figure 4.6: *Turbo Space-Time Coded MIMO-CDMA System*

The coded symbols are then passed through the channel interleaver. All the interleaved data is demultiplexed by the Space-Time Demultiplexer (ST-Demux), into sub-streams. For the *k*th user, the demultiplexed symbols are then spread before transmission using that user's spreading sequence c_k of duration T_c. All sub-streams are BPSK modulated. Each user transmits its sub-stream through n_T transmit antennas. The transmitted data per symbol time can be described as:

$$\mathbf{d} = \left[\mathbf{d}_1, \mathbf{d}_2, \cdots, \mathbf{d}_K\right] \tag{4.32}$$

where

$$\mathbf{d}_k = \left[d_k^1, d_k^2, \cdots, d_k^{n_T}\right] \tag{4.33}$$

Each transmit antenna has an average transmitter power of $\left(B_k^m\right)^2$ where $\left(B_k\right)^2$ is the *k*th user's overall average power. It is assumed that all transmit antennas have equal transmit power of:

$$B_k^m = \frac{B_k}{\sqrt{n_R}} \tag{4.34}$$

University of Cape Town

Channel

All the n_T transmitted data streams for all K users are combined during the wireless transmission process. A synchronous Rayleigh flat fading uplink MIMO-CDMA channel is considered.

4.5.1 Turbo Space-Time Multi-user Receivers[3]

The received signal on the η th receiver antenna is given by:

$$r_\eta(t) = \sum_{k=1}^{K} \sum_{m=1}^{n_T} c_k(t) H_k^{\eta,m} \frac{B_k}{n_T} d_k^m + n_\eta(t) \tag{4.35}$$

As in previous sections, $c_k(t)$ is the kth user's spreading sequence and $n_\eta(t)$ is the AWGN on the η th receiver antenna.

Here $H_k^{\eta,m}$ represents the fading factor from the kth user's mth antenna to the η th receiver antenna. To facilitate the expressing of (4.35) in discrete-form, we express $\mathbf{H}$ as a $Kn_R \times Kn_T$ diagonal matrix whose elements are the sub-matrix $\mathbf{H}_k$:

$$\mathbf{H} = diag\left[\mathbf{H}_1, \mathbf{H}_2, \cdots, \mathbf{H}_K\right] \tag{4.36}$$

$$\mathbf{H}_k = \begin{bmatrix} H_k^{1,1} & H_k^{1,2} & \cdots & H_k^{1,n_T} \\ H_k^{2,1} & H_k^{2,2} & \cdots & H_k^{2,n_T} \\ \vdots & \vdots & \vdots & \vdots \\ H_k^{n_R,1} & H_k^{n_R,2} & \cdots & H_k^{n_R,n_T} \end{bmatrix} \tag{4.37}$$

The MIMO-CDMA spreading matrix can be represented by a $Nn_R \times Nn_R$ matrix as:

$$\mathbf{C} = \left[\mathbf{C}_1, \mathbf{C}_2, \cdots, \mathbf{C}_K\right] \tag{4.38}$$

where

$$\mathbf{C}_k = \left[c_k^1, c_k^n, \cdots, c_k^N\right]; \quad n \in \{1, 2, \cdots, N\} \tag{4.39}$$

and

$$c_k^n = diag\left[\underbrace{c_k^n, c_k^n, \cdots, c_k^n}_{n_R}\right] \tag{4.40}$$

[3] The system model in this section follows that of [15].

University of Cape Town

Furthermore the MIMO-CDMA amplitude matrix can be represented by a $Kn_T \times Kn_T$ matrix as:

$$\mathbf{B} = diag\left[\mathbf{B}_1, \mathbf{B}_2, \cdots \mathbf{B}_K\right] \tag{4.41}$$

where

$$\mathbf{B}_k = diag\left[\underbrace{\frac{B_k}{\sqrt{n_R}}, \frac{B_k}{\sqrt{n_R}}, \cdots, \frac{B_k}{\sqrt{n_R}}}_{n_T}\right] \tag{4.42}$$

The discrete-time representation of the received signal is expressed in the conventional matrix form as:

$$\mathbf{r} = \mathbf{CHBd} + \mathbf{n} \tag{4.43}$$

4.5.2 MMSE Space-Time Receiver for MIMO-CDMA

The MMSE receiver of Section (MMSE) is extended to the turbo coded space-time MIMO-CDMA system. Figure 4.7 shows the structure of this receiver.

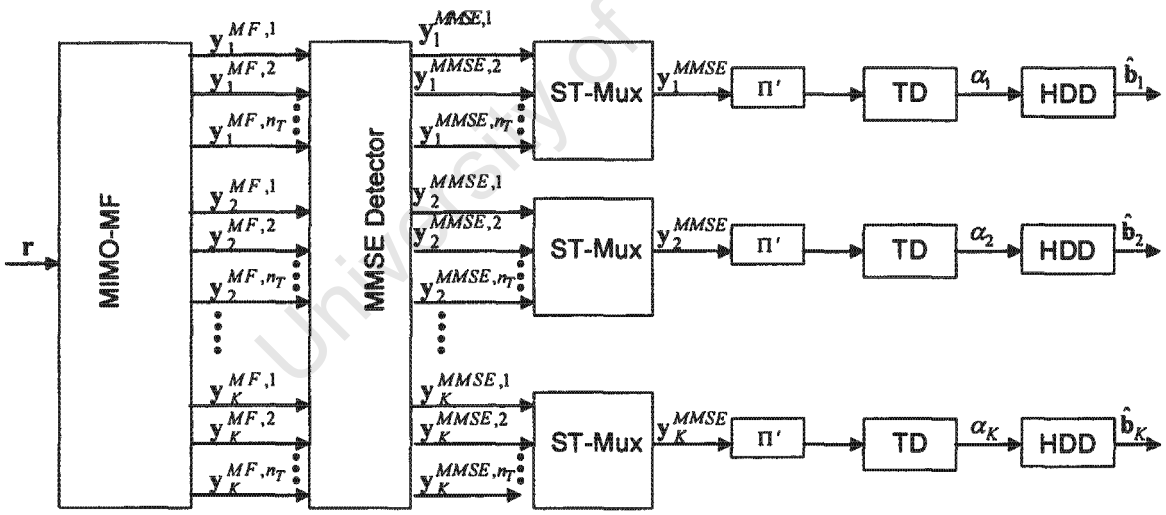

Figure 4.7: *MMSE turbo receiver for MIMO CDMA system*

Each of the n_R receiver antennas is responsible for capturing of the transmitted signals from the fading channel. The received signals are combined and dispread by a bank of

University of Cape Town

MF, as described in Section 3.2. The bank of MIMO MFs will be matched to the corresponding user's signature waveform and also to the fading factors for all receiver antennas. The Maximum Ratio Combining (MRC) technique is used to combine all the MF outputs [2], [33 pages 823-825]. This combining and dispreading process will be repeated for all n_T transmit antennas.

The MIMO MF output is written as:

$$\begin{aligned}\mathbf{y}^{MF} &= \mathbf{B}\mathbf{H}^{H}\mathbf{C}^{T}\mathbf{r} \\ &= \mathbf{B}\mathbf{H}^{H}\mathbf{R}\mathbf{H}\mathbf{B}\mathbf{d}+\mathbf{z}\end{aligned} \tag{4.44}$$

where $\mathbf{H}, \mathbf{C}$ and $\mathbf{B}$ are given by (4.36),(4.38) and (4.41) respectively

and

$$\mathbf{R} = \mathbf{C}\mathbf{C}^{T} = \left\{R_{k,j}\right\}; \quad k, j \in [1,2,\cdots K] \tag{4.45}$$

$$R_{k,j} = diag\underbrace{\left[\rho_{k,j}, \rho_{k,j}, \cdots, \rho_{k,j}\right]}_{n_R} \tag{4.46}$$

Where

$$\mathbf{y}^{MF} = \left[\mathbf{y}_1^{MF}, \mathbf{y}_2^{MF}, \cdots, \mathbf{y}_K^{MF}\right]^{T} \tag{4.47}$$

$$\mathbf{y}_k^{MF} = \left[y_k^{MF,1}, y_k^{MF,2}, \cdots, y_k^{MF,n_T}\right]^{T} \tag{4.48}$$

and

$$\mathbf{z} = \mathbf{B}\mathbf{H}^{H}\mathbf{C}^{T}\mathbf{n} \tag{4.49}$$

Where the conventional transpose of matrix $\mathbf{x}$ is represented by $\mathbf{x}^{T}$ and $\mathbf{x}^{H}$ represents its conjugate transpose (Hermitian conjugate). The inverse of such a matrix is represented as $\mathbf{x}^{-1}$ while its diagonal is denoted by $diag[\mathbf{x}]$.

In Equation (4.48), $y_k^{MF,m}$ represents the *k*th user's MF output for the signal received from transmit antenna *m* given by:

University of Cape Town

$$y_k^{MF,m} = \frac{E_k}{n_R}\chi_{k,k}^{m,m} d_k^m + \frac{E_k}{n_R}\sum_{i\neq n_T}\chi_{k,k}^{m,i} d_k^i + \sum_{\substack{j=0\\ j\neq k}}^{K}\frac{B_k B_j}{n_R}\chi_{k,j}^{m,i} d_j^i + \frac{B_k}{\sqrt{n_R}} n_m \tag{4.50}$$

$\chi_{k,j}^{m,i}$ is the cross-correlation between users k and j due to antennas m and i, given as:

$$\chi_{k,j}^{m,i} = \sum_{\eta=1}^{n_R} H_k^{\eta,m}\rho_{k,j} H_j^{\eta,i} \tag{4.51}$$

The correlation between the kth and jth user is:

$$\chi_{k,j} = \begin{bmatrix} \chi_{k,j}^{1,1} & \chi_{k,j}^{1,2} & \cdots & \chi_{k,j}^{1,n_T} \\ \chi_{k,j}^{2,1} & \chi_{k,j}^{2,2} & \cdots & \chi_{k,j}^{2,n_T} \\ \vdots & \vdots & \vdots & \vdots \\ \chi_{k,j}^{n_T,1} & \chi_{k,j}^{n_T,2} & \cdots & \chi_{k,j}^{n_T,n_T} \end{bmatrix} \tag{4.52}$$

From Equation (4.52) we can structure the combined correlation matrix as:

$$\chi = \{\chi_{k,j}\}; \quad k,j \in [1,2,\cdots,K] \tag{4.53}$$

However, since there is no assumed interference between transmitting antennas of any user, Equation (4.50) reduces to:

$$y_k^{MF,m} = \frac{E_k}{n_R}\chi_{k,k}^{m,m} d_k^m + \sum_{\substack{j=0\\ j\neq k}}^{K}\frac{B_k B_j}{n_R}\chi_{k,j}^{m,i} d_j^i + \frac{B_k}{\sqrt{n_R}} n_m \tag{4.54}$$

From (4.44), the combined correlation matrix can be expressed as:

$$\chi = \mathbf{H}^H \mathbf{R}\mathbf{H} \tag{4.55}$$

The MF output signals, $\mathbf{y}^{MF}$, are fed into the MMSE multi-user-antenna to suppress the MAI. The output of the MMSE multi-user-antenna detector is given by:

$$\mathbf{y}^{MMSE} = \left(\mathbf{B}\chi\mathbf{B} + \sigma^2\mathbf{I}\right)^{-1}\mathbf{BHCr} \tag{4.56}$$

$$\mathbf{y}^{MMSE} = \left[\mathbf{y}_1^{MMSE}, \mathbf{y}_2^{MMSE}, \cdots, \mathbf{y}_K^{MMSE}\right]^T \tag{4.57}$$

and

$$\mathbf{y}_1^{MMSE} = \left[y_k^{MMSE,1}, y_k^{MMSE,2}, \cdots, y_k^{MMSE,n_T}\right]^T \tag{4.58}$$

where $\mathbf{I}$ is a $Kn_T \times Kn_T$ identity matrix.

University of Cape Town

The soft decision of the MMSE detector outputs are multiplexed by the Space-Time Multiplexer (ST-Mux) as shown in Figure 4.7. The multiplexed signal $\mathbf{y}_k^{MMSE}$ is then de-interleaved before it is decoded by the turbo decoder. Here p decoder iterations may be performed before a hard decision is taken on the turbo decoder output. However, the focus of this work is the use of the MMSE space-time receiver in a turbo PIC receiver configuration as introduced in section 3.5.

4.5.3 MMSE Front-end Turbo Space-Time Partitioned Approach Receiver

The MMSE receiver introduced in Section 4.5.2 is combined with the PA receiver structure introduced in Section 3.5.1. The MMSE front-end turbo space-time PA receiver for the MIMO-CDMA system is shown in Figure 4.8.

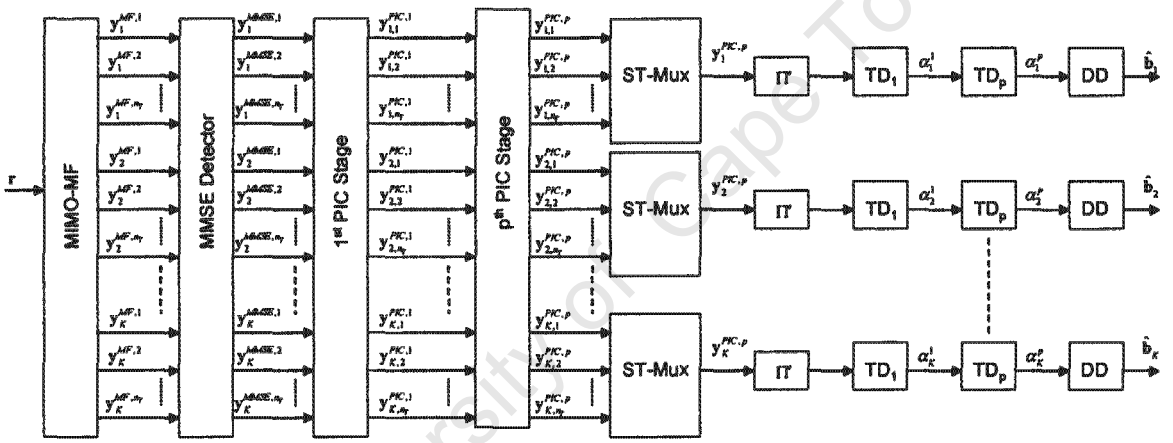

Figure 4.8: *MMSE Front-end Turbo Space-Time PA Receiver Structure*

University of Cape Town

The outputs of the MMSE receiver are passed onto the PIC detector where p IC stages are performed on the multiplexed MMSE output signals $\mathbf{y}_k^{MMSE}$. After p IC stages, the signals $\mathbf{y}_{k,m}^{PIC,p}$ are then multiplexed by the ST-Mux before being de-interleaved.

The PIC detection output after multiplexing is given by:

$$\mathbf{y}^{PIC,p} = \mathbf{y}^{MMSE} - \left(\chi - diag[\chi]\right)\tilde{\mathbf{y}}^{PIC,(p-1)} \tag{4.59}$$

where

$$\mathbf{y}^{PIC,p} = \left[\mathbf{y}_1^{PIC,p}, \mathbf{y}_2^{PIC,p}, \cdots, \mathbf{y}_K^{PIC,p}\right]^T \tag{4.60}$$

$$\mathbf{y}_k^{PIC,p} = \left[y_{k,1}^{PIC,p}, y_{k,2}^{PIC,p}, \cdots, y_{k,n_T}^{PIC,p}\right]^T \tag{4.61}$$

4.5.4 MMSE Front-end Turbo Space-Time Iterative Approach Receiver

The MMSE receiver introduced in Section 4.5.2 is again combined with the IA receiver structure in Section 3.5.2. The MMSE front-end turbo space-time IA receiver structure is shown in Figure 4.9.

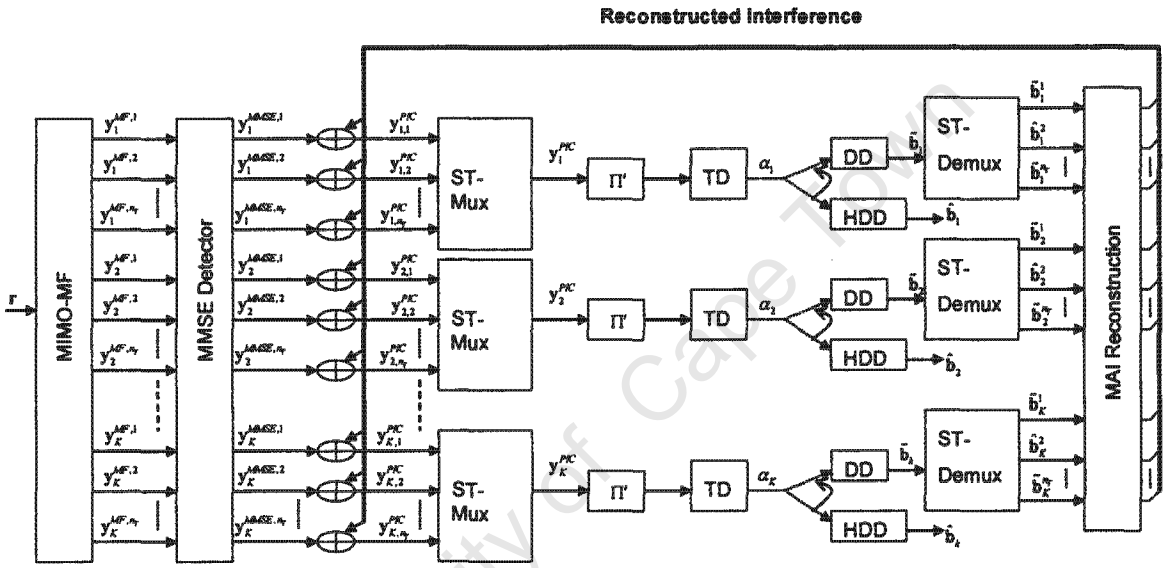

Figure 4.9: *MMSE front-end turbo Space-Time IA receiver structure*

The PIC estimates the signal interference present on the received signal by reconstructing it from the data estimates d_j^l and the cross-correlation values $\chi_{k,j}^{m,i}$ and removing it from the MMSE output signal (Note: on the first iteration there will be no reconstructed estimates of the signal interference).

The output of the PIC detection process is given by:

$$\mathbf{y}^{PIC} = \mathbf{y}^{MMSE} - \mathbf{B}\left(\chi - diag\left[\chi\right]\right)\mathbf{B}\tilde{\mathbf{d}} \tag{4.62}$$

where:

University of Cape Town

$$\mathbf{y}^{PIC} = \left[\mathbf{y}_1^{PIC}, \mathbf{y}_2^{PIC}, \cdots, \mathbf{y}_K^{PIC}\right]^T \tag{4.63}$$

$$\mathbf{y}_k^{PIC} = \left[y_{k,1}^{PIC}, y_{k,2}^{PIC}, \cdots, y_{k,n_T}^{PIC}\right]^T \tag{4.64}$$

The resultant signal $\mathbf{y}^{PIC}$ is expected to have improved, after the reconstructed interference is subtracted from the $\mathbf{y}^{MMSE}$ signal. This signal is multiplexed and fed into the turbo decoder. A soft decision is taken on the decoded signal (which consists of both information and parity LLR values). These data estimates are demultiplexed by the ST-Demux to recover the space-time MIMO-CDMA form.

These demultiplexed data estimates are used in the MAI reconstruction process. The reconstructed interference is subtracted from the $\mathbf{y}^{MMSE}$ signal on the next iteration. This iterative process is repeated for p iterations.

4.6 Numerical Results

In this section we consider the simulated performance of a synchronous turbo coded DS-CDMA system that employs an MMSE front-end turbo space-time multi-user detector at reception. The communication model considered consists of K active users that transmit simultaneously and synchronously through a Rayleigh fading channel. Monte Carlo simulations are used to obtain the performance of the turbo receivers. The receivers all assume perfect knowledge of the CSI. The maximum number of active system users is $K = 15$ and each user transmits an information frame size of $L_{in} = 1024$ data bits. The FEC code used is a rate $r = 1/3$ turbo code with a component encoder with generator polynomial $(7,5)_{octal}$. All spreading codes are of length $N = 15$ and are generated in a pseudo-random manner for each user.

The uplink of the above system is considered with a maximum of 2 transmit antennas at the mobile station and a maximum of 2 receive antennas at the base station.

University of Cape Town

4.6.1 Performance of a simulated PA receiver

In these simulated performance graphs, a combination of 4 multi-user iterations and 4 turbo decoder iterations are applied in the PA receiver structure.

Figure 4.10 shows the BER performance of the PA receiver as a function of the SNR for a $K = 5$ user system with different diversity levels being investigated. The performance for these graphs is evaluated over four combined iterations.

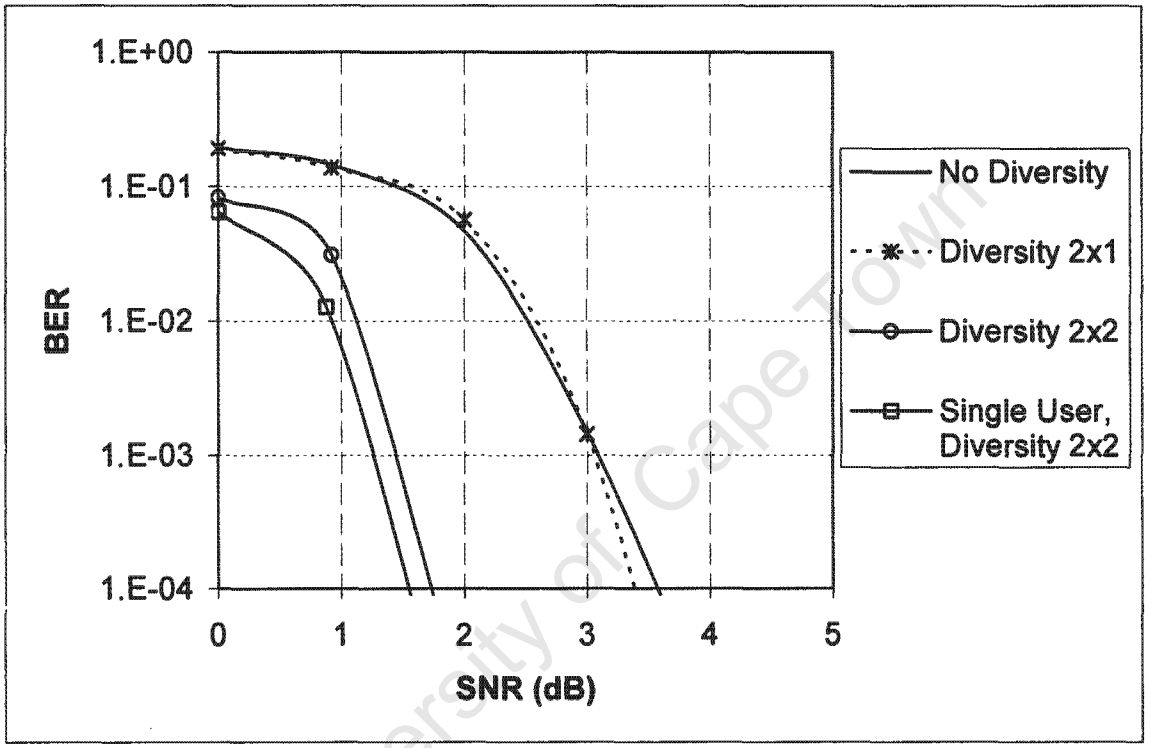

Figure 4.10: *PA receiver BER vs. SNR Performance with diversity for a system with 5 active users*

From the no diversity curve, it can be observed that the PA receiver does effectively cancel the MAI, but due to channel fading, there cannot be any further performance gains attainable. As the diversity levels are increased from 2x1 to 2x2 considerable performance improvements are observed owing to the suppressing of the effects of the fading by the STBC technique.

University of Cape Town

Figure 4.11 shows the BER vs. SNR performance curves for a $K = 5$ users system as the number of PA receiver iterations are varied from 1 to 4. These results are evaluated for a 2x2 diversity system.

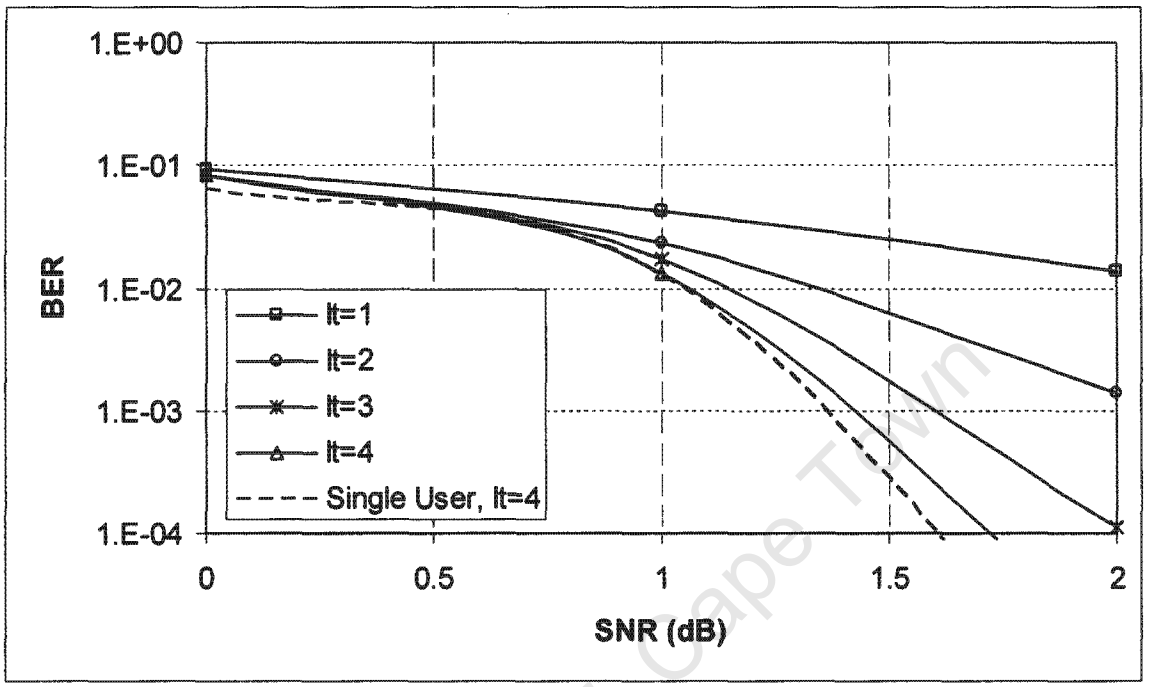

Figure 4.11: *PA receiver BER vs. SNR Performance as a function of number of iterations for a 2x2 diversity system with 5 active users*

As the number of receiver iterations increases to 4, it can be seen that the system still has considerable gains to achieve and approaches the single user performance.

Figure 4.12 shows the BER vs. SNR performance curves for a $K = 5$ users system as the diversity level is varied. The performance of the single-user CDMA system over the Rayleigh fading channel for 1x1 and 2x2 diversity levels is also given for comparative purposes. The performance for all graphs is evaluated over four receiver iterations.

University of Cape Town

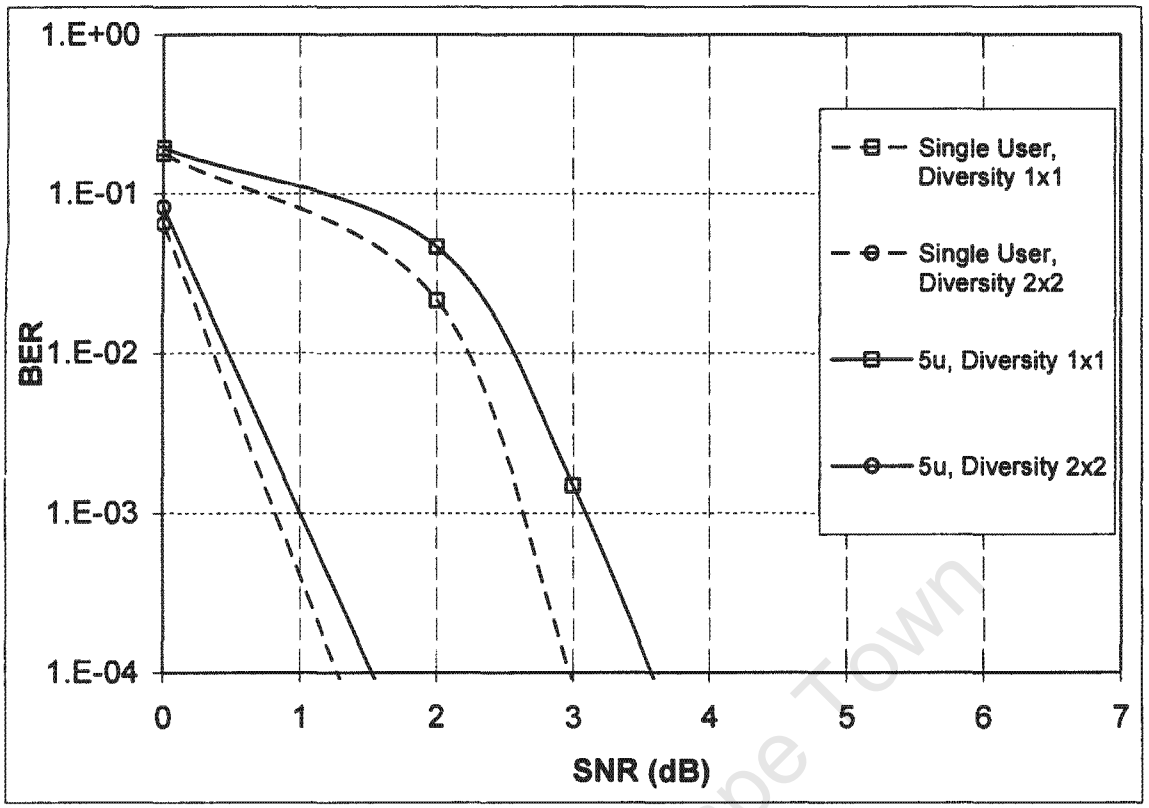

Figure 4.12: *PA receiver BER vs. SNR performance for a 5-user system with varying number of diversity levels*

From Figure 4.12 similar observations can be made as in Figure 4.10 and Figure 4.11 where we observe that the PA receiver effectively cancels the MAI as after 4 iterations the 5 user system approaches that of the equivalent single user performance. This improvement though seems to be limited by the channel fading, thus by applying the 2x2 diversity system the performance of the PA receiver system improves, where we observe that the 5 user curves seem to converge towards the single user performance.

4.6.2 Performance of a simulated IA receiver

Similar simulations to those for a PA receiver in section 4.6.2 are presented here for an IA receiver. However as discussed in section 4.5.4 we perform 4 joint cancellation stages in the case of an IA receiver. The performance of a $K = 5$ users system with different diversity levels evaluated over four iterations is shown in Figure 4.13.

University of Cape Town

Similar observations to the equivalent PA receiver performance can be made. From the no diversity curve, it can be observed that the IA receiver effectively cancels the MAI, and again due to channel fading, there cannot be any further performance gains attainable. As the diversity levels are increased from 2x1 to 2x2 considerable performance improvements are observed owing to the suppressing of the fading effects by utilizing the STBC technique. In the IA receiver, we note a sizable performance gain from the no diversity curve to the 2x1 diversity curve, an observation which could not be made for the PA case.

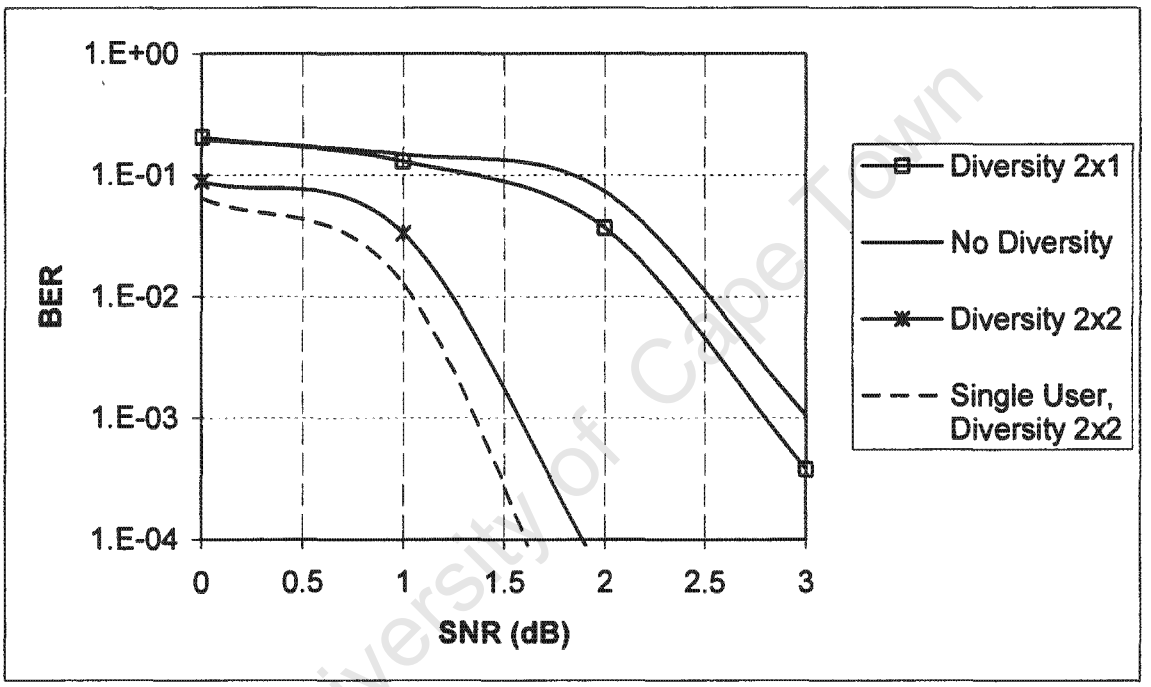

Figure 4.13: *IA receiver BER vs. SNR Performance for a 5-user system with diversity*

From Figure 4.14 it can be noted that as the number of receiver iterations increases to 4, considerable gains are achieve by the 5 user system and it can be imagined from the curves that further improvements can be attained with an increased number of iterations thus edging even closer to the single user performance.

University of Cape Town

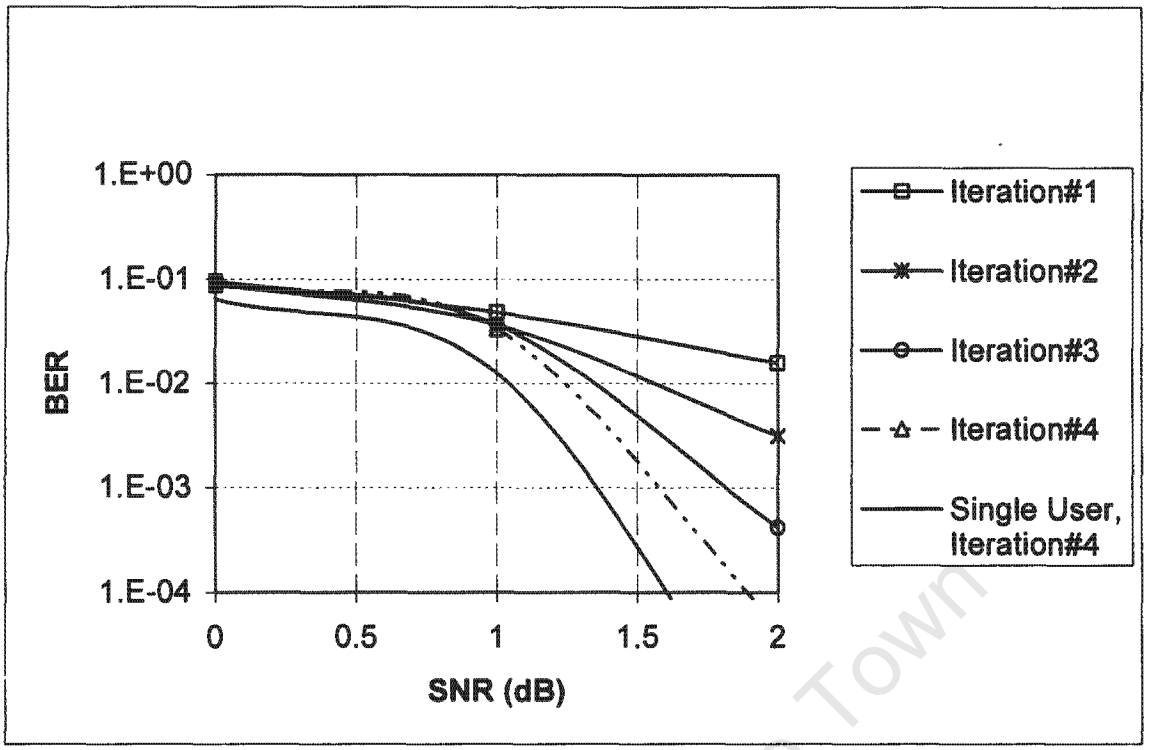

Figure 4.14: *IA receiver BER vs. SNR Performance as a function of the number of iterations for a 2x2 diversity system with 5 active users*

University of Cape Town

4.6.3 Comparison on simulated PA and IA receiver performances

For each approach we perform four iterative cancellation stages (or joint cancellation stages in the case of IA) thus giving a fair comparison, in terms of complexity, between the two systems as both are viewed to perform the same number of floating point operations per user per symbol, however in-depth complexity issues are not discussed in this work.

Figure 4.15 shows the performance comparison of the PA and IA receivers over four receiver iterations for a system with $K = 5$ users. The results show that the IA achieves marginal gains in 4 iterations and reaches a BER of 10^{-3} at SNR of 1.4dB while the PA receiver maintains the same performance at an SNR value of 1.6dB for the 2x2 diversity system. The IA advantage in terms of capacity for low loaded systems seems to be very marginal. This observation holds even for the case of a no diversity system.

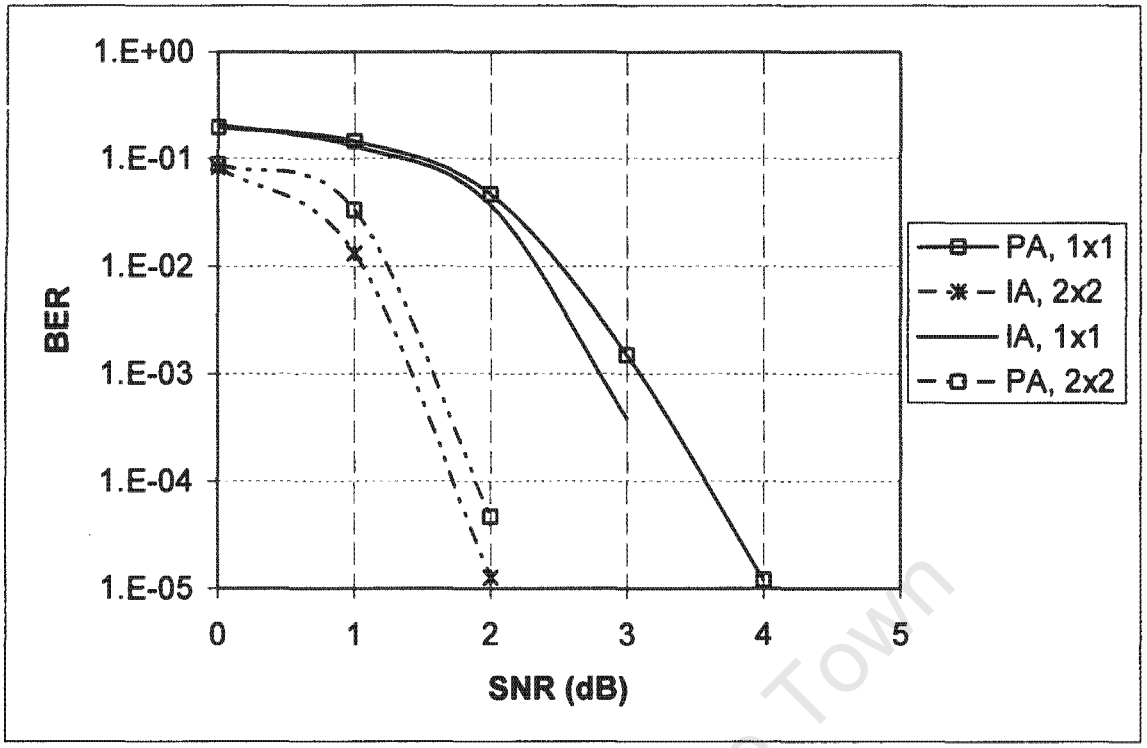

Figure 4.15: *Performance of PA and IA schemes as a function of BER per SNR for a system with 5 active users*

However as the system load increases, the performance gains of the IA receiver become more obvious as indicated in Figures 4.17 – 4.19. These graphs show the capacity performance of both IA and PA receivers in no diversity and 2x2 diversity system configurations evaluated over four receiver iterations. Depending on the diversity configuration employed, it can be noted that the IA receiver maintains a capacity gain of about 5 more users over the PA receiver for a BER performance of 10^{-3} at an SNR value of 2dB and 3dB for the 2x2 and no diversity system configurations, respectively.

University of Cape Town

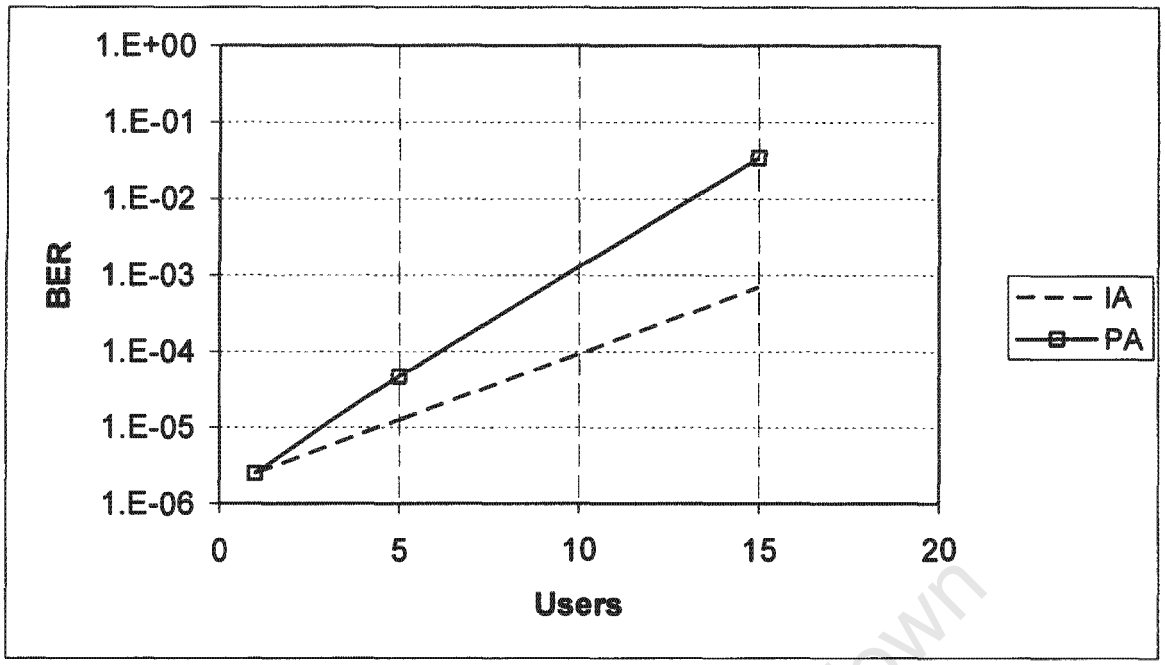

Figure 4.16: *IA and PA system capacity comparison for a 2x2 system configuration at SNR=2dB*

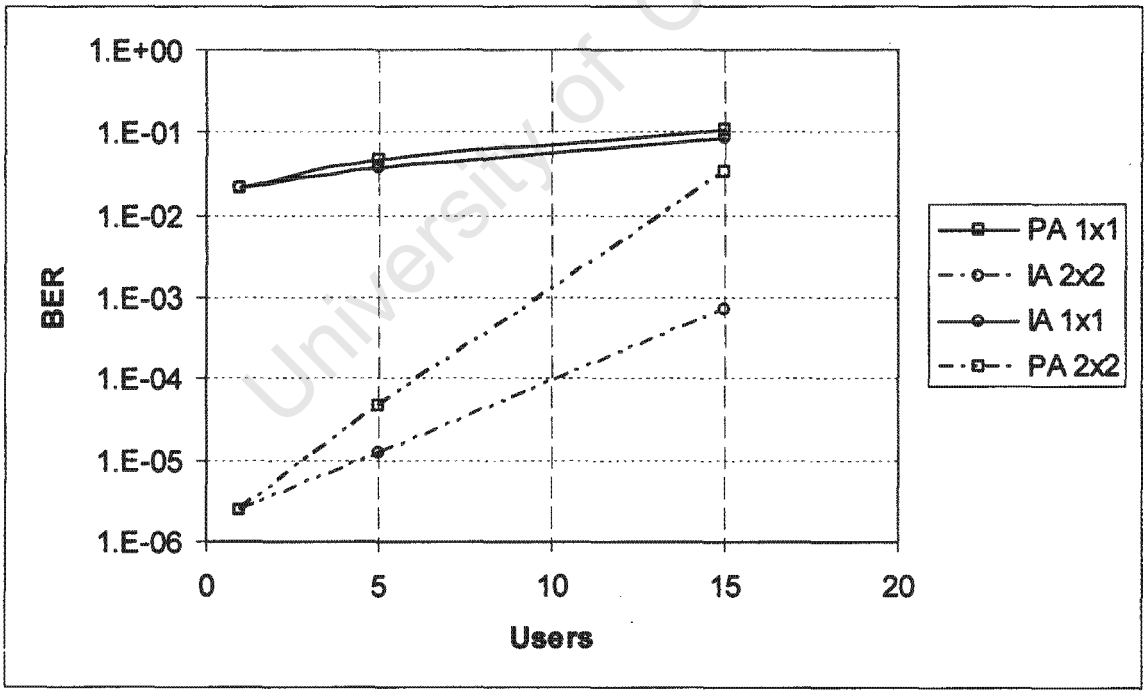

Figure 4.17: *IA and PA system capacity comparison for a 1x1 and 2x2 system configuration at SNR=2dB*

University of Cape Town

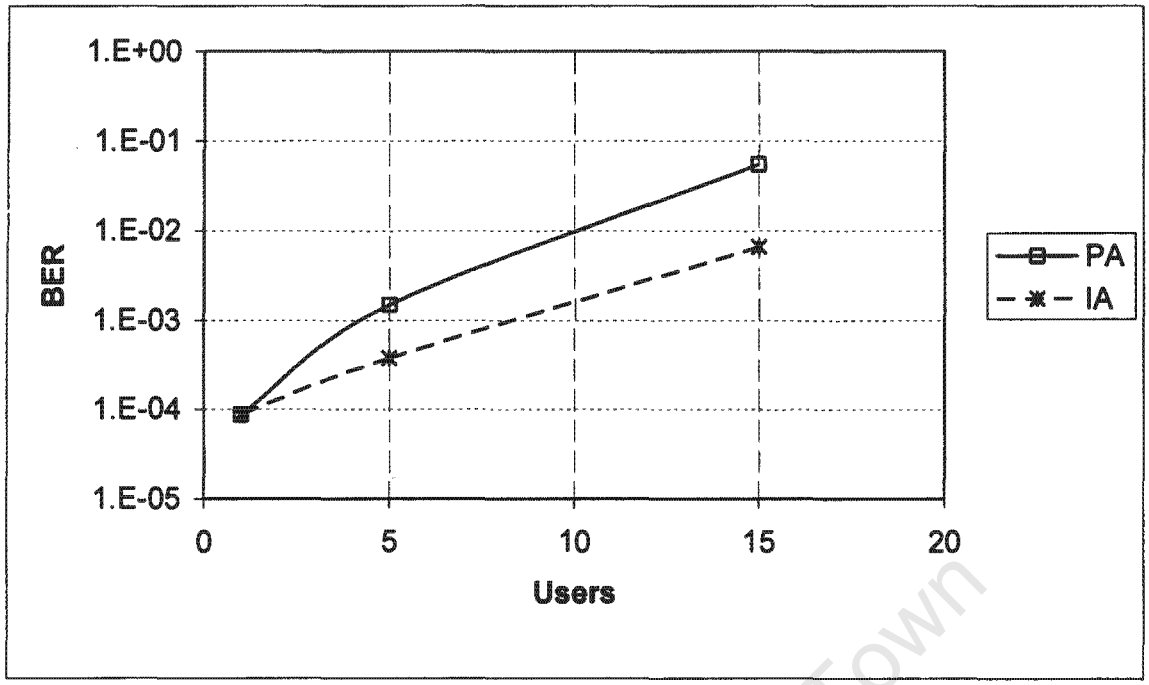

Figure 4.18: *IA and PA system capacity comparison for a 1x1 system configuration at SNR=3dB*

A more in-depth look into the performance of both PA and IA receivers as a function of the number of iterations is shown in Figure 4.19. It can be observed that for highly loaded systems, the PA receiver reaches an error floor just under a BER of 10^{-1} and no amount of additional iterations can improve the performance of this receiver. In contrast, a highly loaded system performance of the IA receiver reveals that more performance improvement is attainable with an increase in the number of iterations.

University of Cape Town

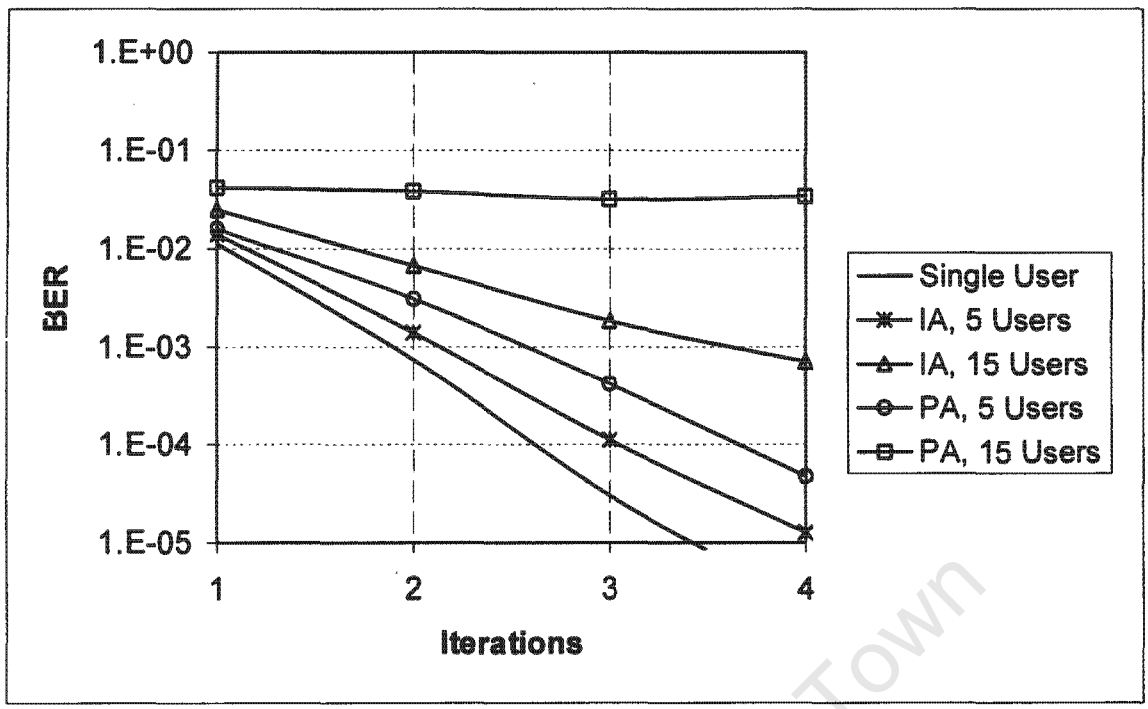

Figure 4.19: *Performance of PA and IA schemes as a function of BER per iteration for a 2x2 diversity system at SNR=4dB*

University of Cape Town

4.7 Summary

In this chapter, two turbo receivers are introduced and are divided into the MMSE front-end turbo space-time partitioned approach receiver (PA) and the MMSE front-end turbo space-time iterative approach receiver (IA). Numerical results reveal that for an equal number of receiver iterations both IA and PA receivers achieve approximately the same performance for a lightly loaded system at any given performance threshold. However as the system load increases the IA starts to gain sizable performance and capacity gains over the PA receiver. The PA receiver is seen to attain no further performance or capacity gains with an increased number of iterations for the case of a highly loaded system. This poor PA performance can possibly be attributed to the poor parity data decoding performance characteristic of turbo codes.

Chapter 5
Turbo Space-Time Receivers with Rate Compatible Punctured Turbo (RCPT) Codes

Contents

5.1 Introduction

In a coded CDMA system, as the system load and data transmitted increases, so does the bandwidth requirement. For a fully-loaded/over-loaded system, the bandwidth required will be $\geq B_{max}$, where B_{max} is the maximum bandwidth available. This strain on the bandwidth required can be relaxed by transmitting fewer bits. Since in the $r = 1/3$ turbo coded system two extra (redundant) bits are transmitted, we can then decide to omit some of the redundant bits in the transmission process.

Higher rate turbo codes can be obtained by puncturing. For example a $r = 1/2$ turbo code can be produced by puncturing one of the parity bits alternately for each data bit – transmit the systematic bits and only the odd indexed parity bits from RSC1 and the even indexed parity bits from RSC2.

If the system load falls to a low value (while still at a higher code rate), then the system becomes bandwidth inefficient as it will only be utilizing B_K bandwidth (where $B_K < B_{max}$), thus the need to lower the system code rate. When multipath fading is considered, the FEC scheme will demand even more bandwidth.

In a conventional application of a communications system the rates of the coding

University of Cape Town

schemes are fixed relative to the acceptable/tolerable error rates for the transmitted data and dependent on the channel characteristics. In a case of fading channels a more adaptive rate would be suitable. This means that the system will chose the most efficient rate, from a set of coding rate schemes, and employ that rate.

Hagenauer [46] introduced Rate Compatible Punctured Convolutional (RCPC) codes, which were formed from a rate $r = 1/M$ parent convolutional encoder. In [47] the RCPC scheme is expanded to consider turbo codes, thus forming RCPT codes. RCPT codes can provide higher throughputs above the $1/M$ rate of the parent encoder. This is done by systematically excluding some code symbols during the transmission process. As more and more code symbols are excluded, the throughput of the system increases [48], however the increased puncturing of more bits expectably results in BER performance degradation. Below we describe the RCPT encoding and decoding as introduced in [47].

5.2 Rate Compatible Punctured Turbo Codes

Encoding

The RCPT encoder will turbo encode the input data sequence of length L_{in} into a coded sequence of length L_{out}. The length of the coded sequence L_{out}, depends on whether the zero termination bits, (tail-bits) used for trellis termination, are included or not. L_{out} is given as:

$$L_{out} = 3\left(L_{in} + [v-1]\right) \tag{5.1}$$

and

$$L_{out} = 3L_{in} \tag{5.2}$$

where (5.1) considers the presence of the tail-bits, while (5.2) does not. It is apparent that the transmission of the tail-bits results in reduced throughput, but we will include them in this thesis since excluding them in the transmission can result in degradation in the MAP decoder performance and/or increased delay in iterative decoding [47].

University of Cape Town

Figure 5.1 shows the puncturing of turbo codes using a rate $1/M$ RCPT encoder that is formed from $M-1$ equal rate, $r=1/2$, RSC encoders. The constituent RSC encoders are those depicted in Figure 2.4. The frame of L_{out} symbols is partitioned into sub-blocks of L_{in}/P symbols, where P is called the puncturing period. For the $r=1/M$ turbo encoder under consideration, the above partitioning will result in MP total sub-blocks. We thus have M matrices (where $M-1$ are from the parity streams and one is from the systematic stream). Each of these M matrices has P columns (where each column is a sub-block) and L_{in}/P bits per column.

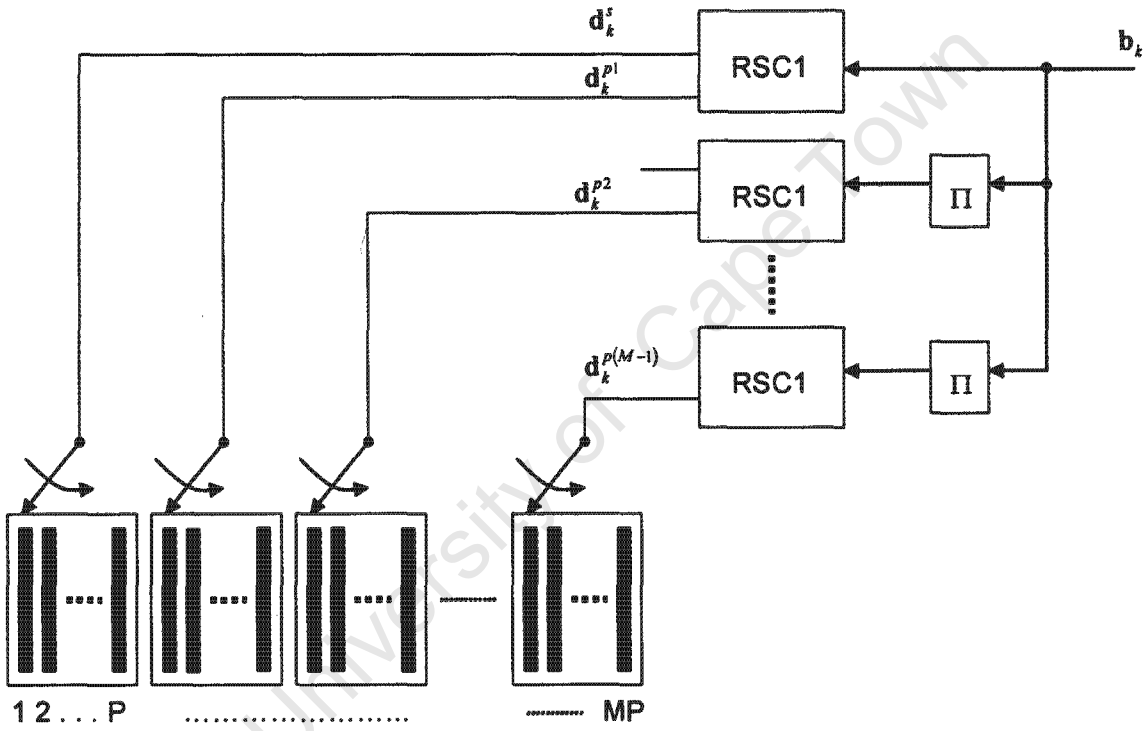

Figure 5.1: *RCPT Encoder Schematic*

These matrices are filled by row and transmitted by column (since a column is a sub-block, then sub-blocks are transmitted).

University of Cape Town

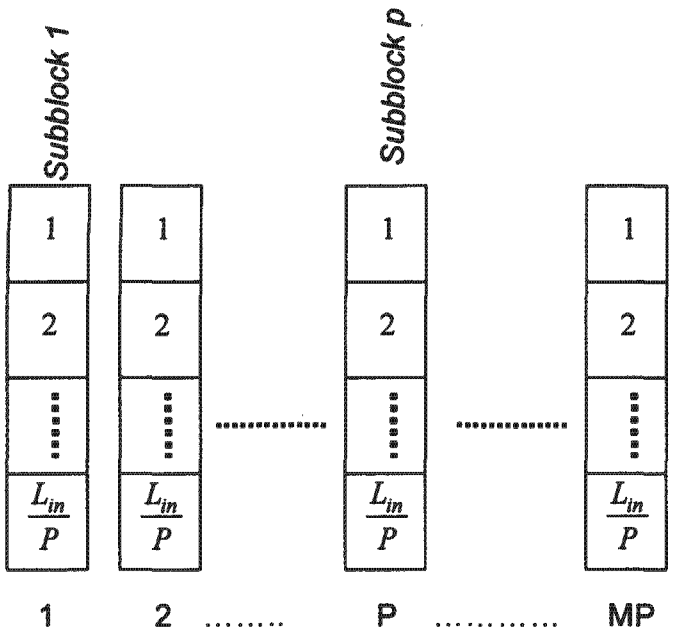

Figure 5.2: *Sub Block illustration*

For a $r = 1/M$ parent encoder, a family of higher rate codes given by:

$$R_l = \frac{P}{P+l}; \qquad l \in \{0,1,\ldots,(M-1)P\} \tag{5.3}$$

These are constructed by employing a $M \times P$ puncturing matrix $\mathbf{P}_M(l)$. This matrix indicates the number of sub-blocks to be transmitted. An entry of 1 in $\mathbf{P}_M(l)$ indicates a column to be transmitted, where the first row of $\mathbf{P}_M(l)$ refers to the systematic matrix and the subsequent rows (i.e. 2 to M) refer to parity matrix from constituent encoders, RSC1 to RSC (M-1). We consider an example of a rate $1/3$ turbo encoder with two rate $1/2$ RSC encoders and a puncturing period $P = 4$.

$$\mathbf{P}_M(2) = \begin{pmatrix} 1 & 1 & 1 & 1 \\ 0 & 0 & 1 & 0 \\ 1 & 0 & 0 & 0 \end{pmatrix} \tag{5.4}$$

University of Cape Town

From the first row of $\mathbf{P}_M(2)$, we note that all $P=4$ columns of systematic bits are sent. From the second row, only the third column of RSC1's parity bits is sent and from the last row, only the first column of RSC2's parity bits is sent. The reader is referred to [47] for a complete list of possible puncturing tables for different turbo code generators, and their derivation.

Worth noting is that [48]:

a) the transmitted frame size will be variable in size, but is lower bounded by L_{in} (when $l=0$) and upper bounded by L_{out} (when $l=(M-1)P$), that is $L_{in} \le L_{trans} \le L_{out}$, where L_{trans} is the number of transmitted bits.

b) to satisfy the lower bound condition in (a), at lest P columns must be sent $(L_{trans} \ge L_{in})$ and to satisfy the upper bound condition, no column must be sent twice $(L_{trans} \le L_{out})$.

Puncturing Tables

Given a puncturing period P and a rate $1/M$ turbo encoder, the authors of [49] devised a scheme for selecting optimal puncturing tables. Optimal tables are those puncturing tables that maximize the system throughput.

Several turbo encoders of varied information size and puncturing period of 4 and 8 were investigated by [49] for their optimal puncturing tables. For their search, they employed a criterion which they dubbed the Average Distance Spectrum (ADS) slope criterion. Thus the term 'optimal puncturing' refers to optimal subject to the ADS slope criterion. A detailed description of the search procedure can be found in [49].

From their search [49] made the following observations

i) for a given encoder and puncturing period, the resulting optimal puncturing tables are not necessarily the same for different information sizes

University of Cape Town

ii) for a given encoder and puncturing period, as the information size increases, the ADS gets better and better

iii) for a given encoder and information size, the ADS for the larger puncturing period $(P=8)$ is almost always better than the ADS for the smaller puncturing period $(P=4)$.

The conclusion in (iii) agrees well with [48] where it was concluded that the $P=8$ scheme is the best performing, this is true because the larger values of P we have, the more degrees of freedom we have in how to implement the puncturing. In [49] the rate 1/3 turbo encoder with generators $(1,33/31)_{octal}$ and $(21/37)_{octal}$ was observed to be the best performing encoder. The optimal puncturing tables results for this encoder with puncturing period $P=8$, are given in Table IV in [49] and is summarised in Table 1 below.

8/9	4/5	8/11	2/3	8/13	4/7	8/15	1/2	8/17	4/9	8/19	2/5	8/21	4/11	8/23	1/3
376	377	377	377	377	377	377	377	377	377	377	377	377	377	377	377
002	002	002	042	052	052	252	252	253	253	253	353	373	373	377	377
001	001	011	011	011	051	051	071	071	073	173	173	173	177	177	377

Table 1: *Puncturing tables (in octal) for turbo encoder with generators* $(1,33/31)_{octal}$ *and* $(21/37)_{octal}$ *for* $P=8$ *and* $L_{in}=1024$

University of Cape Town

The top row of each table indicates the achievable code rates given by $\mathbf{R}_l$, for $l=1,...,P(M-1)$. The next set of $M=3$ rows are the puncturing tables (in octal). This puncturing table represents a binary $M \times P$ matrix.

Decoding

If no parity symbols have been received for two or more RSC encoders, then iterative decoding will not be possible as the corresponding decoders will be excluded in the

iterative process, [47]. In order to take advantage of the iterative MAP decoders, more parity symbols will be transmitted and the possibility of puncturing some of the systematic symbols arises [49].

5.3 Numerical Results

As stated earlier, the main requirements for next generation mobile communication systems is increased capacity and the demand for higher data rates. Battery life is also a great concert thus the implementation of more power efficient transmission/reception schemes is vital. In chapter 3 we investigated possible methods of increasing the system capacity through the use of multi-user detection schemes to mitigate the effects of MAI. Further, in chapter 4 we studied and investigated MIMO techniques as a means of combating the signal degradation experienced in transmission through a wireless communication channel.

Combined MUD and MIMO techniques have shown significant performance improvement over systems that do not utilize turbo space-time multi-user detection. In this chapter we exploit these performance improvements by acknowledging the fact that in more relaxed channel conditions, there is an unnecessarily large amount of redundancy being transmitted in the encoded data, thus introducing the possibility of achieving higher data rates through puncturing the mother code.

In the following section, we investigate the RCPTC scheme based on a rate $r = 1/3$ mother code for a Rayleigh fading channel model. The data bits of each user for the rate $r = 1/3$ encoder are assigned according to the puncturing tables in Table 1 with puncturing period $P = 8$. For performance evaluation purposes we consider values of $l = 2, 8$ and 16 thus giving rates $r = 4/5, 1/2$ and 1/3, respectively.

These code rates are adopted for the two receiver schemes discussed in chapter 4, namely the partitioned approach (PA) and iterative approach (IA) schemes. Since full rate space-

University of Cape Town

time block codes are being used, the overall code rate of both systems in not affected, thus the puncturing pattern used determines the total system code rate. Furthermore, we assume that the effects of puncturing on the overall system complexity are negligible. This assumption can be quantified by reasoning that puncturing merely involves the removal of a subset of the encoded bits, through the pattern defined in Table 1, at transmission and the addition of dummy bits at the receiver end.

Simulations were conducted to investigate the degree of performance degradation due to the implementation of punctured rates $r = 4/5$ and $r = 1/2$ for a single user system with no diversity and also a 2x2 diversity system both which are bench-marked against the rate $r = 1/3$ equivalent system. Throughout this section we use the same system parameters as discussed in section 4.6 and adopt all assumptions accordingly.

Figure 5.3 and Figure 5.4 show the BER performance of a punctured single user system as a function of the SNR for the 1x1 and 2x2 diversity systems, respectively.

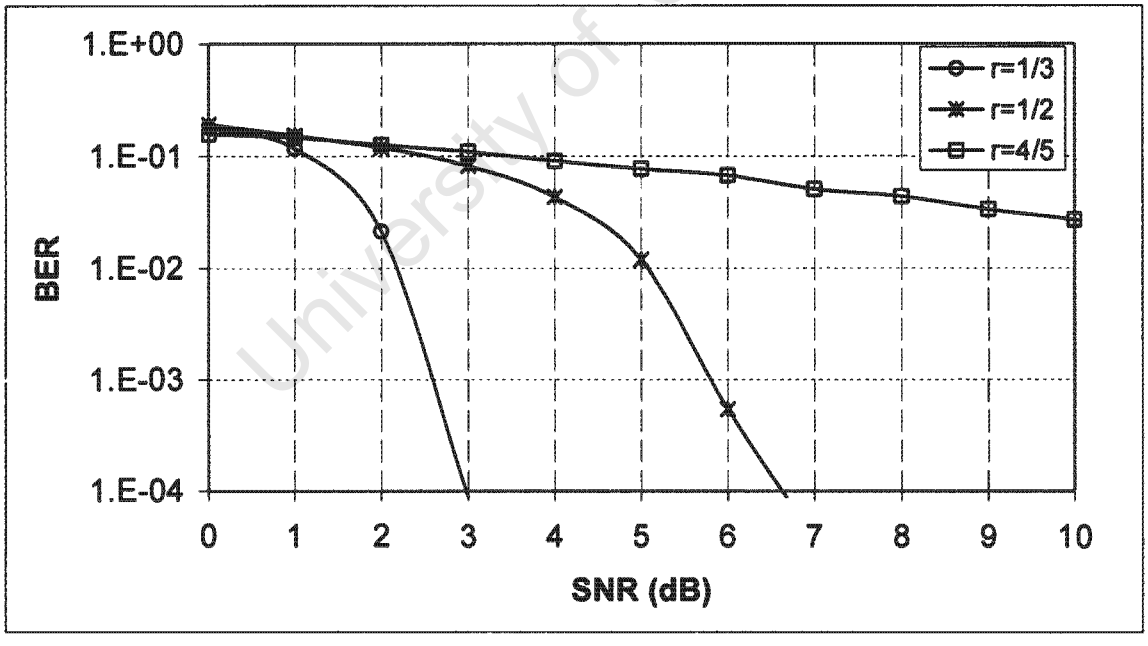

Figure 5.3: *BER vs. SNR performance graph for punctured single user 1x1 diversity system*

University of Cape Town

For a BER performance requirement of 10^{-3}, it is observed that the rate $r=1/3$ system achieves this at an SNR of 2.6dB whilst more power, i.e. 5.8dB, is required for the rate $r=1/2$ system to reach the same performance threshold. The rate $r=4/5$ system, however, does not attain this performance threshold for any of the low power levels in consideration. Therefore, for a no diversity single user system with a stipulated maximum power level of 6dB and a required BER performance of 10^{-3}, puncturing can be used to obtain a data rate increase of 25% and more. However, using code rates much higher than $r=1/2$ will lead to serious performance degradation and failure to meet the system requirements.

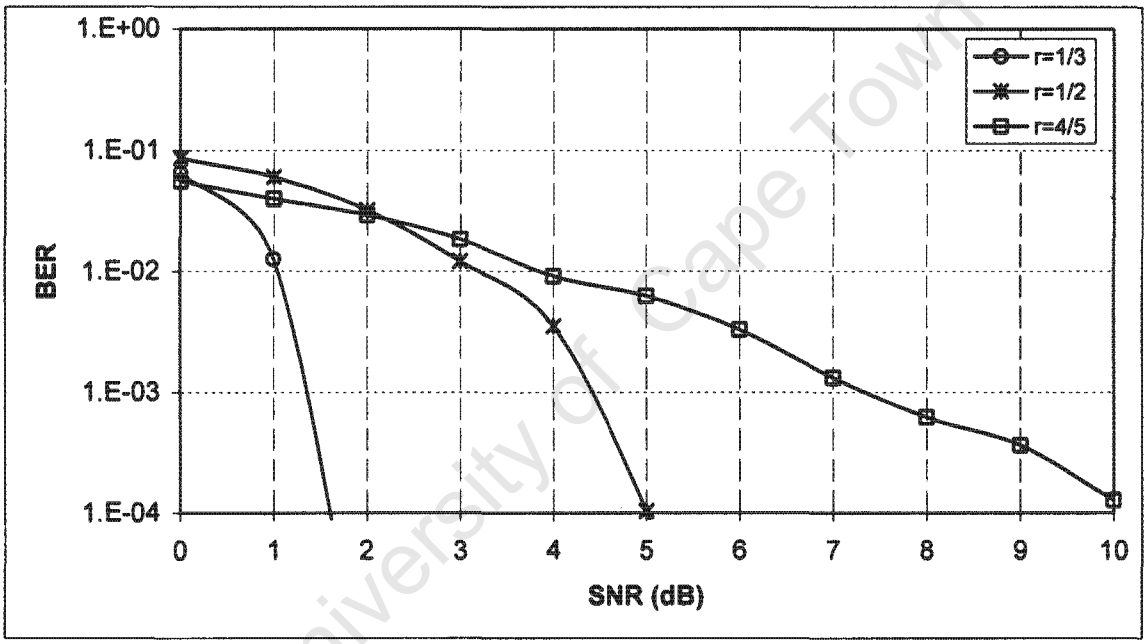

Figure 5.4: *BER vs. SNR performance graph for punctured single user 2x2 diversity system*

In Figure 5.4 it is noted that for a BER performance requirement of 10^{-3} the 2x2 diversity systems attains this threshold at SNR of: 1.4dB for the rate $r=1/3$ system, 4.4 dB for the rate $r=1/2$ and 7.4 dB for the rate $r=4/5$ system. Again, for a system with a stipulated maximum power level of 6dB and a required BER performance of 10^{-3}, It is observed that puncturing can be used to obtain significant data rate increases by utilizing a code rate slightly lower than $r=4/5$ but higher than $r=1/2$. We use Figure 5.5 to

University of Cape Town

explore the exact code rate needed to meet the stipulated system requirements for both no diversity and 2x2 diversity systems.

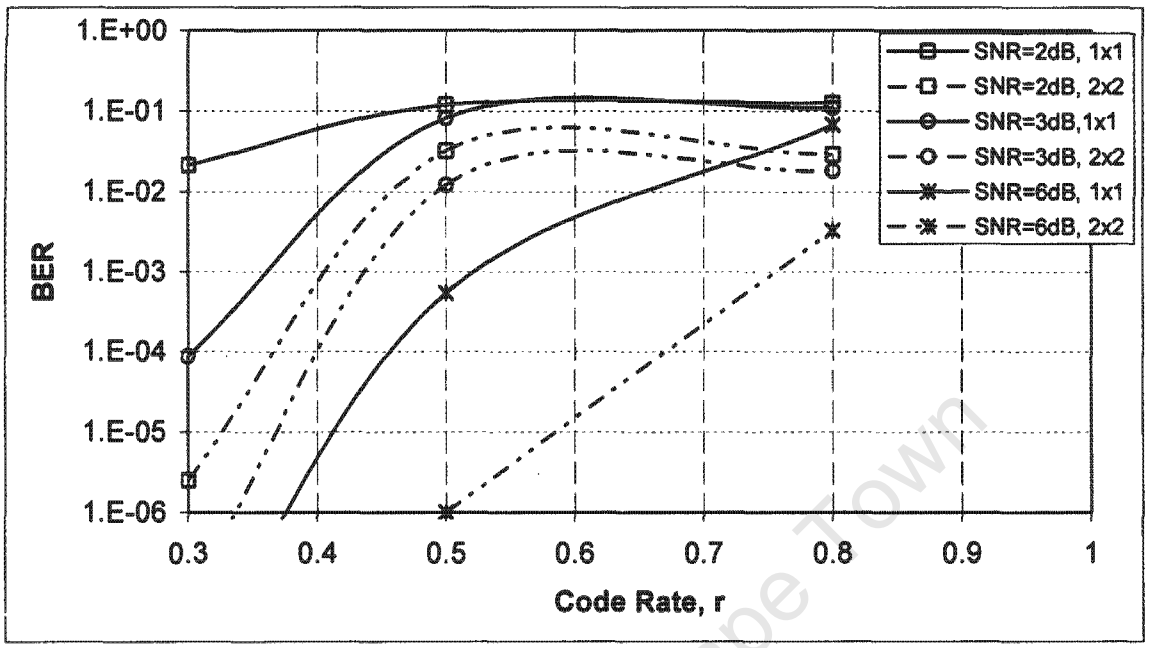

Figure 5.5: *Punctured single user BER performance as a function of the code rate for various power levels*

Figure 5.5 shows the punctured single user BER performance as a function of the code rate for various SNR levels. The following observations are made from Figure 5.5:

- At SNR of 2dB the 1x1 system does not, for any given code rate, achieve the 10^{-3} Performance threshold, i.e. no amount of redundancy can help us achieve this threshold. The 2x2 system however attains the 10^{-3} performance at a rate of 0.4 or less, thus as stated in earlier observations, we achieve a maximum data rate gain of about 25% to that of the no diversity system.
- By increasing the power by 1dB we note that the 1x1 system now achieves 10^{-3} performance at a code rate of $r = 0.36$, indicating that any further puncturing of the mother code can lead to an undesirable loss in performance. The 2x2 system, on the other hand, attains this threshold at a rate of $r = 0.44$, yielding only a slight improvement in terms of achievable data rates as compared to the 2dB 2x2

University of Cape Town

system. This highlights a negligible data rate improvement with a slight increase in power.

- However, by doubling the power to 6dB it can be noted that the earlier stipulated system requirements of a maximum power level of 6dB and a required BER performance of 10^{-3}, can be achieved at a code rate of $r = 0.51$ with the 1x1 diversity system and at a higher code rate of $r = 0.76$ with the 2x2 diversity system.

These investigations are taken further and considered for the multiple users' scenario. Figure 5.6 and Figure 5.7 show the punctured IA receiver BER vs. SNR performance graphs for the K=5 and K=15 user systems, respectively. Simulations are considered for a synchronous system with $N = 15$ for both non diversity and 2x2 diversity turbo coded systems employing an iterative approach detection scheme at reception.

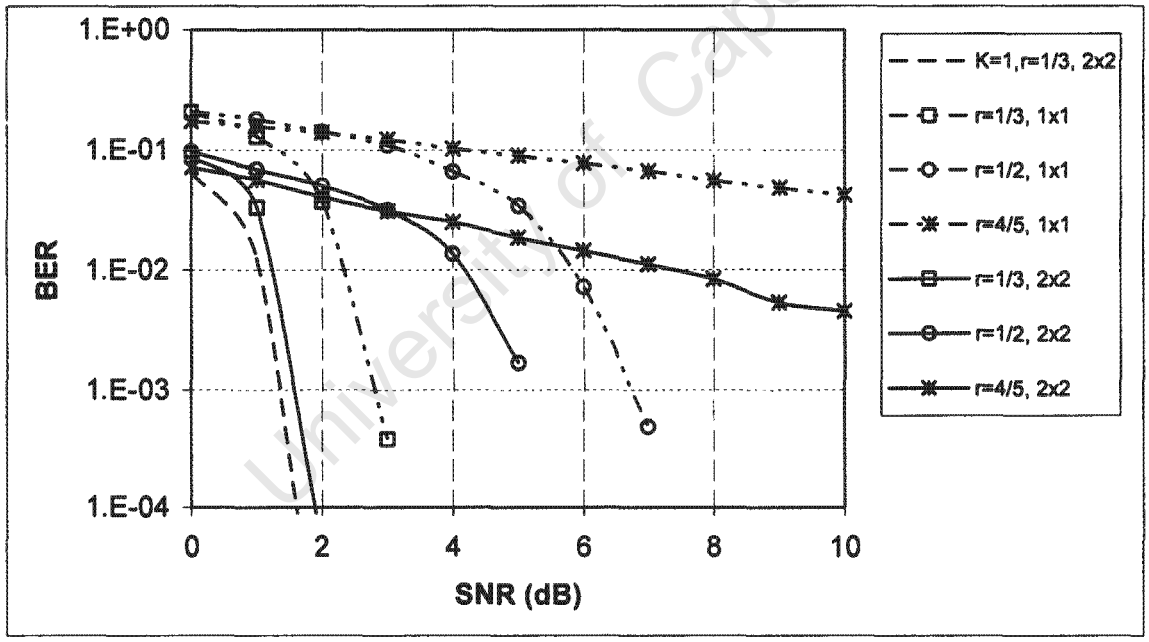

Figure 5.6: *BER vs. SNR performance graph for punctured K=5 users IA system with diversity*

University of Cape Town

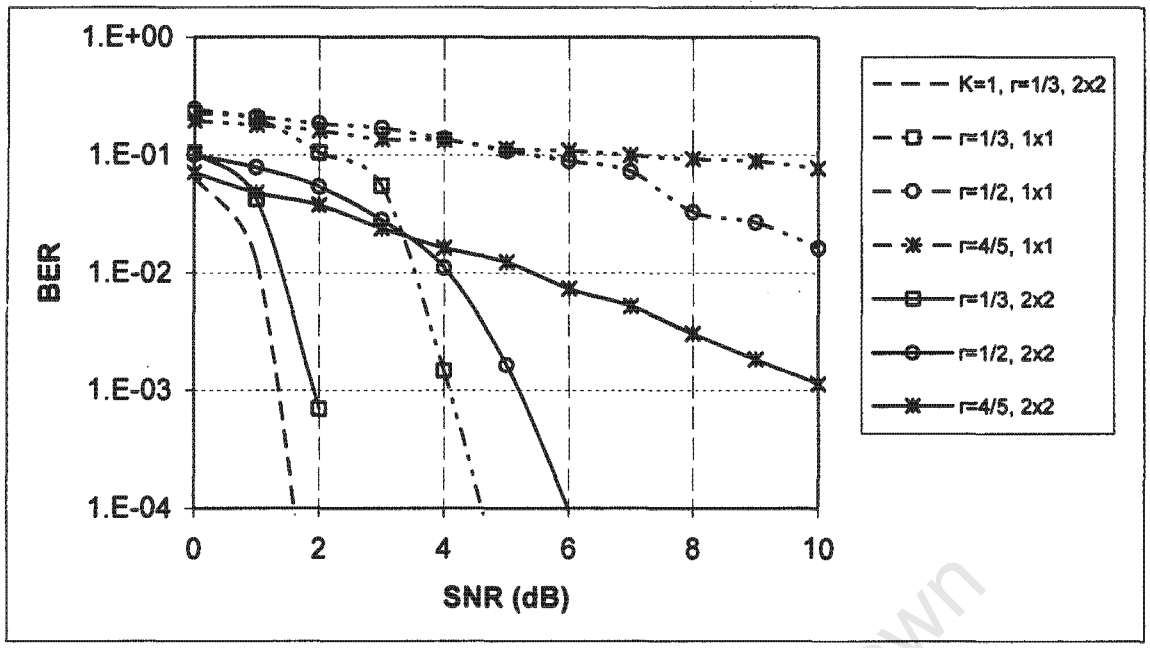

Figure 5.7: *BER vs. SNR performance graph for punctured K=15 users IA system with diversity*

In both graphs there is expected system degradation due to MAI, as discussed in chapter 4. The higher code rate shows a further loss in performance for both the K=5 and K=15 systems.

The effects of increasing the system capacity coupled with an increase in the system code rate can be better observed in Figure 5.8 for the PA system and Figure 5.9 for the IA system.

University of Cape Town

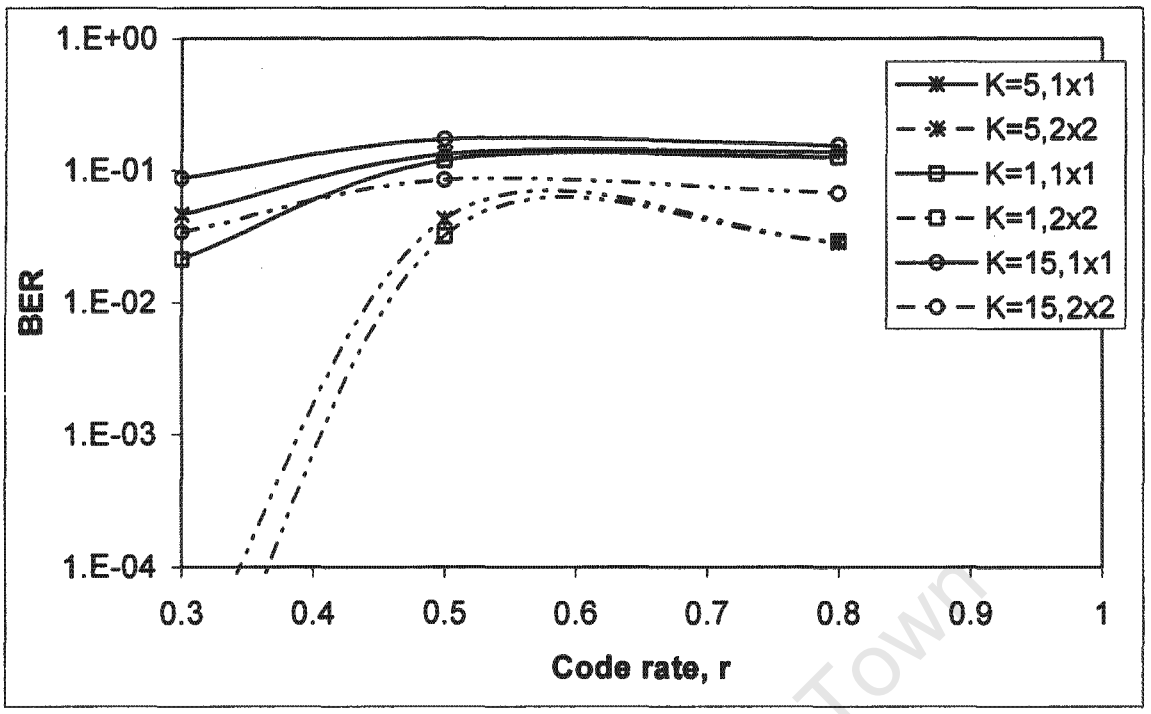

Figure 5.8: *Punctured multiple user BER performance as a function of the code rate at SNR=2dB for PA receiver*

Figure 5.8 shows punctured BER performance as a function of the code rate at SNR=2dB for PA receiver with system loads of K=5 and K=15. The single user performance graphs for both the no diversity and 2x2 diversity systems are also given for comparison reasons. From Figure 5.8, it is clear that at such a low SNR value, the multiple user systems fail to reach the 10^{-3} BER performance threshold for both no diversity and 2x2 diversity systems. This poor performance can, however, be attributed to the choice of receiver used.

Figure 5.9 illustrates the simulated punctured multi-user BER performance as a function of the code rate at SNR=2dB for an IA receiver.

University of Cape Town

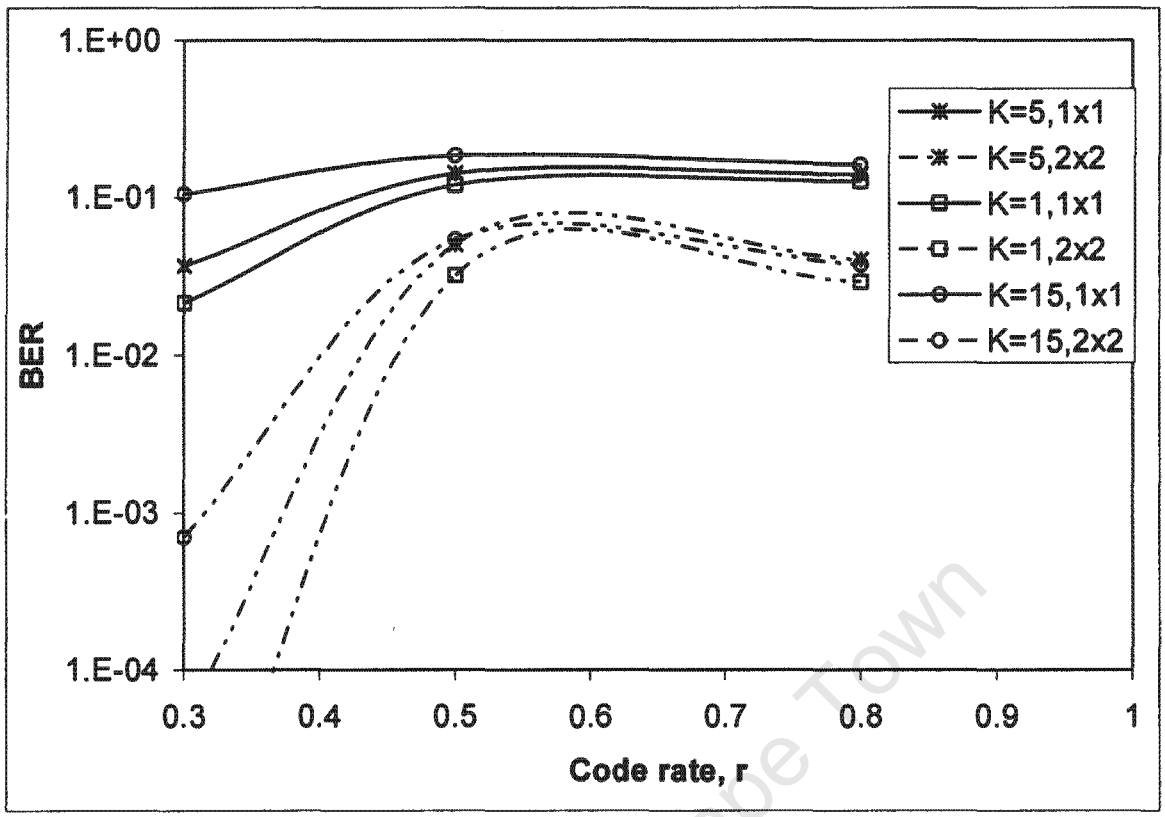

Figure 5.9: *Punctured multiple user BER performance as a function of the code rate at SNR=2dB for IA receiver*

From Figure 5.9, it is observed that the no diversity systems for all system loading values performs similarly to that of the PA receiver and fails to achieve the performance threshold. However as the diversity is increased to 2x2, the IA system performs much better than the PA system, as discussed in chapter 4, and attains the performance threshold at a code rates of $r = 0.39$ and $r = 0.32$ for the K=5 and K=15 systems, respectively. The comparative code rate requirement as a function of system load for both PA and IA systems is shown in Figure 5.10.

University of Cape Town

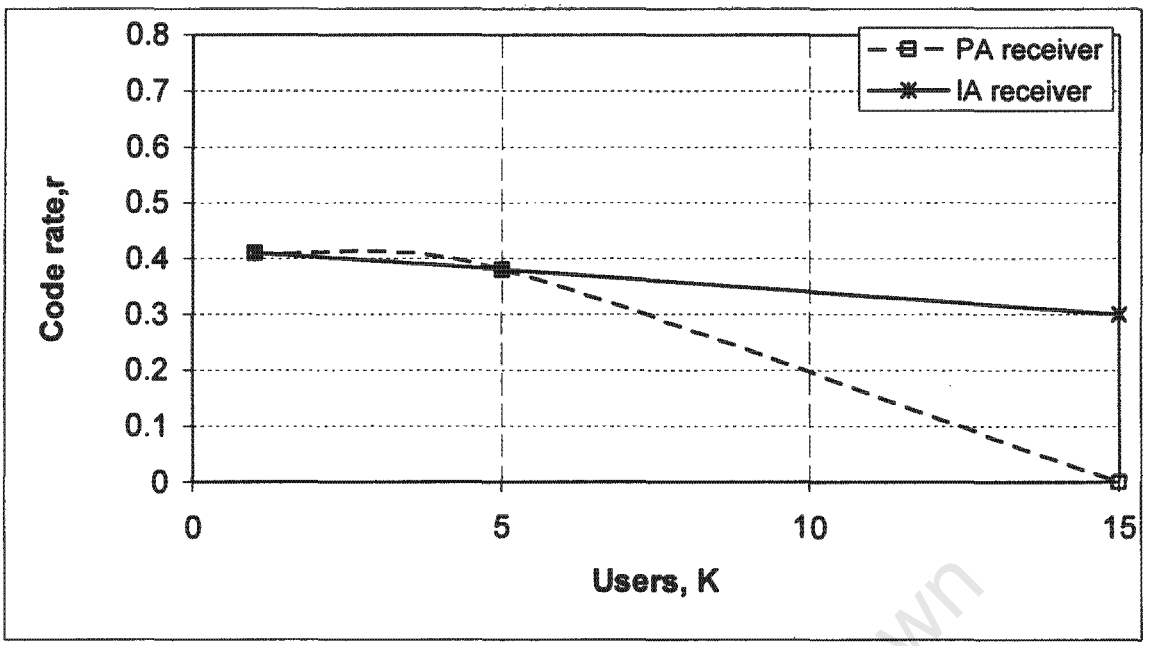

Figure 5.10: *IA and PA graph indicating minimum Code rate required for* 10^{-3} *performance as a function of the system load for a 2x2 diversity system at SNR=2dB*

Figure 5.10 shows the minimum code rate required by both IA and PA systems in order to achieve a BER performance of 10^{-3} in a 2x2 diversity system at SNR value of 2dB. The following observations can be made from Figure 5.10:

- For the IA system, a minimum code rate of $r = 1/3$ is sufficient to attain a BER performance of 10^{-3} at SNR of 2dB for any K users, where $1 \leq K \leq N$.
- For the PA system, no amount of redundancy added to the coded data can achieve the 10^{-3} BER performance at an SNR of 2dB, this is indicated by the code rate of approximately zero.
- The maximum code rate necessary for both systems to achieve the said performance cannot exceed $r = 0.4$.

University of Cape Town

5.4 Summary

Rate compatible punctured turbo codes are investigated in a turbo space-time coded MIMO-CDMA system as a possible way of achieving higher data rates in DS-CDMA uplink. Results show that by using two transmitting antennas and two receiving antennas, the attainable data rate is as high as 25% when compared with the no diversity system. There is, however, a limit to the degree of puncturing that can be done, this limit is generally dictated by the required system performance threshold.

With an increase in SNR, the stipulated system performance can even be attained by using higher code rates, thus significantly increasing the achievable data rates. However, it is observed that as the system load increases the degree of freedom on puncturing becomes greatly reduced. This is attributed to the choice of receiver being employed at reception. The IA receiver is observed to be a better receiver choice than the PA receiver when considering the achievable data rates in a heavily loaded CDMA system.

University of Cape Town

Chapter 6
Conclusion

In this thesis, our aim has been to evaluate the performance of turbo space-time DS-CDMA multi-user detectors with a special emphasis on system capacity and data rates that these receivers can possibly achieve.

The following section summarises the work done in this thesis and highlights all contributions made in this work. We then conclude this chapter by outlining open areas and further research work that can be pursued on this topic.

6.1 Thesis Summary and Contributions

The key concepts from existing literature that form the essence of this thesis are presented and reviewed in chapter 2. The turbo coded DS-CDMA system model for K synchronous users is introduced for the uplink scenario where transmission is observed over both AWGN and Rayleigh fading channels. From this system model, a detailed description of the transmitter, communication channel and receiver are presented. The MAP decoding technique is discussed and its algorithm is explained and the simulated system performance of the said turbo coded system is shown to be consisted with previous work from other researchers for both AWGN and Rayleigh fading channels.

In chapter 3 we evaluate the performance of a matched filter receiver in AWGN channels and it is observed that such a receiver has a capacity limit imposed on it by the MAI. The optimum multi-user detector is introduced to mitigate the effects of the MAI. However due to its computational complexity, it is found to be prohibitive thus sub-optimal schemes are sought. In light of this capacity and complexity limitations, a general review of existing MUD schemes as they are used in combating the MAI that limits the capacity of a CDMA system is undertaken. We then introduce the multi-user detection principle where we divide such detectors into either Partitioned Approach (PA) or Iterative Approach (IA) receivers. The main contribution in this chapter is the application and choice of a turbo multi-user concatenation scheme as a receiver in a turbo coded

University of Cape Town

synchronous DS-CDMA system in an AWGN channel. Simulation results demonstrate that the IA receiver that employs an MMSE detector as its front end provides outstanding capacity gains in comparison to the IA receiver with no MMSE front end and also to the PA receiver with and without an MMSE front end detector. This observation is substantiated since the MMSE receiver balances MAI mitigation with noise enhancement thus has a smooth degradation in performance which when used as the detector front-end gives reliable initial data estimates to the first stage of the detector, thus making all subsequent stages of the detection process more accurate.

MIMO antenna techniques are introduced in chapter 4 as a means of suppressing channel fading. The Turbo space-time MIMO-CDMA system model and two turbo receivers are introduced and these are divided into the MMSE front-end turbo space-time partitioned approach receiver (PA) and the MMSE front-end turbo space-time iterative approach receiver (IA). A comparative study of these two receiver structures through simulations reveals that for an equal number of receiver iterations both IA and PA receivers achieve about the same performance for a lightly loaded system at any given performance threshold. However as the system load increases the IA receiver starts to gain sizable performance and capacity gains over the PA receiver. The PA receiver is seen to attain no further performance or capacity gains with an increased number of iterations for the case of a highly loaded system. These results show that the IA receiver is more robust and yields more performance gains with an increasing number of iterations, for all system load levels.

In chapter 5 the use of RCPT codes in turbo space-time coded MIMO-CDMA systems for the uplink scenario is considered. Performance results for the punctured multiple user systems in Rayleigh fading channels are evaluated for both the PA and IA receiver schemes with diversity and no-diversity considerations. Simulation results show that by using two transmitting antennas and two receiving antennas, data rates higher than the no-diversity system can be achieved. It is observed that there is a limit to the degree of puncturing that can be performed; this limit is generally dictated by the required system performance threshold. Further simulation results indicate that with an increase in SNR, a

University of Cape Town

stipulated system performance can generally be attained by using higher code rates, thus significantly increasing the achievable data rates. However, it is observed that as the system load increases the degree of freedom on puncturing becomes greatly reduced. This however is attributed to the choice of receiver being used at reception and the IA receiver is found to be a better receiver choice than the PA receiver when considering the achievable data rates in heavily loaded CDMA systems.

6.2 Suggestions for Future Work

An extensive study of iterative space-time multi-user detection schemes for synchronous DS-CDMA systems for both AWGN and Rayleigh fading channels has been done in this thesis. However, there are still open areas and possible further research work that can be undertaken. Below we highlight suggestions about future work based on this thesis:

- For simplicity, we assume synchronous transmission throughout this thesis. However, in practice all system users will each transmit at different time intervals, thus asynchronous transmission considerations could possible yield different results to those of synchronous transmission.
- Partitioned and Iterative approach receivers in frequency selective channels. It is anticipated that the receiver structure will be considerably different.
- The receivers under study are assumed to have perfect channel state information. The consideration of the degradation due to channel estimation should give an insight into the practical performance of such receivers.
- The use of higher-order modulation constellations could be considered as a means of providing higher transmission rates.
- The effect on the system performance and overall system code rate when considering diversity levels higher than the 2x2 system in punctured PA and IA receivers.
- A third form of receiver which is a hybrid between the PA and IA receiver can be investigated. In this approach we can possibly perform one PIC cancellation stage and one turbo decoding iteration for each iteration of every iterative approach receiver stage. It is expected that this will lead to better data estimates through more accurate MAI reconstruction and cancellation. We further expect

University of Cape Town

this hybrid receiver to be more complex than either the PA or IA receiver.

- A comparative complexity study of PA and IA receivers is not considered in this thesis. It would be interesting to investigate the possible performance and complexity tradeoffs in PA and IA receivers.

University of Cape Town

References

[1] B. Sklar, *Digital Communications*, Prentice Hall, second edition, 2001.

[2] J. G. Proakis, *Digital Communications*, McGraw Hill, fourth edition, 2001.

[3] B. Sklar, "Rayleigh fading channels in mobile digital communication systems .I. Characterization," *IEEE Communications Magazine,* vol. 35, no. 7, pp. 90-100, 1997.

[4] B. Sklar, "Rayleigh fading channels in mobile digital communication systems .II. Mitigation," *IEEE Communications Magazine,* vol. 35, no. 7, pp. 102-109, 1997.

[5] W. Jakes, Jr., "An Approximate Method to Estimate an Upper Bound on the Effect of Multipath Delay Distortion on Digital Transmission," *IEEE Transactions on Communications, [legacy, pre - 1988]*, vol. 27, no. 1, pp. 76-81, 1979.

[6] L. Bahl, J. Cocke, F. Jelinek, and J. Raviv, "Optimal decoding of linear codes for minimizing symbol error rate (Corresp.)," *IEEE Transactions on Information Theory,* vol. 20, no. 2, pp. 284-287, 1974.

[7] W. E. Ryan, "A turbo code tutorial," *New Mexico State University*, Las Cruses, New Mexico

[8] P. Patel and J. Holtzman, "Analysis of a simple successive interference cancellation scheme in a DS/CDMA system," *IEEE Journal on Selected Areas in Communications,* vol. 12, no. 5, pp. 796-807, 1994.

[9] L. B. Nelson and H. V. Poor, "Iterative multiuser receivers for CDMA channels: an EM-based approach," *IEEE Transactions on Communications,* vol. 44, no. 12, pp. 1700-1710, 1996.

sity of Cape Town

[10] D. Divsalar, M. K. Simon, and D. Raphaeli, "Improved parallel interference cancellation for CDMA," *IEEE Transactions on Communications,* vol. 46, no. 2, pp. 258-268, 1998.

[11] J. Shen, "Iterative Multiuser Detection," PhD thesis, Department of Electronics, University of York, 30 Sept 2004.

[12] X. Wang and H. V. Poor, "Iterative (Turbo) soft interference cancellation and decoding for coded CDMA," *IEEE Transactions on Communications*, vol. 49, no. 7, pp. 1046-61, 1999.

[13] S. Moshavi, "Multi-user detection for DS-CDMA communications," *IEEE Communications Magazine,* vol. 34, no. 10, pp. 124-136, 1996.

[14] S. Verdu, *Multiuser Detection*, Cambridge University Press, 1998.

[15] A. Duel-Hallen, J. Holtzman, and Z. Zvonar, "Multiuser detection for CDMA systems," *IEEE Personal Communications,* vol. 2, no.2, pp. 46-58, 1995.

[16] M. Honig and U. Madhow, "MMSE Interference Suppression for Direct Sequence Spread-Spectrum CDMA," *IEEE Transactions on Communications*, vol. 42, no. 12, pp. 3178-88, 1994.

[17] D. Divsalar, M. Simon, and D. Raphaeli, "A new approach to parallel interference cancellation for CDMA," *IEEE Global Telecommunications Conference, GLOBECOM '96, vol. 3, pp. 1452-1457, London, Nov* 1996.

[18] T. R. Giallorenzi and S. G. Wilson, "Multiuser ML sequence estimator for convolutionally coded asynchronous DS-CDMA systems," *IEEE Transactions on Communications,* vol. 44, no. 8, pp. 997-1008, 1996.

[19] T. R. Giallorenzi and S. G. Wilson, "Suboptimum multiuser receivers for convolutionally coded asynchronous DS-CDMA system," *IEEE Transactions on Communications*, vol. 44, no. 9, pp. 1183-96, 1996.

University of Cape Town

[20] P. D. Alexander, A. J. Grant, and M. C. Reed, "Iterative detection in CDMA with error control coding," *European Transactions on Telecomms*, vol. 9, pp. 419-25, 1998 .

[21] C. Berrou and A. Glavieux, "Near optimum error correcting coding and decoding: Turbo-codes," *IEEE International conference on communications (ICC)*, vol. 2, pp. 1064-1070, Geneva, Switzerland, May 1993.

[22] A. R. Muller and B. J. Huber, "Iterated soft decision interference cancellation for CDMA," *Tyrrhenian International Workshop on Digital Communications 1997,* In *Broadband Wireless Communications*, Luise and Pupolin eds., Springer, London, U.K., 1998.

[23] H. El Gamal and E. Geraniotis, "Iterative multiuser detection for coded CDMA signals in AWGN and fading channels," IEEE Journal on Selected Areas in Communications, vol. 18, no. 1, pp. 30-41, 2000.

[24] H. Jah-Ming and W. Chin-Liang, "A low-complexity iterative multiuser receiver for turbo-coded DS-CDMA systems," IEEE Journal on Selected Areas in Communications, vol. 19, no. 9, pp. 1775-1783, 2001.

[25] E. O. Bejide and F. Takawira, "An iterative multiuser detector for turbo-coded DS-CDMA systems," EURASIP Journal on Applied Signal Processing, vol. 2005, no. 6, pp. 883-91, 2005.

[26] J. Shen and A. G. Burr, "Turbo multiuser receiver for space-time turbo coded uplink CDMA over frequency-selective fading channel," European Personal Mobile Communications Conference, vol. 5, no. 492, pp. 357-361, 2003.

[27] M. K. Howlader and B. D. Woerner, "Iterative Interference Cancellation and Decoding for DS-CDMA Systems," *Proc. of the IEEE 50th Vehicular Technology Conference*, vol. 3, pp. 1815-1819, 1999.

University of Cape Town

[28] J. M. Luna Rivera, D. G. M. Cruickshank, and J. S. Thompson, "Iterative multiuser receiver for a coded DS-CDMA system," *Proc. of the IEEE Vehicular Technology Conference, VCT '01-Spring,* vol. 2, pp. 1581-1522, Greece, May 2001.

[29] G. J. Foschini and M. J. Gans, "On limits of wireless communications in a fading environment when using multiple antennas," *Wireless Personal Communications*, vol. 50, no. 3, pp. 311-335, March 1998.

[30] V. Tarokh, H. Jafarkhani, and A. R. Cakderbank, "Space-time block codes from orthogonal designs," *IEEE Transactions on Information Theory,* vol. 45, no. 5, pp. 1456-1467, 1999.

[31] H. E. Gamal and A. R. Hammons, "New approach for the spacetime transmitter/receiver design," *IEE Transaction Information Theory*, 2001.

[32] I. E. Telatar and D. N. C. Tse, "Capacity and mutual information of wideband multipath fading channels," *IEEE Transactions on Information Theory,* vol. 46, no. 4, pp. 1384-1400, 2000.

[33] S. M. Alamouti, "A simple transmit diversity technique for wireless communications," *IEEE Journal on Selected Areas in Communications,* vol. 16, no.8, pp. 1451-1458, 1998.

[34] C. Berrou and A. Glavieux, "Near optimum error correcting coding and decoding: Turbo-codes," *IEEE Transactions on Communications*, vol. 44, no. 10, pp. 1262-1271, 1996.

[35] R. Kohno, H. Imai, M. Hatori, and S. Pasupathy, "Combinations of an adaptive array antenna and a canceller of interference for direct-sequence spread-spectrum multiple-access system," *IEEE Journal on Selected Areas in Communications,* vol. 8, no.4, pp. 675-682, 1990.

University of Cape Town

[36] S. Y. Miller and S. C. Schwartz, "Integrated spatial-temporal detectors for asynchronous Gaussian multiple-access channels," *IEEE Transactions on Communications,* vol. 43, no. 234, pp. 396-411, 1995.

[37] W. Xiaodong and H. V. Poor, "Space-time multiuser detection in multipath CDMA channels," *IEEE Transactions on Signal Processing,* vol. 47, no. 9, pp. 2356-2374, 1999.

[38] M. C. Reed and P. D. Alexander, "Iterative multiuser detection using antenna arrays and FEC on multipath channels," *IEEE Journal on Selected Areas in Communications,* vol. 17, no. 12, pp. 2082-2089, 1999.

[39] J. Thomas and E. Geraniotis, "Soft iterative multisensor multiuser detection in coded dispersive CDMA wireless channels," *IEEE Journal on Selected Areas in Communications*, vol. 19, no. 7, pp. 1334-1351, 2001.

[40] W. Hamouda and P. McLane, "Performance analysis of space-time MMSE multiuser detection for coded DS-CDMA systems in multipath fading channels," *IEEE Transactions on Wireless Communications,* vol. 5, no. 4, pp. 829-838, 2006.

[41] D. B. Mashwama and E. O. Bejide, "Turbo Space-Time Multiuser Detection for DS-CDMA Systems in Rayleigh Fading Channels," *Proceedings of Southern African Telecommunication Networks & Applications Conference (SATNAC2007)*, Mauritius, 2007.

[42] T. R. Derryberry, S. D. Gray, M. D. Ionescu, D. Mandyam, and B. Raghothaman, "Tranmit Diversity in 3G CDMA Systems," *IEEE Communication Magazine*, vol. 40, no. 4, pp. 68-75, April 2002.

[43] S. Baro, G. Bauch, and A. Hansmann, "Improved Codes for Space-time Trellis-coded Modulation," *IEEE Communication Letters*, vol. 4, no. 1, pp. 20-22, Jan 2000.

University of Cape Town

[44] J. M. L. Rivera and D. G. M. Cruickshank, "A High Capacity Space-Time FEC Coded DS-CDMA System for use over Multipath Channels," *IEEE Transactions on Wireless Communications*, 2002.

[45] T. H. Liew, J. Pliquett, B. L. Yeap, L. L. Yang, and L. Hanzo, "Comparative study of space time block codes and various concatenated turbo coding schemes," *Proc. of the 11th IEEE International symposium on Personal, Indoor and MobileRadio Communications*, vol. 1, pp. 741-745, London, Sept 2000.

[46] J. Hagenauer, "Rate Compatible Punctured Convolutional Codes (RCPC) and their Applications," *IEEE Transactions on Communications*, vol. 36, no. 4, pp. 389-400, 1988.

[47] D. N. Rowitch and L. B. Milstein, "Rate Compatible Punctured Turbo (RCPT) Codes in a Hybrid FEC/ARQ System," in *Proc. IEEE Communication Theory Mini-Conference, held in conjunction with GLOBECOM '97*, pp. 55-59, Phoenix, Ariz, USA, November 1997.

[48] D. Garg and F. Adachi, "Throughput of RCPT hybrid ARQ for DS-CDMA with diversity reception and rake combining," *Proc. of the 57th IEEE Vehicular Technology Conference, VTC '03-Spring*, vol. 4, pp. 2730-2734, April 2003.

[49] D. N. Rowitch and L. B. Milstein, "On the Performance of Hybrid FEC/ARQ Systems Using Rate Compatible Punctured Turbo (RCPT) Codes," *IEEE Transactions on Communications*, vol. 48, no. 6, pp. 948-59, Jun 2000.

University of Cape Town